Titre: Title:	Heat transfer effect on operation and performance of auto cyclic catalytic reactor
Auteur: Author:	Banafsheh Rafii Sereshki
Date:	2007
Type:	Mémoire ou thèse / Dissertation or Thesis
Référence: Citation:	Rafii Sereshki, B. (2007). Heat transfer effect on operation and performance of auto cyclic catalytic reactor [Mémoire de maîtrise, École Polytechnique de Montréal]. PolyPublie. https://publications.polymtl.ca/7823/

URL de PolyPublie: PolyPublie URL:	https://publications.polymtl.ca/7823/
Directeurs de recherche: Advisors:	Danilo Klvana, & Michel Perrier
Programme: Program:	Non spécifié

UNIVERSITÉ DE MONTRÉAL

HEAT TRANSFER EFFECT ON OPERATION AND PERFORMANCE OF AUTO CYCLIC CATALYTIC REACTOR

BANAFSHEH RAFII SERESHKI

DÉPATEMENT GÉNIE CHIMIQUE

ÉCOLE POLYTECHNIQUE DE MONTRÉAL

MÉMOIRE PRÉSENTÉ EN VUE DE L'OBTENTION
DU DIPLÔME DE MAÎTRISE ÈS SCIENCES APPLIQUÉES
(GÉNIE CHIMIQUE)
JANVIER 2007

Your file Votre référence
ISBN: 978-0-494-25568-1
Our file Notre référence
ISBN: 978-0-494-25568-1

UNIVERSITÉ DE MONTRÉAL

ÉCOLE POLYTECHNIQUE DE MONTRÉAL

Ce mémoire intitulé :

HEAT TRANSFER EFFECT ON OPERATION AND PERFORMANCE OF AUTO CYCLIC CATALYTIC REACTOR

présenté par : RAFII SERESHKI Banafsheh

en vue de l'obtention du diplôme de : Maîtrise ès sciences appliquées

a été dûment accepté par le jury d'examen constitué de:

M. LEGROS Robert, Ph.D., président

M. KLVANA Danilo, Ph.D., membre et directeur de recherche

M. PERRIER Michel, Ph.D., membre et codirecteur de recherche

M. DUBOIS Charles, Ph.D., membre

To my parents and my brother

Acknowledgments

I would like to express my deepest gratitude to my director, Professor Danilo Klvana and my co-director Professor Michel Perrier for their support, guidance, and continuous encouragement throughout my Master's Degree project.

A special thanks goes to Dr. Jitka Kirchnerova for revising my project and for many helpful suggestions and discussions. I would like to thank the jury members Professor Robert Legros and Professor Charles Dubois who have accepted to evaluate this thesis.

I would like to thank my colleague, Mr. Massimiliano Zanoletti, for his help, invaluable discussions, advices, and for the very pleasant time during these two past years. I would also like to express my appreciation to Mr. Robin Giguère for his support and encouragement throughout this work.

I would like to thank Ms. Caroline Duphily from *Centre des Technologies du Gaz Naturel* (CTGN), Professor Christophe Guy, and Mr. Alexander Meneses Jacome for participating in our group meetings.

Words are indeed insufficient to express my gratitude to my family for their endless love, spiritual support, and encouragement. Without them this would not have been possible even if they are miles and miles far from me.

Résumé

Ce travail fait partie d'un projet de recherche qui consiste à développer un réacteur auto cyclique (ACR) pour le traitement du méthane imbrûlé des effluents des moteurs au gaz naturel pour les autobus. Le ACR est un réacteur catalytique composé de deux lits fixes concentriques conçu pour permettre la récupération de la chaleur générée par la réaction de combustion du méthane. Du lit se trouvant dans le tube interne, la chaleur est transférée vers le lit externe annulaire du réacteur. Cette configuration permet de préchauffer les gaz d'alimentation et d'améliorer l'autothermicité dans le réacteur.

Ce projet de maîtrise porte sur le transfert thermique dans le ACR, l'objectif étant d'approfondir la compréhension du phénomène de transfert de chaleur impliqué pour permettre l'amélioration de la conception et de l'opération du ACR. D'une part, il s'agissait de modéliser le transfert de chaleur afin de concevoir l'isolation et les ailettes fixées au tube interne du réacteur ACR incorporé à une unité pilote de laboratoire. D'autre part, de réaliser des expériences avec l'unité pilote afin de vérifier expérimentalement l'influence du transfert de chaleur sur la performance du réacteur et de comparer les résultats obtenus avec les prédictions numériques.

Dans un premier temps, un modèle en deux dimensions a été développé pour concevoir l'isolation du réacteur et les ailettes envisagées. Ce modèle résout les équations de conduction de chaleur en utilisant la méthode des éléments finis en 2D avec le logiciel FEMLAB et permet d'estimer le profil de température dans le matériau isolant ou dans les ailettes.

Les résultats du modèle 2D montrent que la présence des ailettes augmente significativement le transfert de chaleur entre les deux tubes concentriques formant le réacteur. Les simulations réalisées indiquent que l'installation sur le tube interne de 14 ailettes droites en acier inoxydable permet d'augmenter le transfert de chaleur entre les tubes par un facteur de l'ordre de 1,4 par rapport au scénario sans ailettes. Le modèle 2D a également permit d'évaluer sept matériaux pour l'isolation de l'unité pilote. Le Kaowool a été choisi comme isolant et les dimensions de la boite où doit être installé le réacteur est 40×40 cm, pour une température maximale à la paroi du réacteur isolé de 60-65°C.

L'unité pilote a été construite et une série d'expériences a été réalisée pour étudier la performance du réacteur avec des conditions expérimentales réelles. Ces expériences ont permis d'obtenir le profil de température à différentes positions dans le réacteur et de mesurer la conversion du méthane pour différentes températures et compositions du gaz d'alimentation. Il a été trouvé que la combustion catalytique du méthane est pratiquement complète pour toutes les concentrations en méthane étudiées et ce, si la température d'alimentation est plus élevée que 350°C.

Finalement, un modèle appelé HT 1D-t, a été élaboré en collaboration avec Zanoletti pour simuler le profil de température et de concentration dans le réacteur. Ce modèle résout les équations de bilan de matière et d'énergie en 1D pour chacune des phases, en utilisant la méthode des différences finies et une stratégie de couplage des équations de bilans. En général, le modèle HT 1D-t produit des prédictions comparables aux mesures expérimentales provenant de l'unité pilote. Ces résultats suggèrent que ce modèle simplifié

produit une approximation raisonnable du profil de température et de concentration dans le réacteur, permettant de ainsi décrire le transfert de matière et d'énergie et éventuellement d'améliorer la conception du ACR.

En résumé, les modèles utilisés dans ce travail ainsi que les résultats expérimentaux sur l'unité pilote ont permis d'approfondir la compréhension des phénomènes de transfert de chaleur dans le ACR. Les modèles ont notamment permis de concevoir l'isolation et les ailettes pour le ACR. Finalement, le modèle HT 1D-t prédit raisonnablement les profils de température et de concentration devenant ainsi un outil pour étudier la performance du ACR.

Abstract

This work is a part of the research project which consists to develop an auto-cyclic reactor (ACR) as a post combustor for the treatment of unburned methane in exhaust emissions from natural gas fueled engines. The project was motivated by the need to remove methane from emissions of natural gas engines since the unburned methane contributes significantly to green house effect. The ACR is a catalytic bed type reactor consisting of two concentric catalyst filled tubes. The design of the ACR permits to transfer the heat released by the methane combustion from the internal tube towards annulus in order to warm up the feed flow in the annular tube and thus improve the autothermicity.

The objective of this master project was to model the heat transfer involved in the ACR in order to improve understanding of reactor performance. Numerical techniques solving energy and mass balance in 1D and 2D were utilized to model heat transfer in the ACR. These models were used to describe the temperature profile and to design the insulation part and the fins effectiveness of a new pilot unit reactor. Then, experiments with the pilot unit were carried out to assess reactor performance under experimental conditions and to compare them with numerical prediction.

Numerical simulations in two dimensions, based on energy balance, were used to design the insulation part of the reactor and to determine the performance of the internal fins. Commercial software FEMLAB, using the finite element method, was utilized to solve the thermal problem with temperature dependent correlations for the physical parameters and the heat transfer coefficients. Using this model, seven different insulation materials were

studied and Kaowool bulk fiber was chosen to insulate the reactor and enclosed it in a metallic box, with the simulated cross sectional dimensions of 40×40 cm. Investigation of the fin performance indicates that the choice of 14 straight fins is a good compromise, which increases significantly the heat transfer between the internal and annular tube.

The ACR pilot unit was constructed and experiments were conducted to study the performance of the reactor under different operating conditions. From these experiments, it was found that the combustion reaction is almost complete for all inlet methane concentration if inlet temperature is above 350°C.

Finally, the 1D heterogeneous transient model (HT 1D-t) for the catalytic combustion in the ACR was elaborated in collaboration with Zanoletti. This model solves the energy and mass balance for both the gas and solid phases using the finite difference method in order to estimate the axial temperature and concentration profile of the gas flowing inside the reactor. Results obtained with the HT 1D-t model are in a reasonable agreement with the experimental data from the pilot unit. This suggests that this simplified model provides a useful approximation for axial temperature and concentration profile, and can be used to describe the heat and mass transfer in the reactor and potentially improve the design of the ACR.

In summary, this work concerns the modeling of heat transfer involved in the auto-cyclic catalytic reactor by using both numerical and experimental techniques. Simplified strategies in 1D and 2D show good potential to model the complex multi-physics problem of

transport phenomena in the ACR. These models permit to progress the understanding of the influence of heat transfer on reactor performance and to improve design and operation of the reactor. Moreover, experimental results are in agreement with numerical predictions and indicate that the methane combustion is almost complete if the inlet temperature is sufficiently high.

Condensé en français

Ce travail de maîtrise fait partie d'un projet de recherche, réalisé à en collaboration avec le Centre des Technologies du Gaz Naturel (CTGN), qui vise à mettre au point une technologie rendant plus écologique l'utilisation du gaz naturel comme carburant pour les moteurs d'autobus. Ce projet consiste à évaluer la possibilité d'utiliser un réacteur auto cyclique (ACR) pour éliminer les émissions de méthane imbrûlé des moteurs au gaz naturel pour les autobus. Pour ce faire, un réacteur auto cyclique, à l'échelle pilote de laboratoire, est en développement au département de génie chimique à l'École Polytechnique de Montréal.

Dans le contexte actuel de l'augmentation des besoins et des coûts en énergie à l'échelle mondiale ainsi que du défi de réduction des gaz à effet de serre, beaucoup d'efforts sont mis en œuvre pour développer des alternatives aux combustibles fossiles provenant du raffinage du pétrole. En particulier dans le domaine du transport, qui est responsable d'une quantité importante de la consommation d'énergie et des émissions de gaz à effet de serres. Parmi les alternatives, le gaz naturel est reconnu comme le plus propre des combustibles fossiles en terme d'émissions de CO_2 et de NO_x. De plus, des grandes réserves de gaz naturel sont disponibles, à un prix raisonnable en comparaison avec le pétrole ce qui rend cette option encore plus attrayante.

La combustion complète du gaz naturel est par contre difficile puisque la structure de la molécule du méthane est très stable. Dans les effluents des moteurs fonctionnant au gaz naturel, on retrouve une concentration relativement élevée de méthane imbrûlé, de l'ordre

de 500-1000 ppm ou même plus si le moteur est froid. Puisque la contribution du méthane à l'effet de serre est plus de vingt fois plus importante que celle de dioxyde de carbone, les émissions de méthane non brûlé des moteurs au gaz naturel réduisent significativement l'avantage de l'utilisation du gaz naturel comme alternative aux produits pétroliers.

En réalité, la présence d'émissions de méthane s'avère un obstacle important pour l'acceptation des moteurs au gaz naturel dans le domaine des transports, même si la concentration en méthane imbrûlé est faible. Dans les circonstances, une technologie de traitement des effluents des moteurs au gaz naturel doit être développer afin de minimiser les émissions de méthane et de permettre l'acceptation du gaz naturel comme carburant alternatif dans le domaine du transport.

Parmi ces technologies, la combustion catalytique est une solution prometteuse pour traiter les émissions de méthane imbrûlé. Par contre, il existe plusieurs défis reliés à la combustion catalytique du méthane. D'une part, la réactivité du méthane est faible et la température des effluents de combustion des moteurs au gaz naturel est elle aussi relativement faible (<550°C). D'autre part, la concentration et la température des effluents varient en fonction du travail réalisé par le moteur. Avec ces variations, il est difficile de maintenir un front de combustion stable et l'autothermicité dans le réacteur à lit fixe en raison des phénomènes de «*creeeping*».

Le réacteur auto cyclique (ACR) est composé de deux tubes concentriques formant un lit catalytique annulaire qui entoure le lit catalytique dans le tube interne. Les gaz sont

alimentés dans le réacteur par le tube extérieur. Arrivés à l'autre extrémité, les gaz s'écoulent à contre-courant par le tube intérieur avant de sortir du réacteur. Cette configuration permet d'utiliser la chaleur dégagée par la combustion catalytique pour réchauffer les gaz d'alimentation et favoriser le démarrage de la réaction catalytique à l'entrée du réacteur, ce qui permet une sorte d'autorégulation du ACR.

Ce projet de maîtrise porte sur le transfert thermique dans le ACR, l'objectif étant l'approfondissement de la compréhension du phénomène de transfert de chaleur impliquée dans le ACR pour permettre d'en améliorer la conception et l'opération. Il s'agissait d'une part de modéliser le transfert de chaleur afin de permettre la conception de l'isolation du réacteur à l'échelle pilote et d'évaluer la performance des ailettes internes. Il s'agissait aussi d'autre part de faire ressortir l'influence du transfert de chaleur sur la performance du ACR en comparant des données expérimentales de l'unité pilote avec les prédictions des solutions numériques.

La modélisation des phénomènes de transfert thermique dans le ACR présente plusieurs défis. Il s'agit d'une part d'un système multiphasique où se déroulent des phénomènes de transfert de matière, d'énergie et de quantité de mouvement qui sont représentés par des équations différentiels. D'autre part, la géométrie du réacteur est complexe en raison de la présence des deux tubes concentriques munis d'ailettes et nécessite l'utilisation de méthodes numériques pour obtenir et par la suite simuler les profils de température et de concentration dans le ACR.

Dans un premier temps, un modèle en deux dimensions a été développé pour concevoir l'isolation du réacteur et évaluer la performance des 14 ailettes envisagées pour le combusteur de l'unité pilote. Ce modèle est basé sur les équations de conduction de chaleur en deux dimensions. Le profil de température dans le matériau isolant ou dans les ailettes est résolu à l'aide du logiciel FEMLAB, un logiciel basé sur la méthode des éléments finis et bien adapté aux problèmes de conduction thermique. Il permet aussi d'introduire les propriétés physiques et les coefficients de transfert comme fonction de la température. Les conditions opératoires du ACR sont, quant à elle, prises en compte en spécifiant la température des gaz dans le réacteur lors du choix des conditions aux limites.

Les résultats du modèle 2D indiquent que la présence des ailettes augmente significativement le transfert de chaleur entre les deux tubes du réacteur. Les simulations réalisées indiquent que l'installation sur le tube interne de 14 ailettes droites en acier inoxydable permet d'augmenter le transfert de chaleur entre les tubes par un facteur de l'ordre de 1,4 par rapport au scénario sans ailettes.

D'après l'étude de sensibilité aux différents paramètres, la performance des ailettes est un compromis entre la résistance de convection entre le gaz et les ailettes et la résistance thermique de conduction, qui est associé au matériau et à la géométrie des ailettes. En effet, la présence des ailettes introduit davantage de surface d'échange, ce qui diminue la résistance de convection, mais introduit davantage de matériau, ce qui augmente la résistance de conduction. Ainsi, il s'avère que la performance des ailettes est d'autant plus élevée que la conductivité thermique des ailettes est élevée et que la surface d'échange est

élevée. En conséquence, l'utilisation de matériau un peu plus conducteur que l'acier inoxydable, comme le fer, permettrait d'augmenter légèrement la performance des ailettes. Par contre, pour des raisons de résistance à la corrosion le choix de l'acier inoxydable s'avère incontournable.

Le modèle 2D a également permis d'évaluer différents scénarios pour la conception de l'isolation sur l'unité pilote ACR. Concrètement, la performance de sept matériaux isolants utilisés pour envelopper le ACR a été comparée. Pour ce faire, les profils de température correspondant à différentes épaisseurs d'isolation ont été simulés pour chacun des sept matériaux isolants avec le modèle 2D.

La comparaison de la température de surface de la paroi du réacteur après isolation indique, comme prévu, que c'est l'isolant le moins conducteur qui nécessite la plus faible épaisseur pour atteindre une température de surface raisonnable, d'environ 60-65°C. Ainsi, en utilisant le Kaowool qui est le matériau le moins conducteur parmi ceux étudiés, une épaisseur minimum de 15 cm d'isolant est nécessaire. Avec ce matériau, les dimensions de la boite dans laquelle a été installée le ACR ont été estimées à 40×40 cm pour une température maximale à la surface de 60-65°C.

Dans un deuxième temps, un modèle HT 1D-t pour représenter la combustion catalytique a été élaboré en collaboration avec l'étudiant au doctorat M. Zanoletti. Ce modèle a été mis au point pour prédire le profil axial de la température et la concentration du gaz s'écoulant dans le ACR. Pour ce faire, les bilans de matière et d'énergie des phases solide et gazeuse

ont été couplés et résolus en utilisant la méthode des différences finies en une dimension combinés à une stratégie de couplage des équations. En somme, ce modèle permet d'estimer les profils de température et de concentration dans le ACR en spécifiant seulement les conditions opératoires du gaz alimenté au réacteur, tel que la température, la concentration en méthane et le débit.

Les résultats obtenus avec le modèle HT 1D-t ont été comparés avec des données de températures prises à différentes positions à l'intérieur du réacteur de l'unité pilote, et ce pour différentes conditions opératoires. La comparaison entre les résultats expérimentaux et les prédictions du modèle HT 1D-t est relativement bonne. Les profils de température suivent la même tendance et les valeurs prédites sont similaires aux valeurs mesurées. De plus, les positions et les valeurs des maximums en température correspondent bien. Finalement, les concentrations du méthane mesurées à la sortie du ACR correspondent bien aux valeurs prédites par le modèle. Le modèle HT 1D-t permet donc une approximation raisonnable du profil axial de température à l'intérieur du réacteur, ainsi que du profil axial de concentration.

Il est important de souligner que le modèle HT 1D-t est une version simplifiée d'un problème tridimensionnel de phénomène d'échanges. Sommes toutes, une dimension n'est pas suffisante pour prendre en compte adéquatement le transfert de chaleur entre les deux tubes du réacteur et les ailettes. C'est pourquoi un modèle complet en 3D devrait être développé pour les travaux futurs afin de mieux prendre en compte l'échange de chaleur entre les tubes.

La stratégie utilisée dans ce travail pour modéliser le transfert de chaleur dans le ACR a montré de bons résultats avec des simplifications en 1D et 2D. Cela indique aussi qu'un choix approprié des corrélations a été utilisé pour définir les propriétés physiques et les coefficients de transfert pour le modèle. De plus, la méthode utilisée pour résoudre le couplage des équations de bilan de matière et d'énergie pour chacune des phases peut s'appliquer en 3D.

L'unité pilote du ACR a été construite à l'École Polytechnique et une série d'expériences a été réalisée pour évaluer la performance du réacteur. L'instrumentation de l'unité pilote a été conçue pour étudier la combustion catalytique dans le ACR, à partir des mesures de température et de composition du gaz à la sortie du réacteur. La température et la composition du gaz alimenté au réacteur sont contrôlées par l'usager. Des thermocouples installés à différentes positions à l'intérieur du réacteur permettent de mesurer la température tandis que la composition du gaz de sortie du réacteur est déterminée par chromatographie.

Le programme expérimental réalisé dans le cadre de ce travail a permis de mesurer le profil de température pour différentes conditions opératoires. Tel que mentionné précédemment, ces mesures ont été utilisées pour comparer les prédictions du modèle HT 1D-t. Il a aussi été observé que la conversion en méthane est pratiquement complète lorsque la température des gaz d'alimentation est supérieure à 350°C et ce, pour toutes les concentrations de méthane testées.

Toutefois, il est important de mentionner que les expériences et les simulations réalisées dans ce travail, ont été effectuées en absence d'inhibiteur de combustion, tel le CO_2 et l'H_2O présents dans les effluents des moteurs. Puisque la conversion du méthane peut être influencée par la présence de ces inhibiteurs, il serait important dans le futur de considérer ces composés dans la composition du gaz d'alimentation de l'unité pilote afin d'en évaluer la performance dans des conditions plus représentatives des émissions des moteurs au gaz naturel.

En résumé, ce travail portait sur la modélisation des phénomènes de transfert de chaleur dans le réacteur auto cyclique (ACR) en utilisant des méthodes numériques et expérimentales. Les stratégies simplifiées en 1D et 2D ainsi que les résultats expérimentaux sur l'unité pilote, ont permis d'améliorer la compréhension des phénomènes de transfert de chaleur dans le ACR. Concrètement, le modèle 2D a permis de concevoir l'isolation de l'unité pilote du ACR ainsi que d'évaluer la performance des ailettes. Le modèle 1D et une série d'expériences ont permis d'étudier la performance du ACR en terme de conversion du méthane et de profil de température et ce, en fonction de différentes conditions d'alimentation du réacteur.

En conclusion, ce projet de maîtrise a permis de contribuer au développement de la technologie de traitement des émissions de méthane des moteurs au gaz naturel. Les modèles utilisés pour simuler le profil de température dans le réacteur sont utiles pour comprendre les phénomènes de transfert de chaleur et améliorer la conception du ACR. Il est également important de souligner que les résultats expérimentaux présentés dans ce

travail montre que la conversion du méthane dans le ACR est pratiquement complète si la température d'alimentation est suffisante. Cela suggère que cette technologie est envisageable comme traitement pour éliminer le méthane imbrûlé des effluents des moteurs au gaz naturel et ainsi réduire l'émission de ce gaz à effet de serre lorsqu'on utilise le gaz naturel comme carburant pour le transport par autobus.

Table of contents

List of tables

List of figures

List of appendices

Nomenclature

Symbols	Description	units
a_v	Surface area of channels per unit volume of monolith, or of pellets per unit bed volume	m^{-1}
A_C	Cross-sectional area of channel or packed bed	m^2
A_f	Heat transfer surface with fins	m^2
A_w	Heat transfer surface without fins	m^2
C_g	Molar gas concentration of feed	mol/m^3
Cp_g	Constant pressure heat capacity of gas	J/mol.K or J/kg.K
Cp_{inlet}	Heat capacity of flowing gas at inlet temperature of the ACR	J/mol.K or J/kg.K
Cp_{outlet}	Heat capacity of flowing gas at outlet temperature of the ACR	J/mol.K or J/kg.K
Cp_W	Heat capacity of the monolith wall	J/mol.K or J/kg.K
d	Diameter	m
D_{er}	Effective radial dispersion coefficient in packed bed or monolith	m^2/s
D_{ez}	Effective axial dispersion coefficient in packed bed or monolith	m^2/s

Symbols	Description	units
$D_{e\theta}$	Effective angular dispersion coefficient in packed bed or monolith	m^2/s
D_H	Hydraulic diameter	m
D_p	Equivalent particle diameter	m
f	Fanning friction factor	dimensionless
F	Momentum exchange force per unit of volume	N/m^3
$\dot{F}_{CH_4}$	Molar flow rate of methane	mol/s
G	Mass flow rate per unit cross-sectional area	$Kg/m^2.s$
h	Heat transfer coefficient	$W/m^2.K$
h_{gs}	Heat transfer coefficient between gas and catalyst surface	$W/m^2.K$
h_m	Heat transfer coefficient between gas and monolith	$W/m^2.K$
h_{wg}	Heat transfer coefficient between gas and wall	$W/m^2.K$
h_{ws}	Heat transfer coefficient between wall and catalyst surface	$W/m^2.K$
ΔH_R	Heat of reaction	J/mol
j	Heat transfer factor	dimensionless
k	Thermal conductivity	W/m.K
κ_a	Permeability of the monolith	m^2
k_g	Gas thermal conductivity	W/m.K
$k_{m,CH4}$	Mass transfer coefficient of methane	m/s
k_n	Reaction rate constant	m/s

Symbols	Description	units
k_p	Particle thermal conductivity	W/m.K
k_{rg}	Radial gas thermal conductivity in a packed bed	W/m.K
k_{rs}	Thermal conductivity of catalyst particle in radial direction	W/m.K
k_{rm}	Thermal conductivity of monolith in radial direction	W/m.K
k_{ss}	Thermal conductivity of stainless steel	W/m.K
k_w	Thermal conductivity of monolith wall	W/m.K
k_{zg}	Axial gas thermal conductivity in a packed bed	W/m.K
k_{zm}	Thermal conductivity of monolith in axial direction	W/m.K
k_{zs}	Thermal conductivity of catalyst particle in axial direction	W/m.K
$k_{\theta g}$	Angular gas thermal conductivity in a packed bed	W/m.K
$k_{\theta m}$	Thermal conductivity of monolith in angular direction	W/m.K
$k_{\theta s}$	Thermal conductivity of catalyst particle in angular direction	W/m.K
K	Characteristic kinetic energy per unit of volume	J/m^3
L	Length	m
$\dot{m}$	Mass flow rate of air	kg/s
M	Molar mass of a substance	kg/kmol
Nu	Nusselt number	dimensionless
Nu_{gw}	Nusselt number between gas and reactor wall	dimensionless
Nu_m	Nusselt number in monolith channels	dimensionless
P	Pressure	Pa

Symbols	Description	units
P_W	Wetted perimeter	m
P_0	Pressure at entrance	Pa
Pe	Peclet number	dimensionless
P_L	Pressure at position L	Pa
Pr	Prandtl number	dimensionless
q	Heat flux	W/m^2
q_b	Heat flux when the entire fin was at base temperature	W/m^2
q_{fins}	Heat flux by fins	W/m^2
q_{inside}	Heat flux from inside of the internal tube	W/m^2
$q_{outside}$	Heat flux from outside of the internal tube	W/m^2
$q_{without\ fins}$	Heat flux without fins	W/m^2
$\mathcal{Q}$	Heat flow rate	W
Q	Volumetric flow rate	L/min
$\mathcal{Q}_{gen}$	Heat generation	W
$\mathcal{Q}_{inlet}$	Heat flow rate enters the reactor	W
$\mathcal{Q}_{loss}$	Heat loss from the reactor	W
$\mathcal{Q}_{outlet}$	Heat flow rate leaves the reactor	W
r	radius	m
Re	Reynolds number	dimensionless
Re_b	Bed Reynolds number in a packed bed	dimensionless

Symbols	Description	units
Re_j	Reynolds number as defined in (2.10)	dimensionless
$(-R_{CH4})_s$	Rate of disappearance of methane at catalyst external surface	mol/g.s or mol/m^2.s
R_{fins}	Thermal resistance in the case of the tube with fins	°C/W
R_g	Universal gas constant, 8,314	J/mol.K
R_{hwg1}	Convection resistance inside of the internal tube	°C/W
R_{hwg2}	Convection resistance outside of the internal tube	°C/W
R_k	Conduction resistance in the tube	°C/W
$R_{without\ fins}$	Thermal resistance in the case of the tube without fins	°C/W
S_f	Shape factor	dimensionless
t	Time	s
t	Thickness of the fins	m
T	Temperature	°C or K
$T_{ambient}$	Temperature of ambient	°C or K
T_g	Temperature of gas	°C or K
T_{inlet}	Inlet gas temperature of the reactor	°C or K
T_k	Temperature at node k in finite difference method	°C or K
T_{outlet}	Outlet gas temperature of the reactor	°C or K
T_s	Temperature on catalyst surface	°C or K
T_∞	Temperature of ambient	°C or K
U	Overall heat transfer coefficient	W/m^2.K

Symbols	Description	units
U_f	Overall heat transfer coefficient with fins	$W/m^2.K$
U_w	Overall heat transfer coefficient without fins	$W/m^2.K$
v	Average velocity (when subscripted with r ,z, θ indicated velocity component in that direction)	m/s
v_s	Average superficial velocity	m/s
$\dot{V}_{CH_4}$	Volume flow rate of methane	L/s
X	Fractional conversion	dimensionless
Δx	Mesh size of grid in finite difference method	m
Y_{CH4}	Mole fraction of methane	dimensionless
$Y_{CH4,g}$	Mole fraction of methane in gas phase	dimensionless
$Y_{CH4,s}$	Mole fraction of methane on catalyst surface	dimensionless
□	Shape factor in equation (3.4)	dimensionless
δ_w	Monolith reactor wall thickness	m
ε	Bed porosity in a packed bed	dimensionless
ε_m	Monolith porosity	dimensionless
η	Effectiveness factor	dimensionless
μ	Viscosity of gas	Pa.s
μ_w	Viscosity of gas at the wall temperature	Pa.s
ρ	Mass density	kg/m^3
ρ_g	Mass density of gas	kg/m^3

Symbols	Description	units
ρ_s	Mass density of catalyst pellet	kg/m^3
ρ_W	Density of the washcoat	kg/m^3
τ_g	Stress tensor of gas	dimensionless

CHAPTER 1 Introduction

In recent years, one important challenge in industrialized countries all over the world concerns the climate change and so-called green house effect (GHE) resulting in global warming. It is known that emissions from fossil fuels combustion are responsible for the GHE and world-wide efforts are done to reduce the effect of the polluting emissions, such as the Kyoto Protocol. Among emissions components, carbon dioxide is known to contribute the most to GHE because of the large quantity that are emitted and that is why, important efforts must be done to reduce this emission, even if the green house effect of CO_2 is small in comparison to CH_4 or N_2O.

Large part of the GHE emissions comes from combustion of fossil fuels serving as an energy source for transportation vehicles. The transportation sector accounts for about one quarter of Canada's green house gas emissions and is also a major contributor to smog in the urban areas (Figure 0-1). Approximately 70 percent of GHG emissions from transportation are a result of people driving cars and goods being moved by truck and two-thirds of these emissions are generated within urban areas [1].

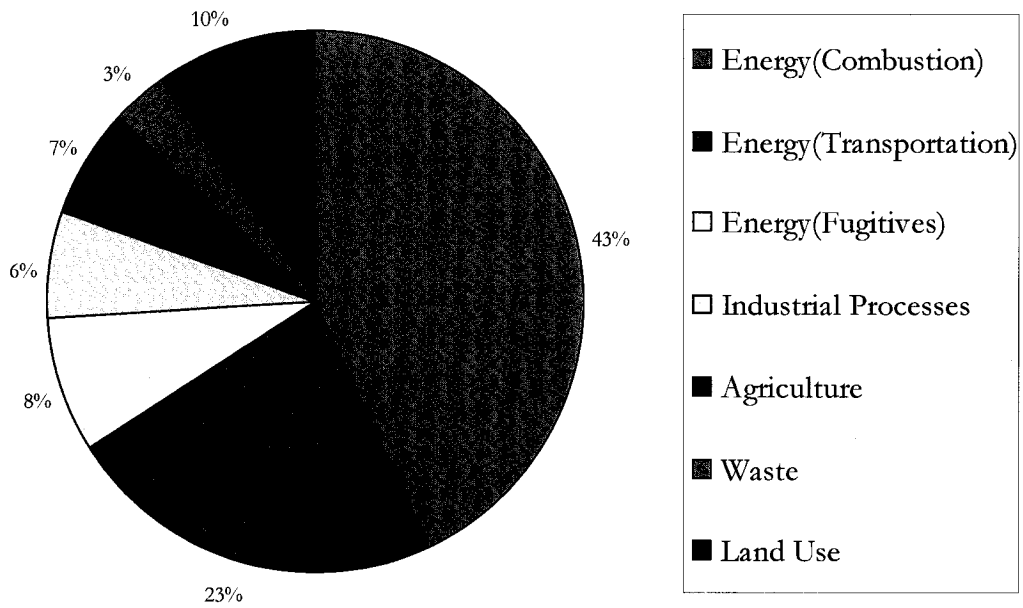

Figure 1-1: Canada's 2004 green house gas inventory [1]

In the context of GHE reduction strategy for transportation vehicles, natural gas (NG) has been recognized as an attractive alternative to classical fossil fuels, such as gasoline or diesel. In fact, the main advantage of NG is the highest hydrogen-carbon ratio (H/C) comparing to other fossil fuels. For the same amount of energy, NG produces not only less CO_2 but also less noxious emissions. As an example, NG combustion generates about 23% less CO_2 than gasoline, 80% less NO_x and more than 99% less SO_x [2]. Thus, natural gas is considered as the cleanest fuel among the existing fossil fuels. Furthermore, NG is available in large amount at relatively low cost. For example, the two largest natural gas fields are probably Urengoy Gas Field in Russia and South Pars Gas Field in Iran with reserves of the

order of 1200 TcF[1]. In Canada, proven reserves of NG are about 57 TcF, while in 2003 the production was close to 6400 BcF[2], which is more than double the amount consumed in Canada [3].

The molecule of methane has a very stable structure and it is difficult to combust completely. Thus, in exhaust emissions from natural gas engines, there is relatively high level of unburned methane, typically 500-1000 ppm (0,05-0,1%), or even higher when the engine is cold. Since methane contribution to GHE is more than twenty times stronger than that of carbon dioxide, the unburned methane reduces the advantage of NG. In fact, this is an obstacle for accepting transport engines using natural gas, even if unburned methane concentration is small. In this context, reduction of at least 60% of methane emission should be reached [2, 4]. Catalytic post-combustion treatment could potentially assure the required reduction of unburned methane emissions.

However, since the methane reactivity is poor [5] and the temperature of the NG engines is relatively low (<550°C), efficient system requires special design. Moreover, concentration and temperature of exhaust emissions vary with time. With all these variations, it is difficult to achieve the autothermicity in a fixed bed reactor because of the creeping phenomenon which means the movement of the reaction zone with time toward outlet of the fixed bed reactor [6]. Consequently, the reaction zone can arrive at the outlet of the reactor and the catalytic conversion will be extinguished.

---

[1] Trillion cubic Feet

[2] Billion cubic Feet

Cyclic change in flow direction by a series of valves, facilitates keeping the combustion front in the catalyst layer [7] and different designs and their applications were proposed [8]. Furthermore, reactor with cyclic feed greatly improves the autothermicity of gas mixtures containing low fuel concentration having low calorific value [9].

A cyclic feed type of reactor was even proposed for post-combustion treatment of NG engines [10, 11]. However, these systems are rather complex and thus not very practical for application in average transportation vehicles.

However, Klvana *et al.* [12] proposed a different reactor (auto-cyclic reactor; ACR) to mitigate the problem of a creeping zone and demonstrated the feasibility of its application for a variety of fuels [13]. Concurrently, similar type of reactor was also studied by Sheintuch and Nekhamkina [14].

As shown in Figure 1-2 this new reactor consists of two concentric tubes. The feed enters the outer annular catalytic bed and at the extremity, the flow returns in counter current direction by inner tube catalytic bed from where it exits. This ACR is applicable for catalytic combustion and other exothermic reactions and takes the advantage of the heat released by chemical reaction to warm up the feed flow before the reaction front leaves the catalytic layer. The heat recuperation makes it possible to re-ignite the reaction at the entrance of the ACR, giving a self-regulating auto cyclic operation. Thus, such reactor can be called auto-cyclic fixed bed reactor.

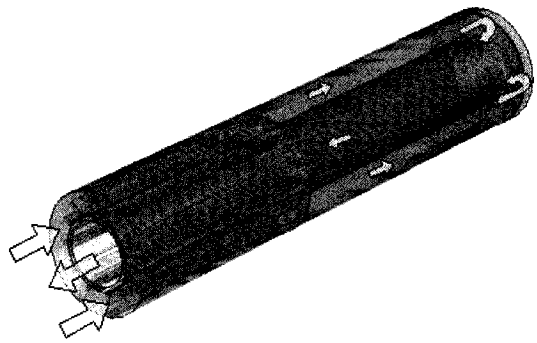

Figure 1-2: Schematic of the auto-cyclic reactor

1.1 Objectives

This research project is a part of a collaboration project with *Centre des Technologies du Gaz Naturel* (CTGN) to evaluate the possibility of ACR operation for eliminating the unburned methane in exhaust emissions from natural gas buses engine.

The general objective of this work is to improve understanding of heat transfer in auto cyclic reactor.

The specific objectives of this project are to:

- Evaluate the heat transfer effect on the performance of the auto cyclic reactor
- Limit the thermal loss from the external tube
- Increase the heat transfer between the two compartments (from the internal tube towards external tube)

1.2 Methodology

This section presents the methodology followed to reach the objectives of the project. Firstly, research activities were done in collaboration with the Ph.D. student M. Zanoletti, aiming to elaborate a model for the catalytic combustion in the ACR in transient regime. As a starting point, the HT 1D-t model for the catalytic combustion in the ACR was elaborated. This model was implemented with MATLAB 7.0.1 in order to simulate the temperature and concentration profiles inside the reactor in axial direction. Efforts were done to develop the 3D model for the catalytic combustion. However, this 3D model is still in progress and the simulations are not terminated.

Also, two-dimensional simulations of heat transfer were done to model temperature profiles for the insulation and the fin material of the ACR. To solve energy, mass and momentum balance equations, various correlations characterizing the heat transfer in the ACR were needed and literature review was performed to find and justify available correlations.

The correlations found from literature were combined with the appropriate energy balance to define a 2D model. The resulting model is in partial differential equation with a set of boundary conditions. However, since the geometry of the ACR is complex, no analytical solution exists and numerical techniques were needed to solve the temperature profile in the ACR. For that purpose, the commercial software FEMLAB (COMSOL, Version 3.2) using the finite element method (FEM) was chosen. Hence, the simplified two-dimensional simulations of heat transfer in ACR were done and the sensitivity of the model was evaluated. This study was useful to estimate the insulation thickness and the fin

performance of the ACR in order to propose a configuration of the ACR which improved its performance and operability, from the heat transfer point of view.

As mentioned before, one of the objectives of this project is to reduce the heat loss from the exterior tube of the reactor. Therefore, a high performance insulation material should be chosen and installed around the reactor in order to decrease the heat loss as much as possible. The temperature in the reactor is high (300-600°C), thus the insulation materials should be non-combustible and resist high temperature. The seven insulation materials studied in this work are listed in Table 1-1 with their descriptions, taken from the thermal insulation handbook [15]. These insulation materials with different thermal conductivities were studied and compared using 2D model in order to design the insulation part of the ACR pilot unit.

Table 1-1: List of insulation materials

Insulation materials	*Description and general characteristics*	*Bulk density (kg/m³)*
Kaolin ceramic fiber	Flexible rolls or sheets	48 to 64
Kaolin ceramic fiber	Flexible rolls or sheets	96 to 128
Mineral wool	Formed into blankets	160 to 224
Alumina silica fiber	Formed into rope, cord and yarn	400
Silica fibers	Formed into woven blankets and felts	96 to 152
Kaowool [16]	Fiber	128
Kaowool [16]	Fiber	256

Another specific objective of this project is to increase the heat transfer from the inner tube towards annulus in order to warm-up the entrance feed of the reactor to improve re-ignition of the reaction. Extended surfaces are a good choice to enhance the heat transfer between a surface and a fluid. In fact, application of extended surfaces provides a combination of conduction and convection systems while heat is conducted through the material and dissipated to the surroundings by convection. In this work, the choice of 14 internal fins to transfer the heat of reaction was evaluated using the 2D model under different operating conditions.

Finally, the new pilot unit of ACR was constructed and experiments were done to study the reactor performance under real experimental conditions. In this pilot unit, the temperatures

along the reactor length were measured using K-type thermocouples, and concentration of the outlet gas was monitored by Gas Chromatograph (GC). However, the temperature, concentration, and flow rate of the reactor feed were controlled by the operator. These experimental data were useful to understand the reactor performance in term of methane conversion and also to compare with the prediction of axial temperature and concentration profiles given by HT 1D-t model.

CHAPTER 2 Modeling of auto-cyclic catalytic reactor

This section presents modeling of the ACR for catalytic combustion of unburned methane in exhaust emissions from natural gas engines. After a brief introduction of the ACR operation, the conservation equations for energy, momentum, and material balances are derived in this section. Furthermore, correlations for heat transfer coefficients and physical properties needed in these balances are presented.

2.1 ACR description

The auto-cyclic catalytic reactor designed for this work consists of two concentric tubes, which are made of standard stainless steel AISI 304 with dimensions given in Figure 0-1. The catalytic bed consists of a combination of pellets and catalytic monoliths. The gas enters through a layer of bare precalcined Alcoa CSS100 3/16 alumina pellets (Zone 1), and then passes through the fins filled by catalytic pellets (0,9 wt%Pd/Al_2O_3, Zone 2) and finally flows into the annular monolith section (Zone 3). At the extremity (Zone 4), the gas enters in counter current direction in the central compartment filled with 6 pieces of monolith (Zone 5) followed by 0,9 wt%Pd/Al_2O_3 catalyst pellets (Zone 6) before exiting the reactor. The outer region of the inner tube is equipped with rectangular outer fins to improve the heat transfer from the inner part toward annulus. This physical coupling of heat transfer between the outlet (inner tube) and inlet (annulus) of the reactor, improves the autothermicity by providing continuous heat recuperation; if the front moves to the outlet of the reactor, its heat may re-ignite the incoming feed in the annulus and a new cycle

begins. In order to decrease the heat loss from the ACR, the reactor should be wrapped with an insulation material and enclosed in a metallic box.

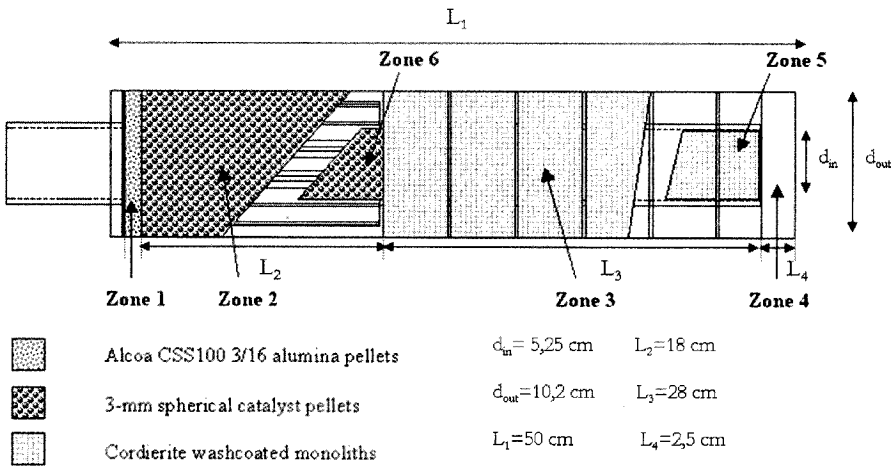

Figure 2-1: Schema of the experimental laboratory ACR

2.1.1 Catalyst

Supported palladium oxide has been found to be the most efficient catalyst for the oxidation of methane to carbon dioxide and water under lean burn conditions [4]. Hence, the catalytic bed in the ACR consists of commercial 0,2 wt%Pd/Al_2O_3 of 3 mm pellets (Procatalyse PC263) enriched with Pd to reach 0,9 wt%Pd in order to increase its performance. This catalyst was impregnated with an ammonia solution of $PdCl_2$ (12,5 mg/ml) and was calcinated at 650°C for 12 hours in air to convert to palladium oxide which is more active than palladium for methane combustion. The resulting enriched PC263 catalyst (5,5 g Pd/L) is more active than the original catalyst.

The other part of catalytic bed consists of a highly active PdO catalyst supported on alumina coated cordierite monoliths (400 CPSI), which gives high geometric area and low-pressure drop through the system. The monoliths were coated with γ-alumina stabilized by 2% CeO_2 (9±1 wt%) and then impregnated by an ammonia solution of $PdCl_2$ (25 mg Pd/ml). Finally they were calcinated at 550°C for 12 hours. The resulting monoliths (6 g PdO/L) are highly active.

2.2 Balance equations

The basis of reactor analysis is to derive the conservation equations for energy, momentum, and mass. Each of these equations has a paramount importance since they describe the relation between temperature, velocity and concentration inside the ACR.

In packed bed reactors, the balance equations could be based on a pseudo-homogeneous or heterogeneous model. In pseudo-homogeneous model, the reactor bed is considered as a single continuous phase, defined by single balance equation. Heterogeneous model considers the fluid and the solid phase separately, hence balance equations are written for each phase.

The pseudo-homogeneous model gives a simplified prediction of reactor performance, considering continuity of temperature and neglecting the difference between fluid and solid. However, in the ACR there is a significant temperature difference between gas and solid. In that context, assumption of temperature continuity between the phases seems inappropriate

to model the gas-solid flow in the ACR and that is why it is preferred to use heterogeneous two-phase model.

For a catalytic combustion, the energy, momentum and mass balances are indeed dependent and should be coupled. Since coupling of these balance equations is mathematically difficult, many correlations are necessary and simplifications are often useful. For instance, when the pressure drop in catalytic combustor is low, coupling with momentum balance may not be necessary since its effect on the solution of the mass and energy balances is small [16]. Since, temperature has a significant effect on the rate of reaction, energy and mass balance must be solved simultaneously.

Moreover, because the fluid flows through the porous media formed by the randomly packed particles, the velocity profile in a packed bed is quite complex. The macroscopic velocity profile in the central part of the packed bed is mostly flat and increases near the wall boundary. However, this rise is negligible and the velocity profile can be considered flat along the cross sectional area of the bed [16]. Furthermore, in monolith channels the velocity is maximum at the centerline and minimum at the wall. Nevertheless, again this rise is negligible and the velocity distribution is considered uniform. In short, the superficial velocity (v_s) which is the velocity based on the total cross sectional area is utilized in this project. The superficial velocity is computed by dividing the volumetric flow rate of the gas by the cross sectional area of the bed. This assumption gives the opportunity to consider a constant velocity profile in the energy balance.

2.2.1 Energy balance equation

Energy balance equation permits to describe the temperature changes along the reactor while the reaction proceeds. Energy balance equation is required for estimating the amount of energy transferred between different sections of the reactor.

The general form of energy balance for steady-state is

$$\begin{bmatrix} Rate\ of\ energy \\ entering\ the\ system \end{bmatrix} - \begin{bmatrix} Rate\ of\ energy \\ leaving\ the\ system \end{bmatrix} = 0 . \qquad (2.1)$$

Since catalytic combustion in the ACR involves heterogeneous reaction: the methane is in gas phase and the catalyst is in solid phase, the energy balance equation is applied for gas and solid phase separately.

The energy balance for gas phase in packed beds is given by

$$\frac{1}{r}\frac{\partial}{\partial r}\left[rk_{rg}\frac{\partial T_g}{\partial r}\right]+\frac{\partial}{\partial z}\left[k_{zg}\frac{\partial T_g}{\partial z}\right]+\frac{1}{r^2}\frac{\partial}{\partial \theta}\left[k_{\theta g}\frac{\partial T_g}{\partial \theta}\right]-v_s\rho_g Cp_g\frac{\partial T_g}{\partial z}+h_{gs}a_v(T_s-T_g)=0 , \qquad (2.2)$$

where r is the radius, k_{rg} , k_{zg}, and $k_{\theta g}$ are the thermal conductivity of gas in radial, axial, and angular direction, ρ_g and Cp_g are density and heat capacity of the gas respectively, h_{gs} is the heat transfer coefficient between gas and catalyst surface, a_v is surface area of the pellets per unit bed volume, T_g is the gas temperature, T_s is the temperature on catalyst surface, v_s is the superficial velocity of gas which would exist in the tube if the packing were absent. It is related to the average velocity in the pores of the bed (interstitial velocity v) by

$$v_s = \varepsilon v . \qquad (2.3)$$

where ε is the bed porosity considered constant.

The energy balance for the gas phase in the monolith section is similar to the energy balance for the gas phase in packed bed. It should be noticed that the porosity of the monolith is different from the packed bed.

The energy balance for solid phase in packed beds is given by

$$\frac{1}{r}\frac{\partial}{\partial r}\left[rk_{rs}\frac{\partial T_s}{\partial r}\right]+\frac{\partial}{\partial z}\left[k_{zs}\frac{\partial T_s}{\partial z}\right]+\frac{1}{r^2}\frac{\partial}{\partial \theta}\left[k_{\theta s}\frac{\partial T_s}{\partial \theta}\right]-\Delta H_R\eta(-R_{CH4})_S\rho_s(1-\varepsilon) \\ +h_{gs}a_v(T_g-T_s)=0 \tag{2.4}$$

where r is the radius, k_{rs}, k_{zs}, and $k_{\theta s}$ are the thermal conductivity of catalyst particles in radial, axial, and angular direction, ρ_s is density of catalyst pellet, ΔH_R is the heat of reaction, η is the effectiveness factor of catalysts, $(-R_{CH4})_S$ is the rate of disappearance of methane at catalyst external surface, h_{gs} is the heat transfer coefficient between gas and catalyst surface, a_v is the surface area of pellets per unit bed volume, T_s is the temperature on catalyst surface, ε is the bed porosity.

The energy balance for solid phase in monolith section is given by

$$\frac{1}{r}\frac{\partial}{\partial r}\left[rk_{rm}\frac{\partial T_s}{\partial r}\right]+\frac{\partial}{\partial z}\left[k_{zm}\frac{\partial T_s}{\partial z}\right]+\frac{1}{r^2}\frac{\partial}{\partial \theta}\left[k_{\theta m}\frac{\partial T_s}{\partial \theta}\right]-a_v\Delta H_R\eta(-R_{CH4})_S \\ -h_m a_v(T_s-T_g)=0 \tag{2.5}$$

where k_{rm}, k_{zm}, and $k_{\theta m}$ are the thermal conductivity of monolith in radial, axial, and angular direction, h_m is the heat transfer coefficient in the monolith, and a_v is the surface area of

channels per unit volume of monolith. It should be noticed that the units of $(-R_{CH4})_S$ vary for packed bed and monolith section. The unit of $(-R_{CH4})_S$, is (mol/g.s) in packed bed and (mol/m^2.s) in monolith section.

To deal with these energy balance equations it is necessary to define heat transfer coefficients and thermal conductivities. In addition, the bed to wall heat transfer coefficient and the fins heat transfer coefficients must be defined since they are involved in boundary conditions defining the differential equations of these energy balances.

Because of the high operating temperature, heat transfer by radiation between reactor wall and flowing gases should in principle be considered. However, due to small dimensions of the system, the radiation interactions can be neglected [16].

2.2.1.1 Heat transfer coefficients

2.2.1.1.1 Heat transfer coefficients in packed beds

In literature, there are many correlations for heat transfer coefficients in packed beds. Hayes and Kolaczkowski [16] described the heat transfer coefficients in terms of dimensionless j factor

$$j = \frac{h_{gs}}{Cp_g G} Pr^{2/3}, \tag{2.6}$$

where G is the mass flow rate per unit cross-sectional area ($G = \rho_g v_s$). The Prandtl number (Pr) is defined as

$$Pr = \frac{Cp_g \mu}{k_g} \quad . \tag{2.7}$$

Bird *et al.* [17] suggested the following correlations which fit the most experimental data

$$j = 0.91 Re_j^{-0.51} S_f \quad Re_j \prec 50, \tag{2.8}$$

$$j = 0.61 Re_j^{-0.41} S_f \quad Re_j \succ 50, \tag{2.9}$$

where S_f is the shape factor, which is 0,79 for a Rashig ring, 0,91 for a short cylinder, and 1 for a sphere. As alumina pellets were used in the ACR, S_f=1 should be employed. The Reynolds number (Re_j) in equation (2.8) and (2.9) is given by

$$Re_j = \frac{\rho_g v_s D_p}{6(1-\varepsilon)\mu S_f} = \frac{GD_p}{6(1-\varepsilon)\mu S_f} \quad , \tag{2.10}$$

where D_p is the equivalent particle diameter, μ is the viscosity of gas, ε is the bed porosity and determined experimentally as 0,42, which is in the typical range of bed porosity for packed bed [16] , ρ_g is density of ideal gas obtained from

$$\rho_g = \frac{PM}{R_g T_g} \quad . \tag{2.11}$$

Thus, the heat transfer coefficient between gas and solid particles in packed beds can be estimated from equations (2.6) to (2.11).

The porosity of the monolith is the ratio of flow area to total area which is the area available for the flow passing through the channels. The dimensions of the monolith are shown in Table 2-1. The porosity of the monolith was estimated around 0,66 [16] for the coated monolith.

Table 2-1: Physical dimensions of monolith (CPSI=400)/washcoat

Inside channel width (uncoated)	1,1 mm
Wall thickness between channels	0,15 mm
Washcoat cross sectional area	0,175 mm^2
Wetted perimeter of channel (with washcoat)	3,8 mm

2.2.1.1.2 Bed to wall heat transfer coefficients in packed beds

There are two wall heat transfer coefficients involved in the reactor. One is the heat transfer coefficient from the solid particles to the wall (h_{ws}) and the other is heat transfer coefficient from the gas to the wall (h_{wg}) [16].

For the solid particles, heat transfer coefficient from the solid to the wall is defined as

$$h_{ws} = 2.12\frac{k_{rs}}{D_p}, \tag{2.12}$$

k_{rs} is the thermal conductivity of the particles and D_p is equivalent particle diameter.

For the gas phase, correlations between Nusselt, Reynolds and Prandlt number are used to estimate the heat transfer coefficient between the gas and the wall (h_{wg}). Yagi and Wakao [18] presented the Nusselt number (Nu_{gw}) as a function of bed Reynolds number (Re_b) and Prandlt number

$$Nu_{gw} = 0.6Pr^{1/3}Re_b^{0.5} \quad 1 \prec Re_b \prec 40, \tag{2.13}$$

$$Nu_{gw} = 0.2Pr^{1/3}Re_b^{0.8} \quad 40 \prec Re_b \prec 2000, \tag{2.14}$$

where Re_b is the bed Reynolds number given by

$$Re_b = \frac{GD_p}{\mu}, \tag{2.15}$$

Since the Nusselt number at the wall is defined by

$$Nu_{gw} = \frac{h_{wg} D_p}{k_g}, \tag{2.16}$$

the heat transfer coefficient between wall and gas h_{wg} can be calculated from equation (2.16) with k_g the thermal conductivity of the gas and D_p the equivalent particle diameter.

2.2.1.1.3 Heat transfer coefficient for fins

Many studies deal with the estimation of heat transfer coefficient on fins. In general, there are two heat transfer coefficients for fins to consider; heat transfer coefficient at the tip and heat transfer coefficient on the lateral part of fins. Heat transfer coefficient at the fin tip is often assumed equal to heat transfer coefficient on the lateral or taken to be equal to zero which is adiabatic tip condition [19]. Furthermore, Razelos and Krikkis [20] showed that the difference between the two cases is negligible in most of the cases such as for effective fins which increase the heat transfer between the primary surface and adjacent fluid. Based on these studies, in this work it was assumed that the heat transfer coefficient at the fin tip is equal to the heat transfer coefficient on the lateral.

In the present work the assumption of uniform heat transfer coefficient was applied which means the heat transfer coefficient is not a function of position on the lateral surface of the

fins. Furthermore, heat transfer coefficient from gas to wall (h_{wg}) in packed beds was employed as the heat transfer coefficient on fins surface

$$h_{wg} = \frac{0.2\, Pr^{1/3}\, Re_b^{0.8}\, k_g}{D_p}, \tag{2.17}$$

where Pr is the gas Prandtl number, Re_b is the bed Reynolds number, k_g is the gas thermal conductivity, and D_p is the equivalent particle diameter.

2.2.1.1.4 Heat transfer coefficient in monolith channels

Each channel of the monolith can be considered as a tube. Thus, the empirical relations for pipe and tube flow can be employed. Since the maximum Reynolds number in monolith channels is less than 400, the heat transfer coefficient can be evaluated by the empirical correlations for laminar flow. Sieder and Tate [21] proposed a empirical relation for laminar flow heat transfer in tubes

$$Nu_m = 1.86(Re\, Pr)^{1/3}\left(\frac{D_H}{L}\right)^{1/3}\left(\frac{\mu}{\mu_w}\right)^{0.14}, \tag{2.18}$$

where Re is the Reynolds number in monolith channel, Pr is the Prandlt number at bulk temperature, L is the length of monolith, μ is the gas viscosity at bulk temperature, μ_w is the gas viscosity at the wall temperature, and D_H is hydraulic diameter defined by

$$D_H = \frac{4A_C}{P_W}, \tag{2.19}$$

where A_C is the cross sectional area of the flow and P_W is the wetted perimeter.

Heat transfer coefficient in the monolith channel can be obtained by

$$h_m = \frac{Nu\, k_g}{D_H}, \tag{2.20}$$

where k_g is the thermal conductivity of the gas at bulk temperature.

2.2.1.1.5 Physical properties

In heterogeneous energy balance given by equations (2.2), (2.4), and (2.5) thermal conductivities in axial, radial, and angular directions are required for the solid phase and for the gas. Dixon and Cresswell [22] showed that solid thermal conductivities in packed bed are a function of bed porosity, gas thermal conductivity and thermal conductivity of particles (alumina)

$$k_{rs} = k_{zs} = k_{\theta s} = \frac{2k_g(1-\varepsilon)^{0.5}}{1-\frac{k_g B}{k_p}}\left[\frac{\left[1-\frac{k_g}{k_p}\right]B}{\left[1-\frac{k_g B}{k_p}\right]^2} ln\left[\frac{k_p}{Bk_g}\right] - \frac{B+1}{2} - \frac{B-1}{\left[1-\frac{k_g B}{k_p}\right]}\right], \tag{2.21}$$

Where

$$B = C\left[\frac{1-\varepsilon}{\varepsilon}\right]^{10/9}, \tag{2.22}$$

and C=1.25 for spheres and 1.4 for crushed particles.

The effective axial thermal conductivity in the monolith section can be related to the thermal conductivity of the monolith wall (k_w) and monolith porosity (ε_m)

$$k_{zm} = (1-\varepsilon_m)k_w. \tag{2.23}$$

The effective radial and angular thermal conductivity of the monolith depends on the monolith structure.

For the gas phase, radial, axial, and angular thermal conductivities can be calculated from equation (2.24) through (2.29) [22] with

$$k_{rg} = \frac{GCp_g D_p}{(Pe)_{rg}}, \tag{2.24}$$

$$k_{zg} = \frac{GCp_g D_p}{(Pe)_{zg}}, \tag{2.25}$$

and

$$k_{\theta g} = \frac{GCp_g D_p}{(Pe)_{\theta g}}. \tag{2.26}$$

Peclet number (Pe) in radial, axial, and angular direction can be estimated from equation (2.27) through (2.29) respectively

$$\frac{1}{(Pe)_{rg}} = 0.1 + \frac{0.66\varepsilon}{Re_b Pr}, \tag{2.27}$$

$$\frac{1}{(Pe)_{zg}} = \frac{0.73\varepsilon}{Re_b Pr} + \frac{0.5}{\left[1 + \frac{9.7\varepsilon}{Re_b Pr}\right]}, \tag{2.28}$$

and

$$\frac{1}{(Pe)_{\theta g}} = 0.1 + \frac{0.66\varepsilon}{Re_b Pr}. \tag{2.29}$$

2.2.2 Continuity and momentum balance equations

The equation of continuity is employed to relate the density and velocity of the gas as follows

$$\frac{1}{r}\frac{\partial}{\partial r}(\varepsilon\rho_g r v_r)+\frac{\partial}{\partial z}(\varepsilon\rho_g v_z)+\frac{1}{r}\frac{\partial}{\partial\theta}(\varepsilon\rho_g v_\theta)=0. \tag{2.30}$$

Momentum balance equations provide information about the variation of velocity and pressure profile across the reactor. Since there may be a large temperature gradient in catalytic combustion reactor, density and viscosity are not constant and their variation should be considered in momentum balance.

The general form of momentum balance in steady-state regime is

$$\begin{bmatrix}Rate\ of\ momentum\\ entering\ the\ system\end{bmatrix}-\begin{bmatrix}Rate\ of\ momentum\\ leaving\ the\ system\end{bmatrix}+\begin{bmatrix}Sum\ of\ forces\\ acting\ on\ the\ system\end{bmatrix}=0. \tag{2.31}$$

As mentioned in section 2.2, there are in fact two phases involved in the ACR, which are the solid catalyst and the flowing gas. To apply momentum balance for the whole volume of ACR (gas and catalyst), bed porosity and momentum exchange (F) between gas and solid catalyst should be considered in momentum equation. Equation (2.32) represents the equation of momentum in packed bed

$$\nabla.(\varepsilon\rho_g vv)-\nabla.(\varepsilon\tau_g)+\varepsilon\nabla p+F=0, \tag{2.32}$$

where ε is bed porosity, which is constant, τ_g is stress tensor defined in equation (2.33) by Newton's law of viscosity

$$\tau_g=(k_g-\frac{2}{3}\mu)(\nabla.v)-\mu\left[(\nabla v)+(\nabla v)^T\right]. \tag{2.33}$$

The definition of the momentum interaction between solid and gas (F) is not trivial and empirical correlations are often used. The term F represents the force per unit of volume associated with the kinetic behavior of the gas. For instance, Tiemersma *et al.* [23] defined the momentum interaction force in the packed bed reactor by Ergun equation

$$F = 150\frac{(1-\varepsilon)^2}{\varepsilon^2}\frac{\mu_g v_s}{D_p^2} + 1.75\frac{1-\varepsilon}{\varepsilon}\frac{v_s^2 \rho_g}{D_p}, \tag{2.34}$$

where ε is the bed porosity, v_s is the superficial velocity, and D_p is particle diameter.

The monolith section can be considered as a porous media and F can be derived by Darcy's law

$$F = \frac{\mu}{\kappa_a}\varepsilon_m v_s, \tag{2.35}$$

where κ_a is the apparent permeability of the monolith that presents the ability of the monolith bed to transmit the fluid. This force can be defined as the product of the perimeter of cross sectional area of the monolith channel P, the length of the monolith L, the characteristic kinetic energy per unit of volume K, and the friction factor f [17],

$$F = PLKf. \tag{2.36}$$

For fully developed flow, the force balance on the reactor in the direction of the fluid is

$$F = (P_0 - P_L)A_C, \tag{2.37}$$

where P_0 is the pressure at entrance, P_L is the pressure at position L and, A_C is the cross sectional area. Combining the equation (2.36) and (2.37), using the definition of the kinetic energy per unit volume, and isolating the term of pressure

$$\frac{(P_0 - P_L)}{L} = \frac{2}{D_H} \rho v_s^2 f, \tag{2.38}$$

D_H is hydraulic diameter is defined by

$$D_H = \frac{4A_C}{P_W}. \tag{2.39}$$

Applying equation (2.38) and Darcy's law, the permeability κ_a is expressed as

$$\kappa_a = \frac{\varepsilon_m \mu}{\left(\frac{2}{D_H}\right) \rho v_s f}. \tag{2.40}$$

Friction factor can be estimated by

$$f = \frac{14.227}{Re}. \tag{2.41}$$

2.2.3 Mole Balance Equation

Mole balance equation provides information about the composition of the species and variation of concentration along the reactor.

The general form of mole balance in steady-state regime is

$$\begin{bmatrix} Molar\ flow\ of \\ methane\ into \\ the\ system \end{bmatrix} - \begin{bmatrix} Molar\ flow\ of \\ methane\ out\ of \\ the\ system \end{bmatrix} - \begin{bmatrix} Disappearance \\ of\ methane \\ by\ reaction \end{bmatrix} = 0. \tag{2.42}$$

Equation (2.43) shows the mole balance equation of methane in gas phase in radial, axial, and angular direction.

$$\frac{1}{r}\frac{\partial}{\partial r}\left(rD_{er}C_g\frac{\partial Y_{CH_4,g}}{\partial r}\right)+\frac{\partial}{\partial z}\left(D_{ez}C_g\frac{\partial Y_{CH_4,g}}{\partial z}\right)+\frac{1}{r^2}\frac{\partial}{\partial\theta}\left(D_{e\theta}C_g\frac{\partial Y_{CH_4,g}}{\partial\theta}\right)-\frac{\partial(C_g v_s Y_{CH_4,g})}{\partial z} \quad (2.43)$$
$$-k_{m,CH_4}a_r C_g(Y_{CH_4,g}-Y_{CH_4,s})=0,$$

where D_{er}, D_{ez}, and $D_{e\theta}$ are the effective radial, axial, and angular dispersion coefficient in packed bed or monolith bed respectively, C_g is the feed gas molar concentration, Y_{CH4} is the mole fraction of methane, v_s is the superficial velocity, $k_{m,CH4}$ is the mass transfer coefficient of methane, a_r is the external surface area of the catalyst packing per unit volume of reactor. It should be noticed that the dispersion coefficients and bed porosity in the packed bed and the monolith section should be distinguished.

Mole balance equation for the solid phase in packed bed is shown by equation (2.44), which is a balance between mass transfer and reaction rate.

$$\frac{1}{r}\frac{\partial}{\partial r}\left(rD_{er}C_g\frac{\partial Y_{CH_4,s}}{\partial r}\right)+\frac{\partial}{\partial z}\left(D_{ez}C_g\frac{\partial Y_{CH_4,s}}{\partial z}\right)+\frac{1}{r^2}\frac{\partial}{\partial\theta}\left(D_{e\theta}C_g\frac{\partial Y_{CH_4,s}}{\partial\theta}\right) \quad (2.44)$$
$$-\eta(-R_{CH_4})_s\rho_s(1-\varepsilon)+k_{m,CH_4}a_r C_g(Y_{CH_4,g}-Y_{CH_4,s})=0,$$

$(-R_{CH4})_s$ is the rate of disappearance of methane at catalyst external surface, $k_{m,CH4}$ is the mass transfer coefficient of methane, C_g is the feed gas molar concentration of gas, η is the effectiveness factor of catalyst, and ρ_s is the mass density of catalyst pellet.

Mole balance equation for solid phase in monolith section is described by equation(2.45)

$$\frac{1}{r}\frac{\partial}{\partial r}\left(rD_{er}C_g\frac{\partial Y_{CH_4,s}}{\partial r}\right)+\frac{\partial}{\partial z}\left(D_{ez}C_g\frac{\partial Y_{CH_4,s}}{\partial z}\right)+\frac{1}{r^2}\frac{\partial}{\partial\theta}\left(D_{e\theta}C_g\frac{\partial Y_{CH_4,s}}{\partial\theta}\right) \quad (2.45)$$
$$-\eta(-R_{CH_4})_s+k_{m,CH_4}C_g(Y_{CH_4,g}-Y_{CH_4,s})=0.$$

Equations (2.43), (2.44), and (2.45) describe the mole balance equation for methane. For a single reaction, only one mole balance equation is required and the concentration of other species can be obtained by the stoichiometry of the reaction.

2.3 Summary

This section presented the operation of the reactor and a description of the catalyst material used in the ACR. Afterward, the balance equations for energy, momentum, and mass governing the ACR, were discussed in this part. Correlations from literature for heat transfer and thermal properties were also presented.

The presented balance equations are partial differential equations that must be solved by numerical methods. In the following chapter the strategy used to solve these equations is presented.

CHAPTER 3 Numerical simulations of heat transfer

As presented in chapter 2, temperature, velocity, pressure and concentration of methane in ACR are governed by partial differential equations. For the complex three-dimensional geometry of the ACR, direct analytical solution does not exist and numerical methods were needed to solve balance equations presented in chapter 2. In this chapter, finite element method was used to model heat transfer in ACR. These simulations were performed to estimate the insulation thickness around the reactor and the fin performance.

3.1 Numerical methods

Numerous numerical methods were developed to find approximate solutions for partial differential equations involved in many engineering problems. Classical techniques are finite difference method (FDM), finite element method (FEM), and finite volume method (FVM). In this section, finite element method was chosen as a reliable technique to solve the partial differential equations involved in describing operation of the ACR.

3.1.1 Finite element method and software

Finite element method was developed in the mid 1950's to solve the complex geometry in transport phenomena problems. This robust method allows dealing with non-linear equations, complex geometries, and different boundary conditions. Another advantage of FEM is the possibility of using not only uniform meshes, but also non-uniform meshes of different element sizes in different parts of the domain. FEM uses interpolation function defined on each element of the mesh giving a continuous interpolation of the unknown variables over the entire domain based on discrete nodal values. In general, linear or

quadratic basis can be chosen for these interpolation functions and discrete values of the variables are found by the resolution of a system of equations.

FEM implementations are now part of many commercial softwares available for engineers, such as FEMLAB (COMSOL, version 3.2) chosen in this project. In most of these softwares, the user needs to create the geometry, generate the mesh, select the desired physical equations and define the boundary conditions in order to properly define the FEM problem. One advantage of FEMLAB is the possibility to define user expressions, which permit to employ non-isothermal physical properties. Moreover, recent FEMLAB software is able to deal with multiphysics problems, which are suitable for the future development of complete ACR model with coupling of energy, momentum and materials balances in 3D.

3.2 ACR 2D model simulation

The auto-cyclic catalytic reactor consists of two concentric cylinders of 50 cm long standard stainless steel pipe; the annular tube has 10,2 cm inside diameter with thickness 0,15 cm and the central tube has 5,25 cm inside diameter and thickness 0,39 cm.

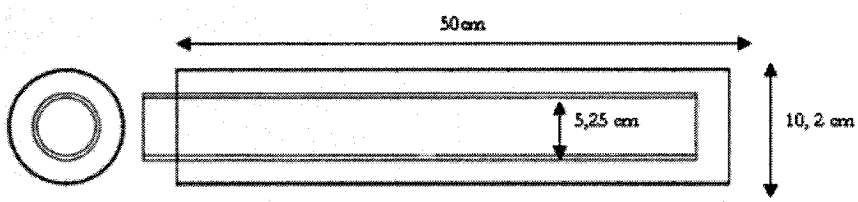

Figure 3-1: Dimensions of ACR

The aim of this section is to model the temperature profile of insulation material, temperature profile of fins, and to estimate the fin performance. For this purpose, only energy balance equation was employed. Thus, the application mode of heat transfer by conduction was selected in FEMLAB with steady-state model.

For three-dimensional simulations of heat transfer by conduction in the ACR, temperature profile of the gas should be specified to define the boundary conditions of the problem. Since this temperature profile should be determined by solving the complete multiphysics problem of the ACR, simplified model was considered in this project. The inlet and outlet gas flows were considered at same constant mass velocity and at temperature of 400°C and 600°C respectively as the boundary conditions. Moreover, there is symmetry of heat conduction in axial direction, thus only two-dimensional (cross sectional) geometries were used for all of the simulations performed in this chapter.

Since the concentration of methane in exhaust emissions from natural gas engine is very low (~1000 ppm) and it is desired to have no methane in outlet of the reactor, the physical properties of air were used for the gas as the first step of approximation.

3.2.1 Insulation

The reactor must be wrapped with insulation material and placed into a metallic box in order to decrease the heat loss from exterior tube of the reactor. The purpose of this study is to find an insulation material requiring the smallest thickness of insulation. Hence, the

idea is to estimate, for different material, the smallest box dimension having the reasonable temperatures on the surfaces of the box during the ACR operation. For security reasons, 60-65°C was considered the reasonable temperature on the surface of the metallic box. This temperature is in fact an upper limit that one can touch the metallic box without risk of burning.

3.2.1.1 Mathematical model

For the insulation part, the heat balance equation is

$$\rho Cp\frac{\partial T}{\partial t} - \nabla.(k\nabla T) = Q, \tag{3.1}$$

where T is temperature, ρ is density of insulation, Cp is heat capacity of insulation material, k is thermal conductivity of insulation, and Q is heat source which is zero in this case. When a steady-state is reached, the temperature does not change with time, thus $\partial T / \partial t = 0$ and the first term of equation (3.1) disappears, leading to

$$\nabla.(k\nabla T) = 0. \tag{3.2}$$

3.2.1.2 Boundary conditions

Since the side walls of the box have convection heat transfer with ambient air, heat flux boundary conditions were assumed on side walls

$$n.(k\nabla T) = h(T_\infty - T), \tag{3.3}$$

where h is the heat transfer coefficient on side walls of the box and it was estimated for each side of the box separately [24]

$$h = \alpha\left(\frac{\Delta T}{L}\right)^{1/4}, \tag{3.4}$$

where α is a factor depending on the type of convection and the surface (Table 3-1), ΔT is the temperature difference between box wall and ambient, and L is the length of the box side.

Table 3-1: Shape factor α for free laminar convection in equation (3.4) [24]

Surface	α
Vertical plane	1,42
Heated horizontal plate facing upward	1,32
Heated horizontal plate facing downward	0,59

Furthermore, the maximum inside temperature of the reactor was fixed at 600°C all along the length and continuity boundary conditions were chosen for interior boundaries.

$$n.(k_1 \nabla T_1 - k_2 \nabla T_2) = 0 \tag{3.5}$$

In addition, all the thermal conductivities involved in equation (3.2), (3.3) and (3.5) were considered a function of temperature (Appendix A).

3.2.1.3 Insulation thickness and temperature profile

Seven different non-combustible insulation materials were investigated using seven box dimensions from 25 cm to 55 cm, in order to determine the appropriate insulation material for the ACR. For each box dimension, FEM mesh was generated, temperature profile was simulated for each insulation material, and surface temperatures on side walls were

compared. An example of mesh and simulated temperature profile is given in Figure 3-2 and Figure 3-3 while the results of all the simulations are summarized in Figure 3-4 and Table 3-2.

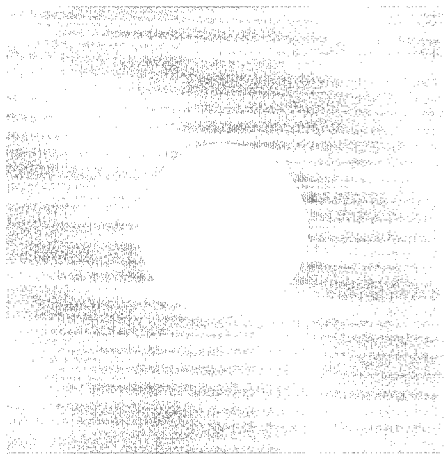

Figure 3-2: FEM meshes for alumina silica fiber (31062 elements) with cross sectional box dimension 30×30 cm

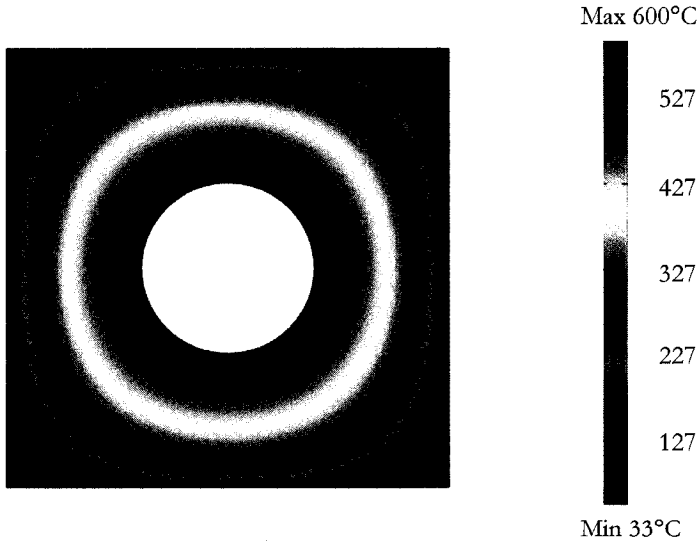

Figure 3-3: Temperature profile for alumina silica fiber with cross sectional box dimension 30×30 cm

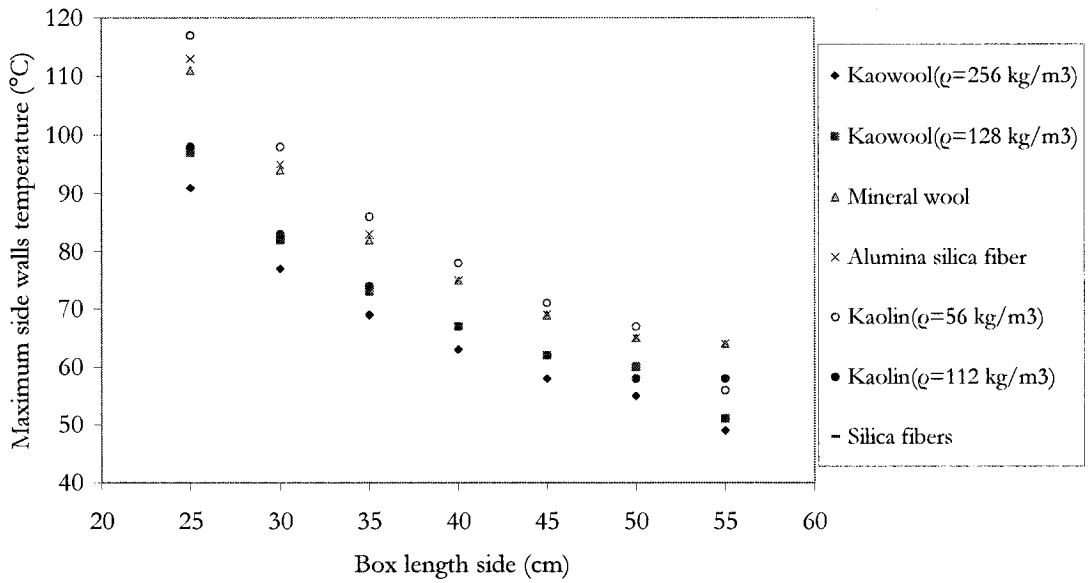

Figure 3-4: Maximum side wall temperature of the metallic box vs. box length side of the reactor

Table 3-2: Insulation thickness with different materials

Insulation materials	*Average density (kg/m^3)*	*Thermal conductivity (W/m.K) at T=500°C*	*Smallest insulation thickness (cm)*	*Box dimensions (cm)*
Kaowool	256	0,098	15	40×40
Kaowool	128	0,111	17,3	45×45
Silica fibers	128	0,120	17,3	45×45
Kaolin ceramic fiber	112	0,125	17,3	45×45
Mineral wool	192	0,150	20	50×50
Alumina silica fiber	400	0,163	20	50×50
Kaolin ceramic fiber	56	0,170	22,3	55×55

As expected, by increasing the box dimensions the surface temperature on side walls decreases. Also, the insulation with the material having the smallest thermal conductivity requires the smallest insulation thickness. The insulation thickness is the length of the box minus the diameter of the reactor.

As documented in Table 3-2 the use of Kaowool leads to the smallest insulation thickness among the studied materials by considering reasonable temperature on side walls of the box. Therefore, the box dimension for the ACR was estimated as 40×40 cm with Kaowool insulation (ρ =256 kg/m^3) and the hottest zone on upper wall and side walls is at 60-65°C as shown in Figure 3-5.

Moreover, the two-dimensional heat loss from the reactor was estimated by FEMLAB. This amount is the result of integration of heat flux q over the exchange boundary Γ as presented in equation (3.6). The heat loss from the reactor box (40×40 cm) per unit length using Kaowool was computed as 163 W/m. The overall heat loss from the reactor can be estimated by multiplying this amount by length of the reactor box (70 cm). Thus, the overall heat loss from the reactor is 114 W.

$$Q = \int_{\Gamma} q d\Gamma \tag{3.6}$$

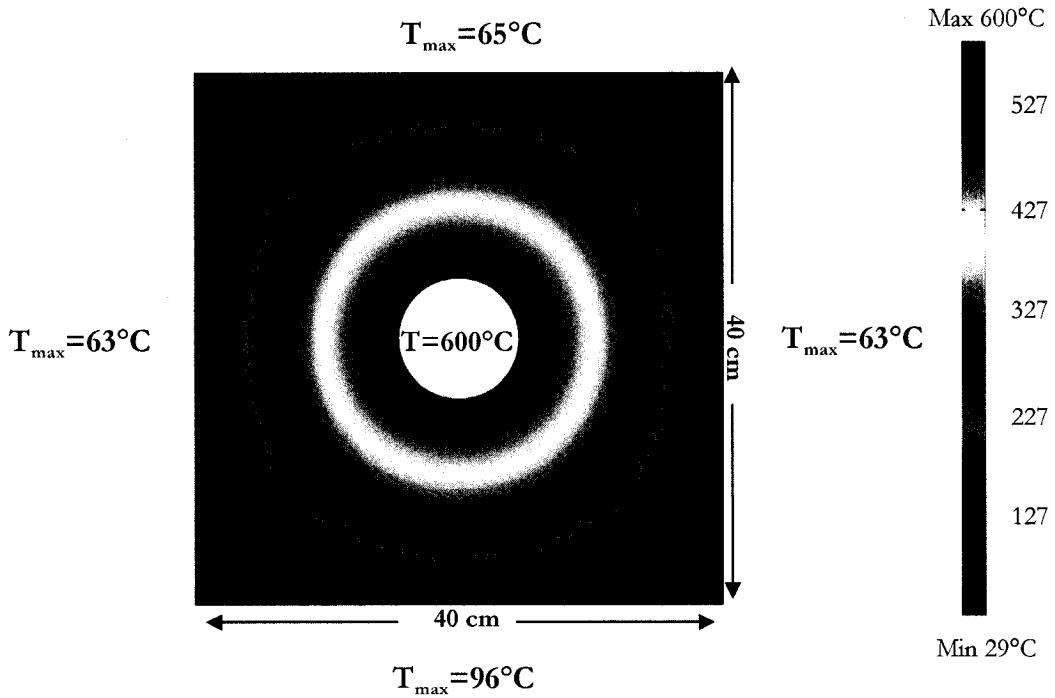

Figure 3-5: Temperature profile of Kaowool insulation material around the reactor

3.3 Pre-heater 2D model simulation

The pre-heater (Figure 3-6) consists of four heating elements (1,33 cm) with total power of 4280 W to warm up the entrance feed of the ACR to the typical temperature of exhaust emissions from natural gas engines. The pre-heater tubes housing the heating elements have the internal diameter of 3,2 cm and length of 25 cm.

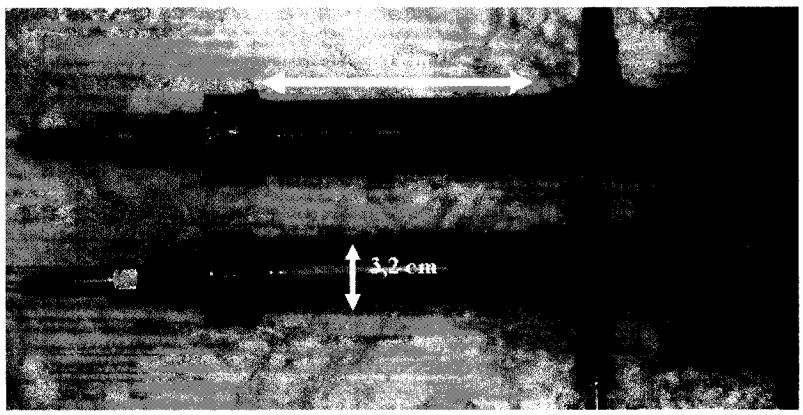

Figure 3-6: Photograph of the Pre-heater, showing two of the elements

3.3.1 Insulation

The same insulation material was used for pre-heater section in order to decrease the heat loss. The objective is to estimate the box dimension by having still the same reasonable temperatures on the box surfaces (60-65°C). The same boundary conditions as for the box surfaces for the ACR were used here and the maximum inside temperature of the pre-heater was fixed at 550°C. The same insulation material Kaowool fiber was used to wrap the pre-heater.

Figure 3-7 shows the variation of maximum surface temperature on the box versus the box dimension. To maintain the reasonable temperature on the box surfaces, the length side of the box was estimated as 35 cm demonstrated in Figure 3-7. In addition, Figure 3-8 presents the temperature profile of insulation material for the pre-heater. The two-dimensional heat loss from the pre-heater was calculated to be 150 W/m by integrating the

heat flux q over the total exchange boundary Γ. Thus, the estimated overall heat loss from the pre-heater being enclosed in a box 40 cm long is 60 W.

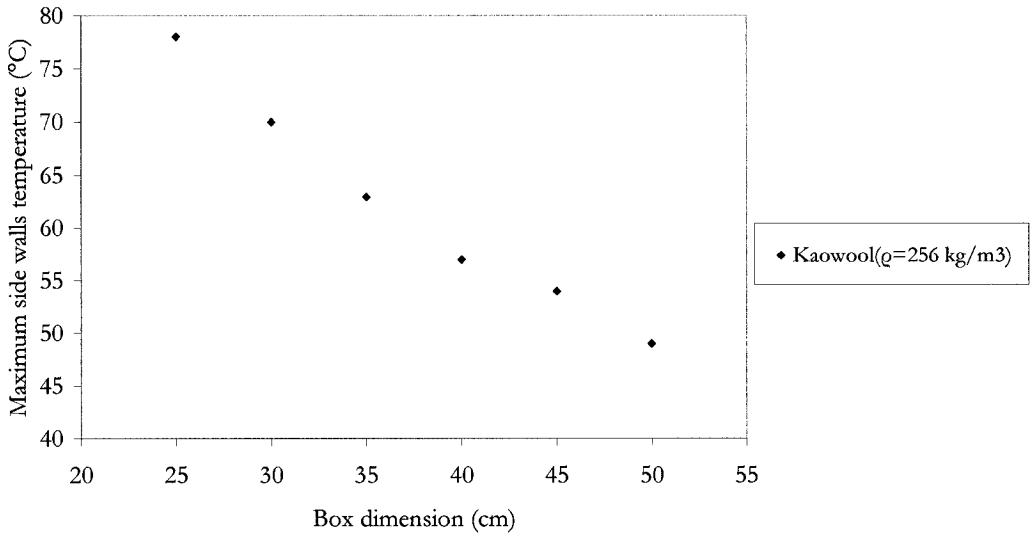

Figure 3-7: Maximum side wall temperature of the metallic box vs. box dimension

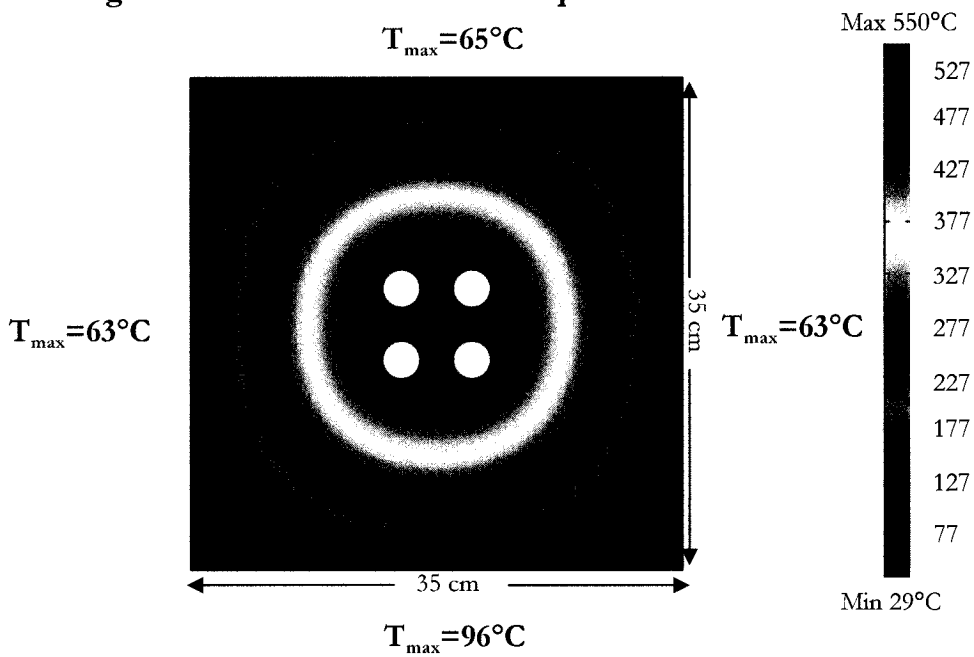

Figure 3-8: Temperature profile of insulation material around pre-heater

3.4 Fin performance

Fourteen straight fins of rectangular profile were welded around the inner tube to improve the heat transfer toward annulus in the ACR in order to warm-up the entrance feed of the reactor and re-ignite the reaction. This number of fins was recommended by «*Thermofin*» company (located in Montreal) as an optimum number of fins, on a tube of diameter 5,25 cm. In this project, the performance of fins for improving heat transfer in the ACR was studied using FEM model of ACR.

The cross sectional geometry of the reactor with fins section and dimension of the fins are presented in Figure 3-9. The objective is to obtain the temperature profile, quantify the heat transfer in the presence of fins and finally estimate the fin performance.

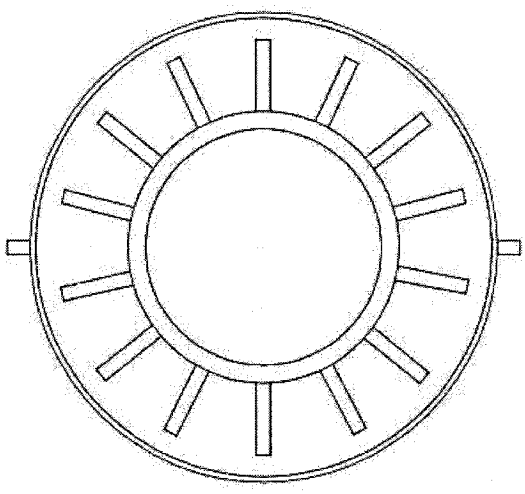

d_{in}_annulus	10,2 cm
d_{in}_tube	5,25 cm
annulus thickness	0,15 cm
tube thickness	0,39 cm
fin height	1,6 cm
fin thickness	0,32 cm
fin length	18 cm
no. of fins	14

Figure 3-9: Geometry and dimensions of the reactor with fins in 2D

3.4.1 Mathematical model

Since the heat transfer in fins proceeds by conduction, the same equation (3.2) was employed in FEMLAB simulation.

3.4.2 Boundary conditions

In view of the fact that the gas enters between the fins and returns in counter current direction by the internal tube, heat flux boundary conditions were assumed on the fin surface and on the internal tube wall as shown in Figure 3-10. Equation (3.7) represents the heat flux boundary condition,

$$n.(k\nabla T) = h_{wg}(T_g - T). \tag{3.7}$$

T_g is the temperature of the gas and T is the temperature of the wall which is variable, and k is the thermal conductivity of fin material (stainless steel). As mentioned in section 2.2.1.1.3, the heat transfer coefficient between wall and gas in packed beds is defined as,

$$h_{wg} = \frac{0.2\, Pr_g^{1/3}\, Re_b^{0.8}\, k_g}{D_p}. \tag{3.8}$$

For purpose of simulation, the temperature of the inlet gas was fixed at 400°C as a typical average temperature of exhaust gases from natural gas fuelled engines while the temperature of the outlet flow was assumed at 600°C, which is the maximum expected temperature in the reactor.

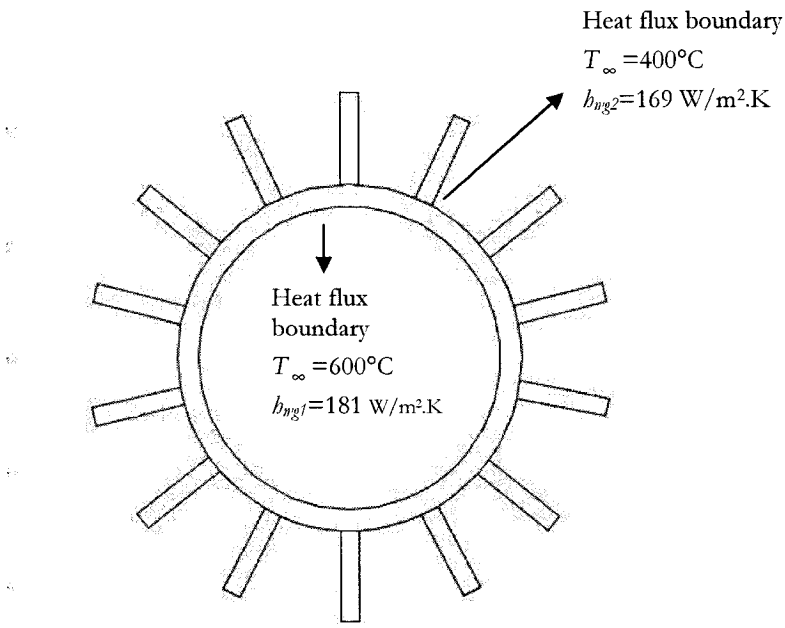

Figure 3-10: Boundary conditions of fins

3.4.3 Fin performance calculation

Fin performance can be expressed either as fin efficiency or fin effectiveness. Fin efficiency is defined as the heat transferred by the fin over the heat that would be transferred if the thermal conductivity of fin were infinite.

$$Fin\ Efficiency = \frac{q_{fins}}{q_b} \tag{3.9}$$

where q_{fins} is actual heat transferred by fin and q_b is the heat that would be transferred if the entire fin was at base temperature. The fin efficiency was estimated approximately 0,65 for the same geometry and the same operating conditions in ACR using charts provided in [24] page 46.

On the other hand, fin effectiveness is defined as the ratio between the heat transferred with fins and the heat which would be transferred without fins

$$Fin\ Effectiveness = \frac{q_{fins}}{q_{without\ fins}}. \tag{3.10}$$

In this case, we need to know the heat transferred for the two situations, with and without fins. Both can be computed easily from FEM solution by integrating heat flux q over exchange surfaces Γ, representing the perimeter simulated temperature profile using equation (3.6).

The temperature profile for the case without fins is shown in Figure 3-11 and result of the simulation for temperature profile for the case with fourteen fins is presented in Figure 3-12.

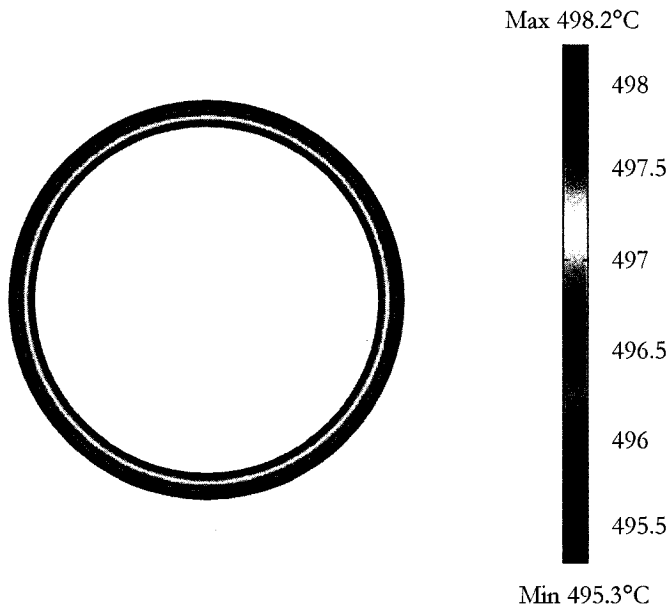

Figure 3-11: Temperature profile of the tube

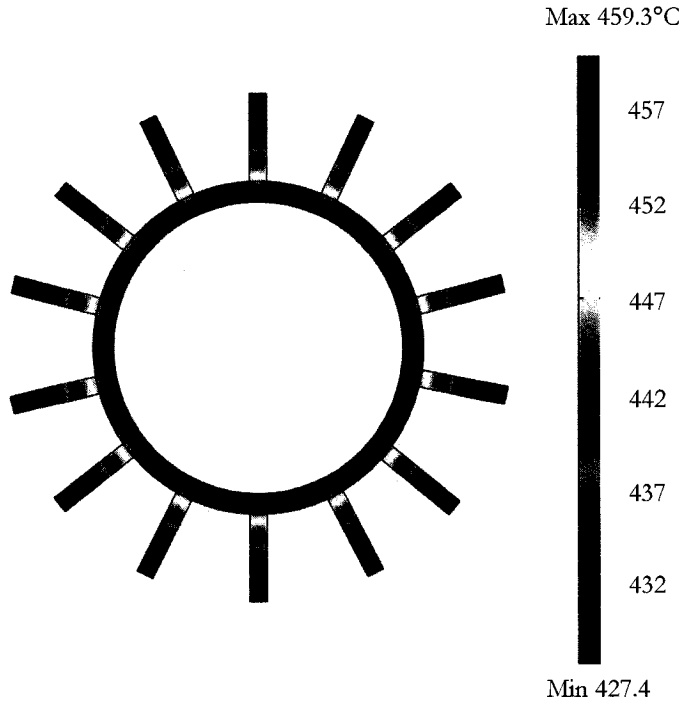

Figure 3-12: Temperature profile of the fins

Using temperature profile of Figure 3-11 and Figure 3-12, the fin effectiveness was estimated and is shown in Table 3-3.

Table 3-3: Fin effectiveness

q with fins (W/m)	4277
q without fins (W/m)	3056
Fin effectiveness	1,4

As a conclusion, by adding the fourteen fins in this case the rate of heat transfer increases by a factor 1,4.

Moreover, for the case of the tube without fins, analytical solution can be found because of the simplified geometry and boundary conditions; in fact this is a one-dimensional problem (see Appendix B). Equation (3.11) shows the total heat flux in the tube without fins which is the ratio of overall temperature difference to the sum of the thermal resistances

$$q_{without\ fins} = \frac{2\pi \Delta T_{\infty}}{\frac{1}{r_1 h_1} + \frac{ln(r_2/r_1)}{k_{ss}} + \frac{1}{r_2 h_2}}. \tag{3.11}$$

Thermal resistance in the case of the tube without fins is expressed as

$$R_{without\ fins} = \frac{1}{2\pi r_1 h_1} + \frac{ln(r_2/r_1)}{2\pi k_{ss}} + \frac{1}{2\pi r_2 h_2}, \tag{3.12}$$

hence

$$q_{without\ fins} = \frac{\Delta T_{\infty}}{R_{without\ fins}}. \tag{3.13}$$

The analytical solution for the tube with fins is not available because of the complex geometry, however the total heat flux with fins can be expressed as

$$q_{fins} = \frac{\Delta T_{\infty}}{R_{fins}}. \tag{3.14}$$

Since fin effectiveness can alternatively be expressed as

$$Fin\ Effectiveness = \frac{R_{without\ fins}}{R_{fins}}, \tag{3.15}$$

Equation (3.15) and data in Table 3-3 indicate that $R_{fins} \prec R_{without\ fins}$.

3.4.4 Influence of mesh size

When using numerical techniques such as finite element methods, it is always important to check the influence of mesh size on simulation results in order to choose an appropriate

mesh size. From FEM theory, it is known that the numerical error of a FEM solution reduces by decreasing mesh size. In practice, the choice of the mesh size for the simulation of most real industrial applications (including the ACR) is a compromise between CPU time, memory, available disk space, and the desired accuracy.

In this project, influence of mesh size was first investigated for the case of the tube without fins where analytical solution is available because of the simplified geometry and boundary conditions (Appendix B).

The analytical solution for temperature along the radial direction takes the following form

$$T = \frac{-C_1}{k} lnr + C_2, \tag{3.16}$$

where, C_1 and C_2 are constants of integral presented in Appendix B, k is the thermal conductivity of tube material, and r is the radius of the tube. Figure 3-13 shows the graph of analytical solution of temperature as a function of the radius of the tube without fins. As can be seen, the analytical solution for this range of r can be approximated as a linear solution.

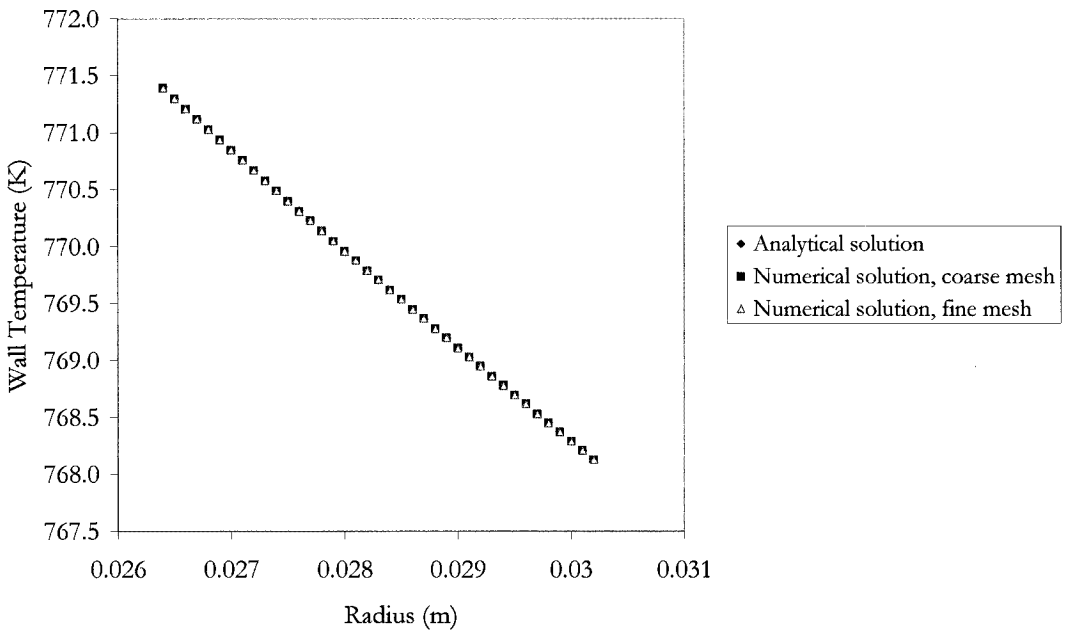

Figure 3-13: Analytical solution of the tube without fins

Analytical solutions are generally useful to study the performance of numerical methods since numerical error can be easily estimated. However, in our case the solution given by equation (3.16) is almost linear and the decrease of the mesh size does not significantly affect the precision of the solution (Figure 3-13). This can be explained by the use of quadratic interpolations for FEM, providing precise solution in the case of quasi-linear problem.

In more complex geometry, such as the tube with fins, the analytical solution is not available and another error criterion must be defined, for example equality of heat flux entering and leaving the exchange surface. Equation (3.17) describes the relative error of heat flux,

$$relative\ \ error = \frac{q_{in} - q_{out}}{q_{average}}. \tag{3.17}$$

Table 3-4 and Table 3-5 present the heat flux for internal and external perimeters for both cases with and without fins. As it was expected, the relative difference between the heat fluxes is very small for the case without fins, while the relative error is significant for the case with fins. It can be noticed that decreasing the mesh size, reduces the relative error of the heat flux at the price of more degrees of freedom. Consequently, by raising the number of equations, the CPU time and the required memory increase.

Table 3-4: Influence of mesh size in the tube without fins

Mesh	No. of elements	Degree of freedom	q_{inside} (W/m)	$q_{outside}$ (W/m)	Relative error
Coarse	188	468	3055,45	3055,12	1,1E-04
Fine	752	1688	3055,72	3055,63	2,9E-05
Finer	3008	6384	3055,83	3055,81	7,9E-06

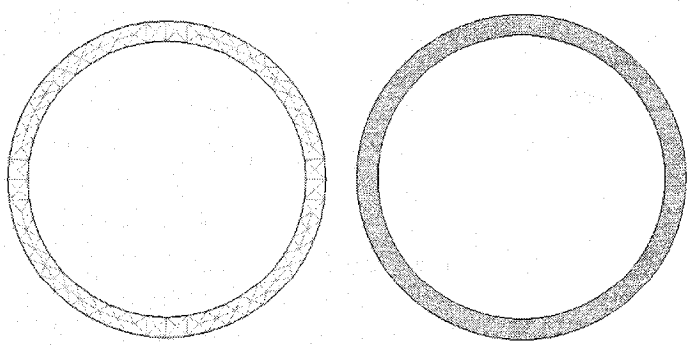

Figure 3-14: Coarse mesh (188 elements) and finer mesh (12032 elements) for tube without fins

Table 3-5: Influence of mesh size in the tube with fins

Mesh	No. of elements	Degree of freedom	q_{inside} (W/m)	$q_{outside}$ (W/m)	Relative error
Coarse	465	1149	4290,62	4584,20	6,60E-02
Fine	1860	4158	4257,87	4407,52	3,50E-02
Finer	7440	15756	4254,87	4337,19	1,90E-02

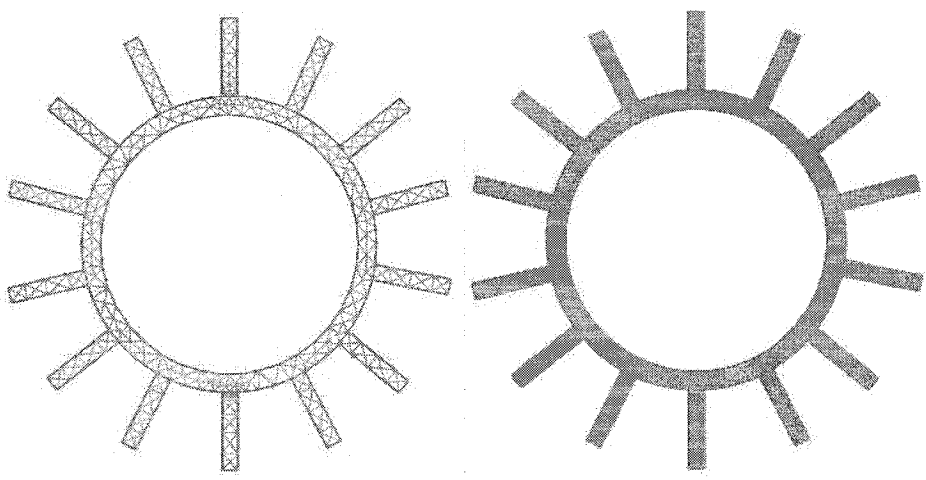

Figure 3-15: Coarse mesh (465 elements) and finer mesh (29760 elements) for tube with fins

3.5 Evaluation of sensitivity of the model to heat transfer parameters

The mathematical models presented in section 3.2 permit us to simulate the heat transfer in the ACR in order to design the insulation thickness and the fin performance. However, these two responses depend also on different parameters such as temperatures, gas velocity, heat transfer coefficients and physical properties. This section is the second step of the ACR modelling where sensitivity of the model was investigated. After choosing the insulation material and estimating the fin performance, it is appropriate to study the sensitivity of the model to different conditions and improve understanding of the thermal sensitivity of the auto-cyclic reactor.

In brief, in previous sections, insulation material and box dimensions were fixed and kept constant while in this section, the response of the ACR to various operating conditions was studied. Moreover, since many correlations were used in the model, it is crucial to know if a small error in correlations produces a big difference in the response of the model. Thus, it is essential to study the sensitivity of the model to the precision of the correlations. Therefore, this section represents the sensitivity of the ACR to heat transfer and the sensitivity of the numerical model to quality of the used correlations.

3.5.1 Influence of different parameters on fin effectiveness

In this section the sensitivity of fin effectiveness to different characterizing parameters was studied. The objective is to verify the influence of thermal conductivity of fin material, inlet gas velocity, inlet and outlet gas temperature, number of fins, and geometry of the fins on

fin effectiveness. For the purpose of simulation, the temperature of the gas at the inlet and at the outlet of the reactor was considered 350°C and 600°C respectively.

3.5.1.1 Thermal conductivity

Thermal conductivity of fin material (stainless steel) can affect the overall heat transfer. Thermal conductivity (k_{ss}) appears in overall heat transfer coefficient (U) which is a combination of convection and conduction defined by

$$U = \frac{1}{R} = \frac{1}{R_{h_{wg1}} + R_k + R_{h_{wg2}}}. \tag{3.18}$$

The overall heat transfer is

$$Q = UA\Delta T_\infty, \tag{3.19}$$

where A is the heat transfer surface. R_{hwg1} and R_{hwg2} are the convection resistance inside and outside of the internal tube, and R_k is the conduction resistance in the tube. It is expected that an increase in thermal conductivity decreases the thermal resistance R_k. Consequently, according to equation (3.18) and (3.19) the overall heat transfer coefficient and heat transfer rate enhance. Thus, higher thermal conductivity of materials leads to higher heat transfer rate. This is illustrated in Figure 3-16. If the material of the fins (stainless steel) was replaced with more conductive materials in Table 3-6, total heat transfer would increase gradually until reaching a constant value. This can be explained by the fact that, when the thermal conductivity tends to a higher value, then the resistance from heat conduction (R_k) tends to a smaller value and the heat transfer is limited by convection on inner and outer surface of the internal tube. Hence, for high conductivity values, increase of thermal conductivity does

not raise significantly the total heat transfer rate since heat transfer is then dominated by convection.

As demonstrated in Figure 3-17, higher thermal conductivity tends to increase fin effectiveness. However, the increase is not very considerable. For instance, if stainless steel is replaced by silver which is 30 times more conducting, the fin effectiveness will be raised only 9% from 1,403 to 1,523.

The curve presented in Figure 3-17 also indicates that there is a value for thermal conductivity for which fin effectiveness asymptotically reaches a constant value. This suggests the use of a material more conductive than stainless steel would improve the performance from heat transfer point of view. The critical value of thermal conductivity in our ACR model is about $k/k_{ss} = 5$ which corresponds to iron. However, from the practical point of view, like corrosion, only stainless steel is suitable for the ACR. Moreover, using very high thermal conductivity material is unnecessary since the overall heat transfer is dominated by convection coefficients. Thus, no further improvement in fin effectiveness is obtained when increasing the thermal conductivity by more than an order of magnitude.

It should also be noted that the precision of thermal conductivity correlations may influence the calculated fin effectiveness (Figure 3-17), but this effect is relatively small.

Table 3-6 : Thermal conductivity of different materials

	Thermal conductivity(W/m.K) (T=273K)	k/k_{ss}
Stainless steel 304	14,9	1
Titanium (100%)	21,9	1,5
Lead (100%)	35,2	2,4
Platinum (100%)	71,6	4,8
Iron (100%)	80,2	5,4
Nickel (100%)	90,7	6,1
Zinc (100%)	116	7,8
Gold (100%)	317	21,3
Aluminium (100%)	373	25
Copper (100%)	401	27
Silver (100%)	429	29

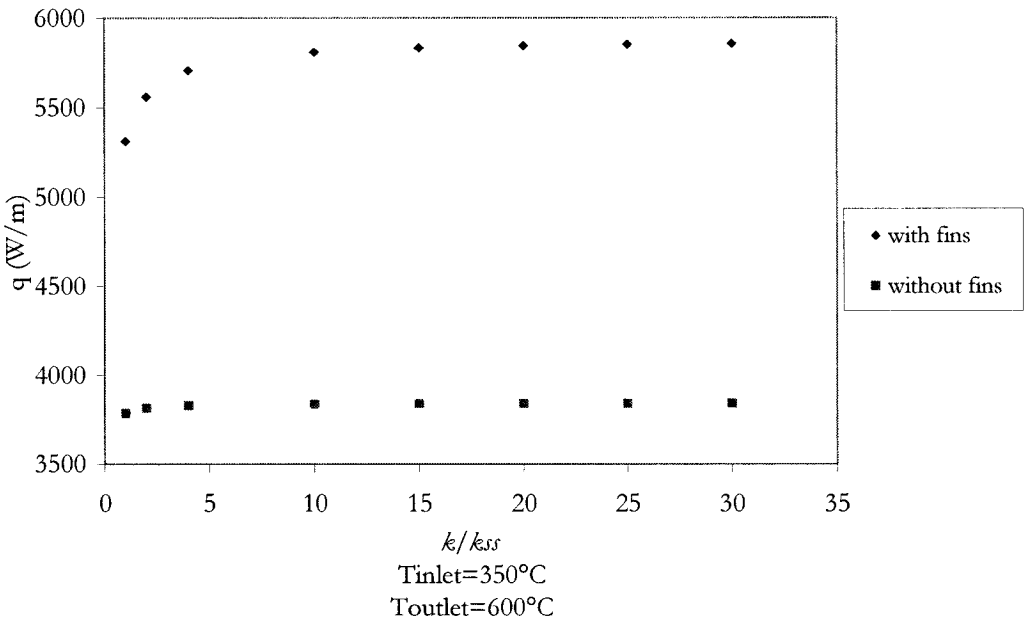

Figure 3-16: Influence of thermal conductivity on total heat transfer

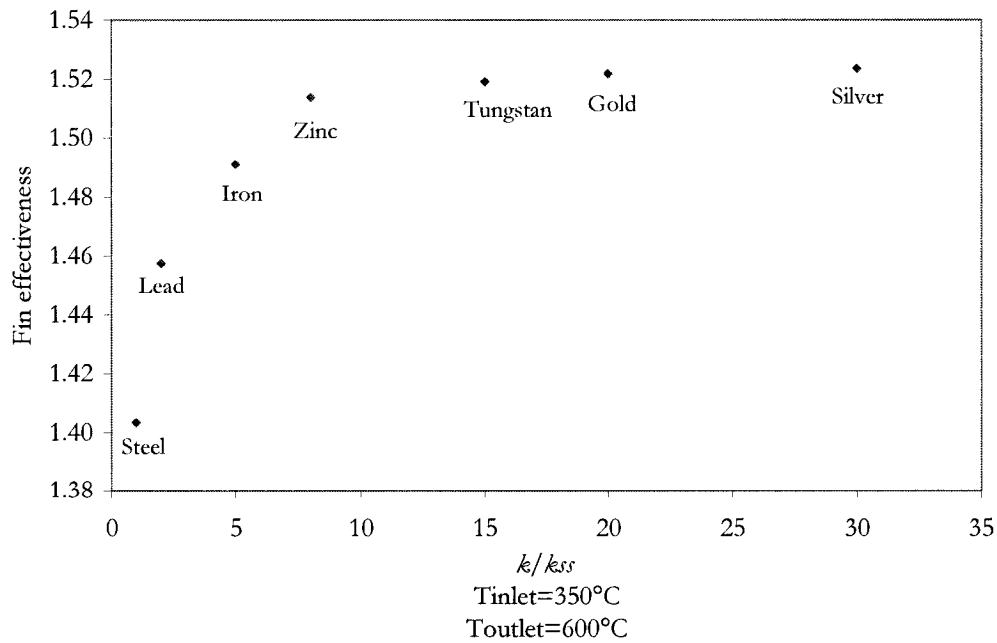

Figure 3-17: Influence of thermal conductivity on fin effectiveness

3.5.1.2 Inlet gas velocity

The variation of inlet gas velocity affects Reynolds number, thus heat transfer coefficients on the inner and outer surface of the internal tube are influenced. By increasing inlet gas velocity, convection heat transfer coefficients increase with $h \propto v^{0,8}$ (equation (3.8) and Figure 3-18). Hence, the terms containing convection resistance (R_{lmg1} and R_{lmg2}) in equation (3.18) decrease and conduction resistance becomes more important. Thus, total heat transfer from the internal tube towards annulus is expected to increase at higher inlet gas velocity. This behavior is illustrated in Figure 3-18 and Figure 3-19.

Conversely, the fin effectiveness reduces when convection coefficients increase. In fact, extending the heat transfer surface by fins is useful to decrease convection resistance, but on the other hand, the presence of fins involves more material, which tends to increase the conduction resistance R_k. According to these results, the fins are most efficient when the convection resistance is dominant since it increases the surface without increasing too much the conduction resistance. In short, when the value of heat transfer coefficients is large, as it is with fluids with high velocity, the conduction resistance becomes dominant so in this case the presence of fins produces a reduction in overall heat transfer coefficient and in fin effectiveness as well.

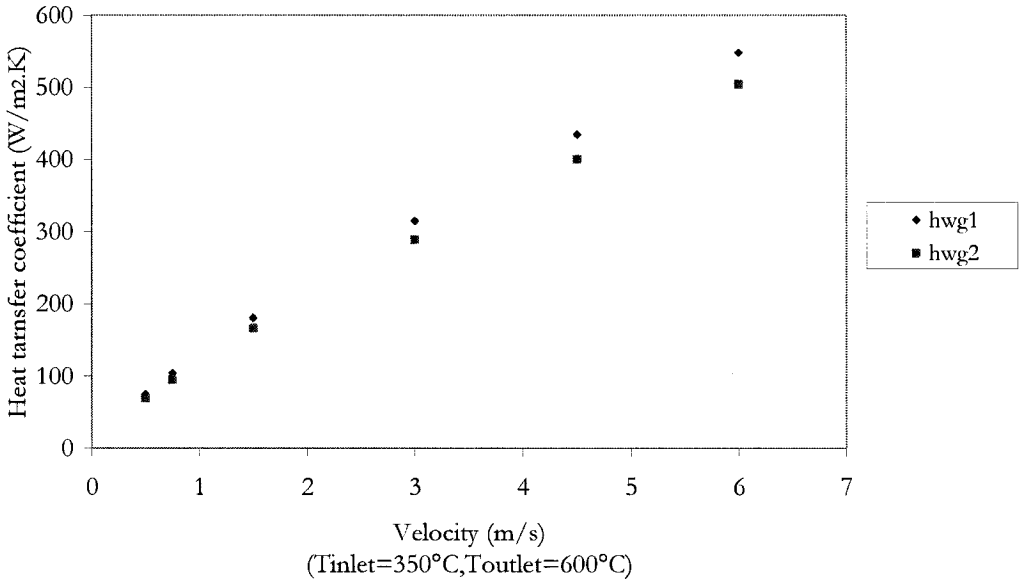

Figure 3-18: Heat transfer coefficients vs. inlet gas velocity

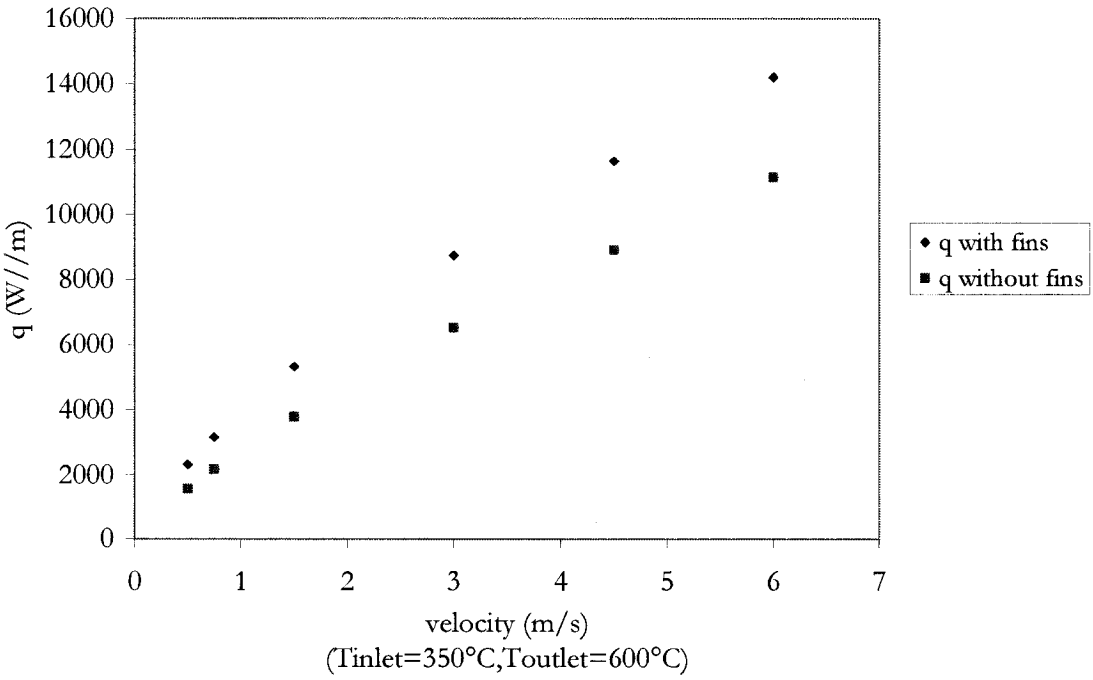

Figure 3-19: Influence of inlet gas velocity on total heat transfer

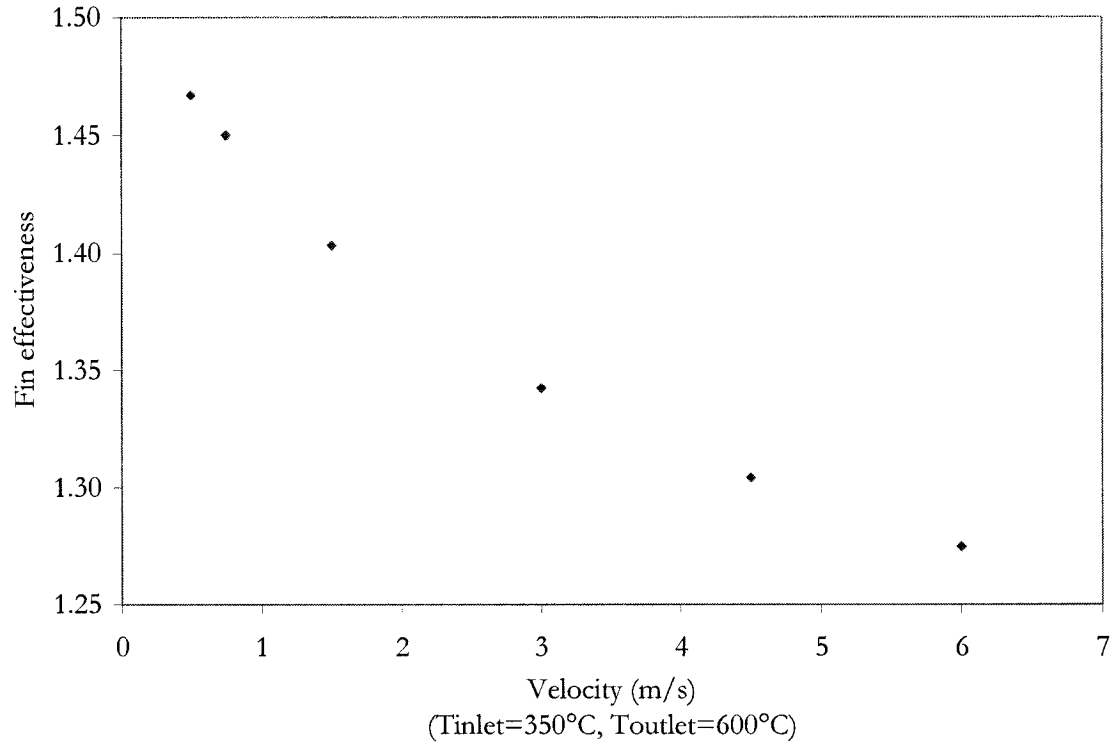

Figure 3-20: Influence of inlet gas velocity on fin effectiveness

3.5.1.3 Inlet and outlet gas temperature

The temperature of the entrance gas of the reactor is variable depending on acceleration of the NG engine, and the distance of the ACR from this engine. Thus, the sensitivity of fin effectiveness to different entrance gas temperature was studied in this work.

Both inlet and outlet temperatures of the reactor affect the physical properties of gas. Similarly, the convection heat transfer coefficient which is function of physical properties varies (see equation (3.8)). Moreover, the temperature gradient between inlet and outlet gas temperatures has a direct effect on total heat transfer (see equations (3.13) and (3.14)).

If the temperature of inlet gas changes from 250°C to 550°C with constant outlet temperature T_{outlet}=600°C, the convection heat transfer coefficient on the outer surface of the inner tube increases. Therefore it is expected that the overall heat transfer coefficient rises as shown in Figure 3-21.

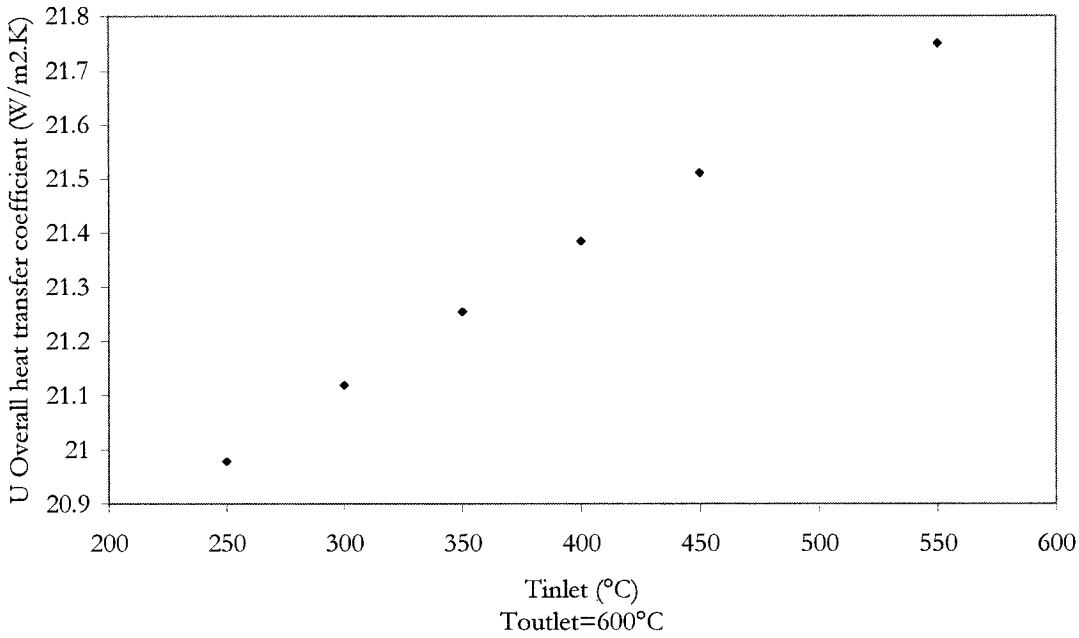

Figure 3-21: Overall heat transfer coefficient vs. inlet gas temperature

Conversely, as presented in Figure 3-22 and Figure 3-23, the overall heat transfer and fins performance are reduced by increasing inlet gas temperature. This phenomenon can be explained by the influence of temperature gradient on total heat transfer between the inlet and outlet gas of the reactor. As the temperature gradient decreases, it reduces the heat transfer and the fin effectiveness.

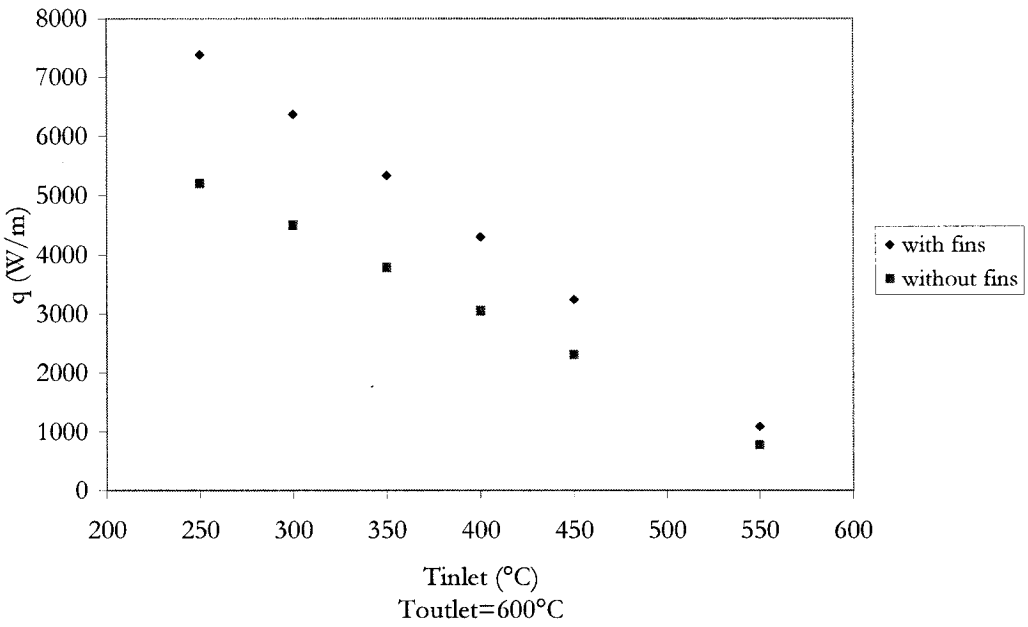

Figure 3-22: Influence of inlet gas temperature on total heat transfer

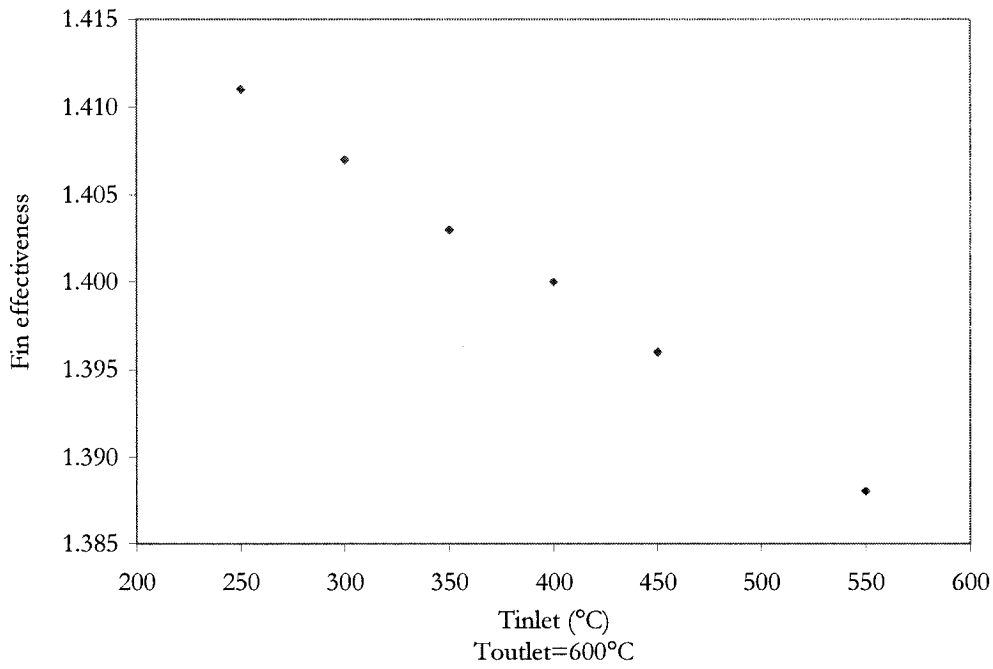

Figure 3-23: Influence of variation of inlet temperature on fin effectiveness

The outlet temperature of the reactor depends on the temperature of the inlet gas, the methane concentration, and the rate of conversion in the reactor. However, regardless the methane concentration, if the temperature of the outlet gas increases from 400°C to 650°C with constant inlet gas temperature T_{inlet}=350°C, the heat transfer coefficients in the outer and inner compartments, the overall heat transfer, and fin effectiveness raise as well. When the outlet temperature rises, there is a greater temperature gradient in the system, thus more heat is transferred and fin effectiveness is enhanced.

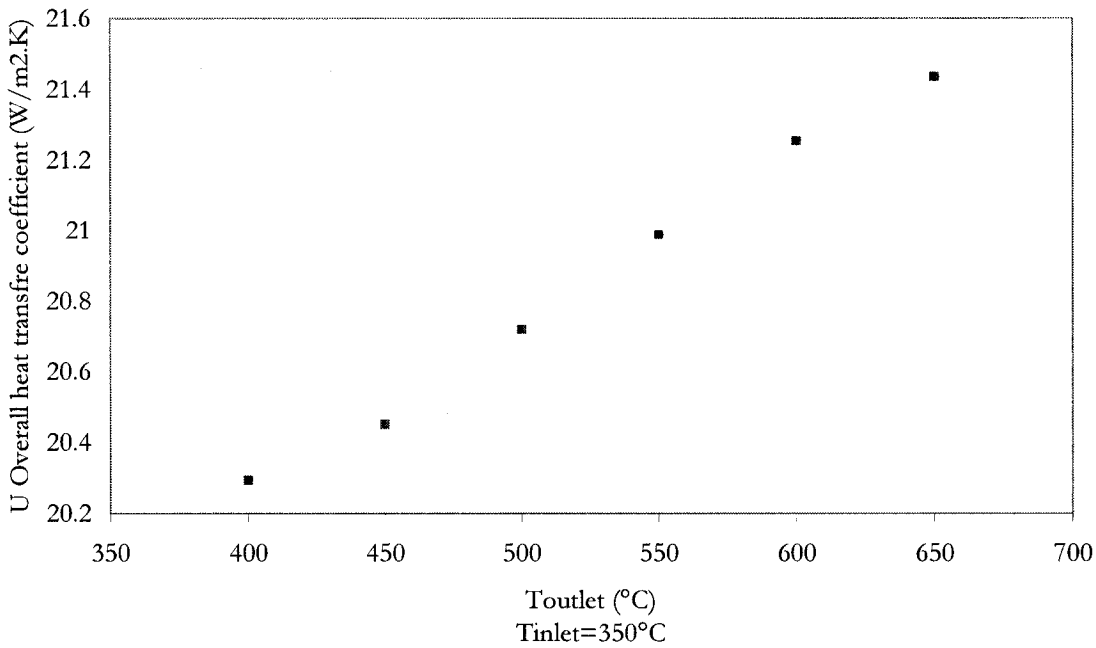

Figure 3-24: Overall heat transfer coefficient vs. outlet gas temperature

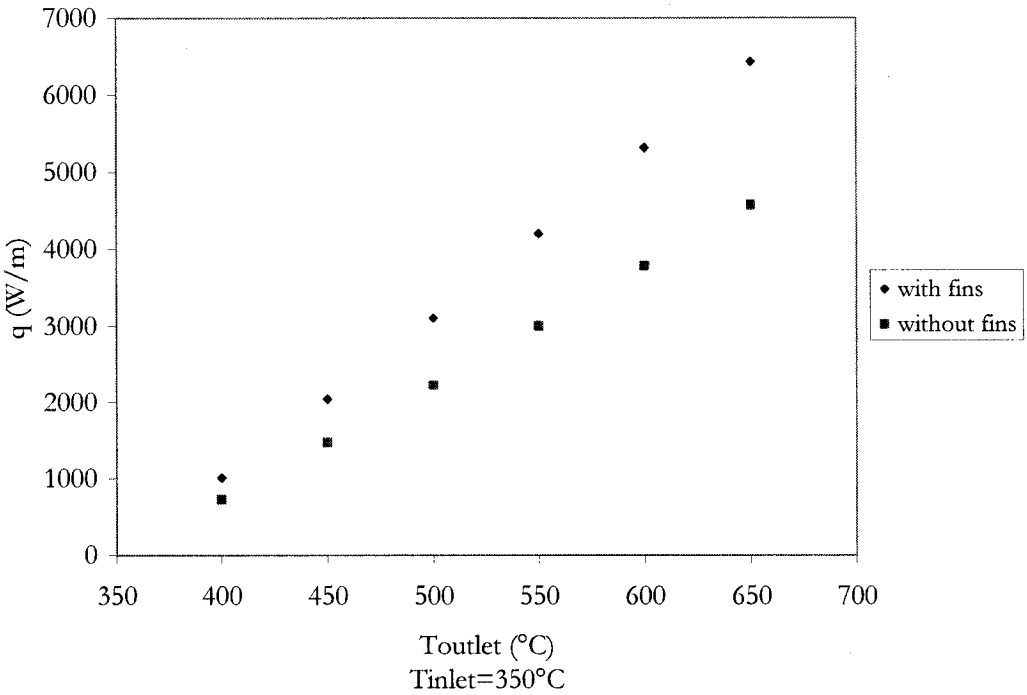

Figure 3-25: Influence of outlet gas temperature on total heat transfer

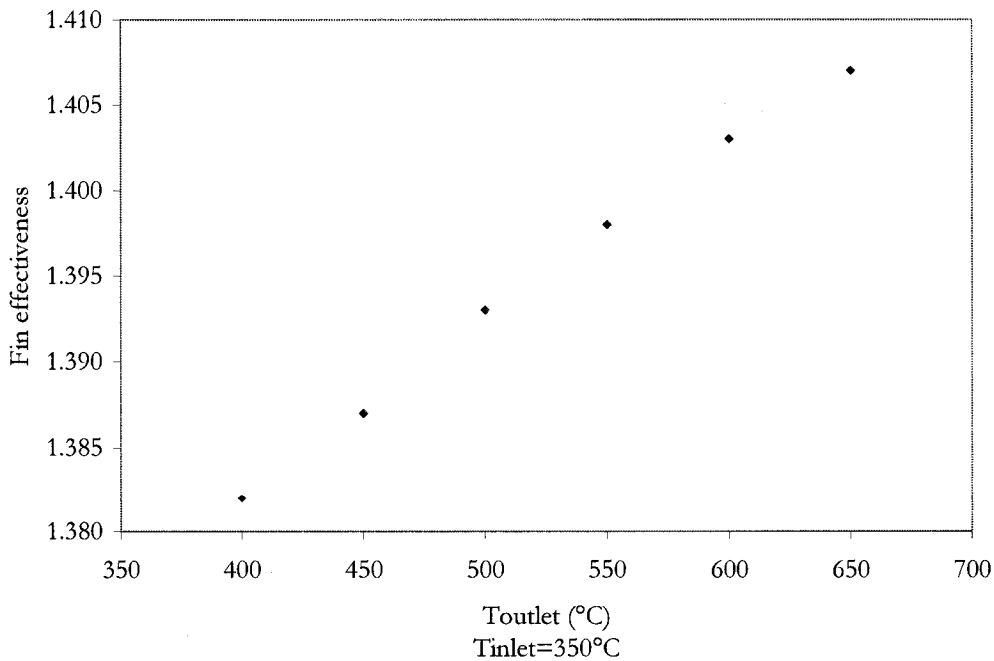

Figure 3-26: Influence of variation of outlet temperature on fin effectiveness

3.5.1.4 Number of fins

In this section the effect of the number of fins was studied by keeping the same geometry of the fin. An increase of around 9% of fin effectiveness was observed by increasing the number of fins from 8 to 14. However, by doubling the number of fins from 14 to 28, there is only 12% of raise on fin effectiveness as shown in Table 3-7. In this table, A_f and A_w indicate the heat transfer surface with fins and without fins respectively while U_f and U_w present the overall heat transfer coefficient with fins and without fins.

Table 3-7: Influence of number of fins on fin effectiveness

No. of fins	Fin effectiveness	A_f/A_w	U_f/U_w
8	1,28	2,32	0,55
14	1,40	3,37	0,42
28	1,57	5,68	0,28

By raising the number of fins, the exchange heat transfer surface increases and the total heat transfer is expected to increase. However, if conduction in the fins is the limiting thermal resistance of the overall heat transfer, the augmentation of total heat transfer can be limited by conduction thermal resistance. In fact, the results of Table 3-7 indicate that an augmentation of number of fins results in augmentation of exchange surface A_f/ A_w while there is a diminution of U_f/U_w from the thermal resistance of the fins.

On the other hand, the increase of the number of fins would result in the reduction of the space for the pellets and also of the cross-sectional area for flowing gas. Thus, the choice of a number of 14 fins recommended by the constructor seems to be a good compromise.

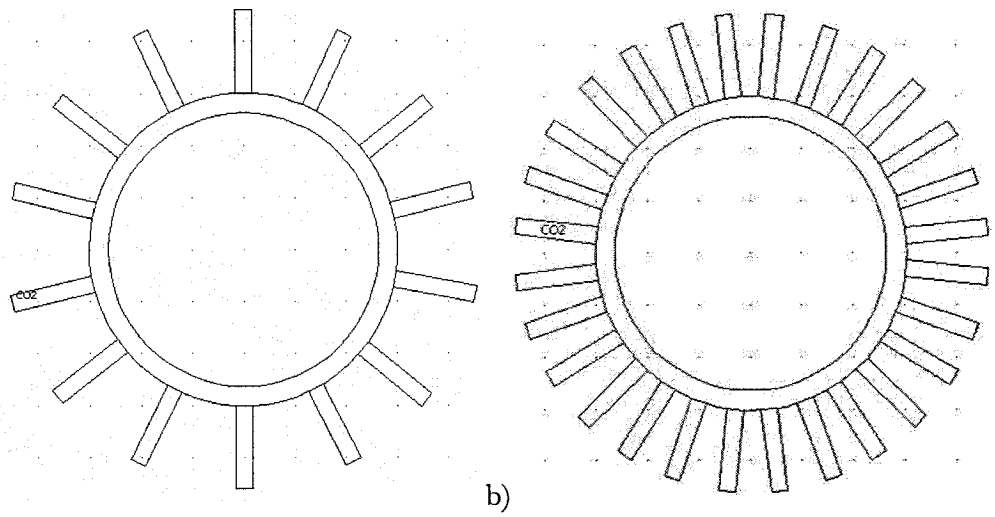

a) b)

Figure 3-27: Variation of number of fins a) 14 fins, b) 28 fins

3.5.1.5 Geometry of fins

The geometry of fins has an influence on heat transfer surface and fins performance. The thickness and the height of the fins are 0,32 cm and 1,6 cm respectively. If the fins were thinner (t=0,32/2 cm) or shorter (L=1,3 cm), the fin effectiveness would decrease because of smaller heat transfer surface.

Table 3-8: Influence of fin dimension on fin effectiveness

Fins dimensions (cm)	Fin effectiveness	A_f/A_w	U_f/U_w
Real Dimensions (L=1,6, t=0,32)	1,40	3,37	0,42
Thinner (L=1,6, t=0,16)	1,36	3,32	0,41
Shorter (L=1,3, t=0,32)	1,37	2,74	0,50

Furthermore, if the geometry of the fins changes from rectangular profile to triangular profile, the fin effectiveness decreases because of the same reason.

Table 3-9: Influence of different type of fin on fin effectiveness

Fin type	Fin effectiveness	A_f/A_w	U_f/U_w
Rectangular(14 fins)	1,40	3,37	0,42
Triangular(14 fins)	1,37	3,11	0,44

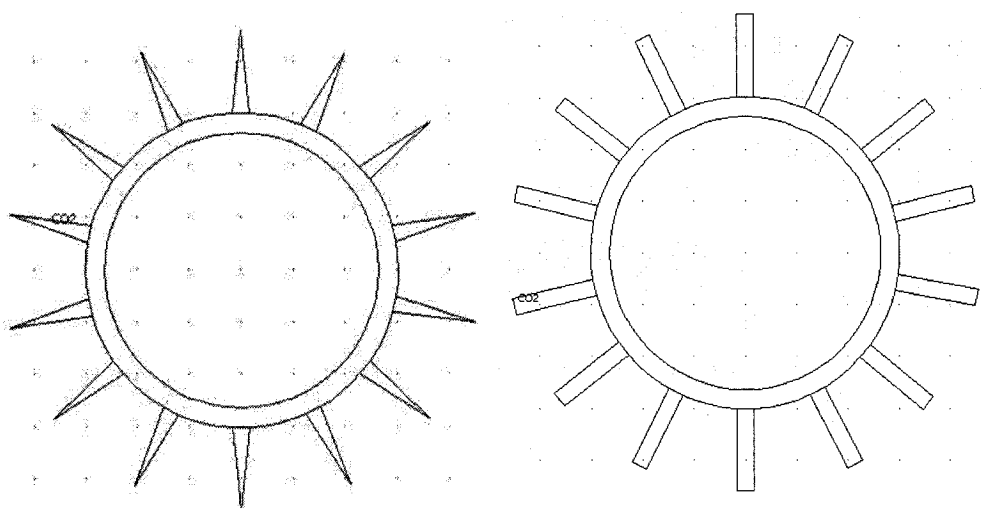

Figure 3-28: Triangular and rectangular fin geometry

3.5.2 Influence of different parameters on insulation thickness

In this section the sensitivity of insulation thickness to different parameters was studied. As it was mentioned before, the inside temperature of the reactor was considered constant in calculation of insulation thickness. Therefore, there are two thermal resistances in this case; one is heat transferred by conduction in insulation material (R_k), and the other one is heat transferred by convection on the surface of the box with ambient air (R_h). The overall heat transfer is defined by

$$Q = U A (T_{inside} - T_\infty), \tag{3.20}$$

where U is the overall heat transfer coefficient. Using the resistance analogy, one can expressed U as

$$U = \frac{1}{R} = \frac{1}{R_k + R_h}. \tag{3.21}$$

The objective is to find the sensitivity of the insulation thickness to the following parameters:

- insulation material,
- maximum inside temperature in the reactor,
- ambient temperature.

Note that for all of these cases, the reasonable temperature for the surface of the metallic box was desired to be 60-65°C.

3.5.2.1 Thermal conductivity

In theory, lower thermal conductivity of insulation material leads to thinner insulation layer around the reactor and smaller box dimensions. This is demonstrated in Figure 3-4 and Table 3-2. Indeed, reducing the thermal conductivity increases the thermal resistance R_k, thus smaller overall heat transfer coefficient is obtained which leads to lower total heat loss of the ACR.

Different insulation materials, listed in Table 3-2, were examined and the smallest insulation thickness was estimated around 15 cm for the reasonable surface temperature using the Kaowool bulk fiber. Figure 3-29 depicts the insulation thickness of materials versus thermal conductivity at 500°C.

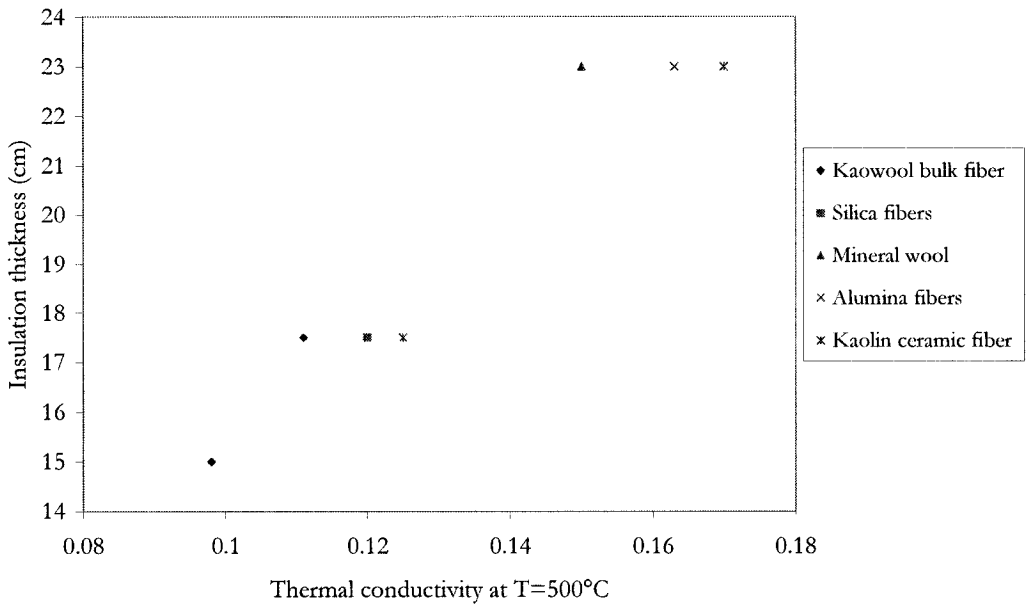

Figure 3-29: Influence of thermal conductivity of insulation materials on insulation thickness

3.5.2.2 Maximum inside temperature of reactor

For the intended application, the temperature of the reactor is not expected to exceed 550°C. However, for security reasons, an upper limit of 600°C for temperature was considered for simulations. By this assumption, the length side of the box was estimated as 40 cm for a maximum surface temperature of 60-65°C on upper and side walls. In this section the variation of maximum inside temperature of the reactor on box dimensions was investigated and results are summarized in Table 3-10. As expected, by lowering the temperature inside the reactor, the size of the box reduces along with the total heat transferred.

Table 3-10: Influence of inside temperature of reactor on box dimension

T_{inside}(°C)	Box side length(cm)	Heat loss (W)
650	45	122
600	40	114
550	35	108

Alternatively, the influence of inside temperature of the reactor on surface temperature of the box was studied with keeping the box dimension as 40×40 cm. By decreasing the maximum temperature inside the reactor, the maximum temperature on the side walls of the box reduces as depicted in Figure 3-30.

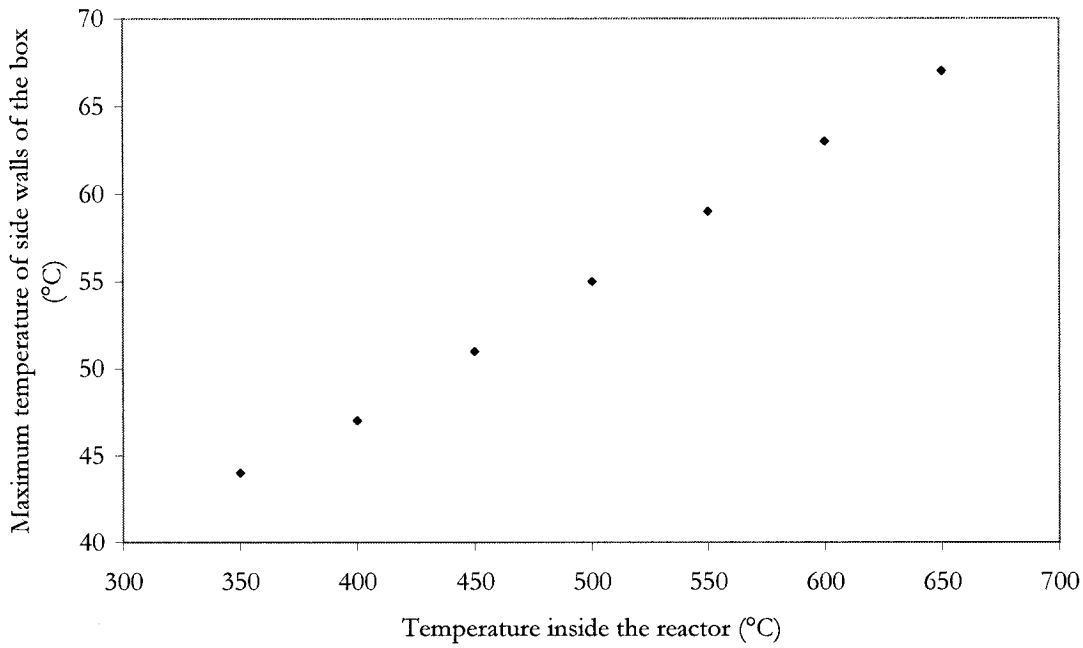

Figure 3-30: Influence of inside temperature of the reactor on temperature of side walls of the box

3.5.2.3 Tube and annulus diameter

By decreasing the diameter of the tube and annulus compartments of the ACR, the box side length reduces as shown in Table 3-11. It is obvious that by decreasing the dimension of the reactor, the whole size of the system becomes smaller.

Table 3-11: Influence of tube and annulus diameter on insulation thickness

d_annulus(cm)	12,7	10,16
d_tube(cm)	8,89	5,25
box side length(cm)	45	40

3.5.2.4 Ambient temperature

In general, the ambient temperature is considered 25°C. However, it is interesting to study the variation of ambient temperature and observe the response of the model. As it is shown in Table 3-12, by increasing the ambient temperature, the box side length would need to be larger in order to maintain the reasonable temperatures on side walls (60-65°C).

Table 3-12: Influence of ambient temperature on insulation thickness

$T_{ambient}$(°C)	box side length(cm)
30	45
25	40
20	35

Furthermore, if the ambient temperature changes for any reason in the laboratory, the temperature on side walls of the box varies. If the ambient temperature rises, the temperature on side walls of the reactor gets higher as illustrated in Figure 3-31.

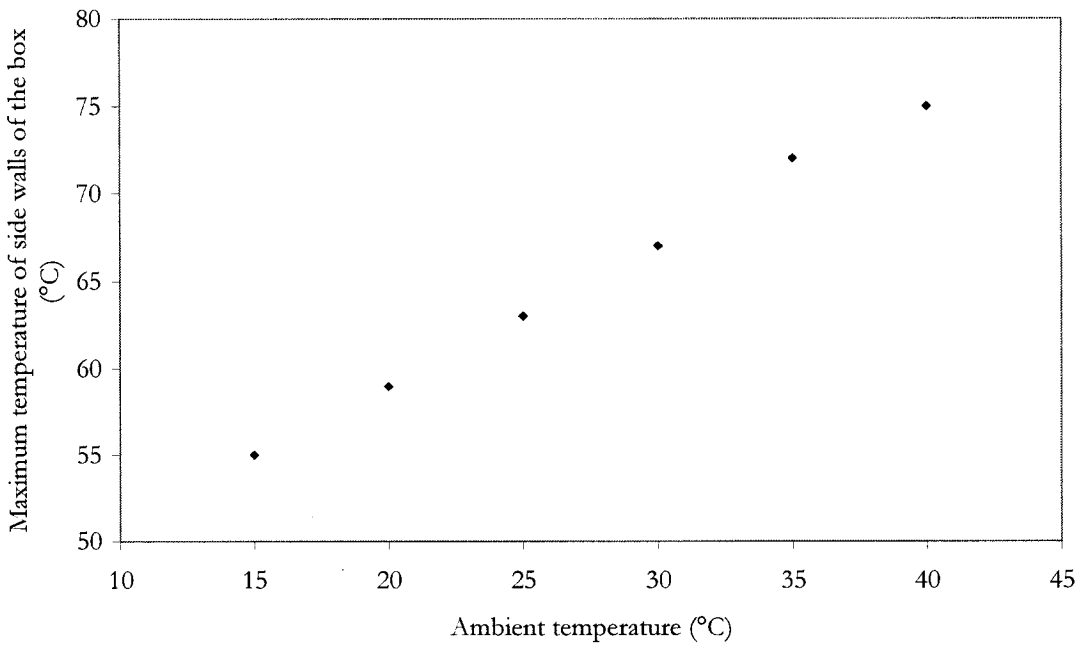

Figure 3-31: Influence of ambient temperature on temperature of side walls of the box 40×40 cm

3.6 Summary

Chapter 3 presented the mathematical model for estimating the insulation thickness and fin effectiveness using software FEMLAB based on finite element method. Kaowool bulk fiber (ρ =256 kg/m^3) was chosen to insulate the reactor enclosed it in a metallic box, with cross sectional dimensions estimated as 40×40 cm for the reactor and 35×35 cm for the pre-heater. The overall heat loss from the reactor and the pre-heater was calculated to be 114 W and 60 W respectively. Fin performance is limited by both the conduction and convection resistance of heat transfer. If the inlet and outlet gas temperatures are considered 350°C and 400°C respectively, the fin effectiveness is estimated as 1,4.

Sensitivity study indicates that by increasing the thermal conductivity, the fin performance increases. Furthermore, there is a condition under which extending the surfaces does not significantly improve the heat transfer. This condition happens with high velocity fluids that results in large convection heat transfer coefficients. Thus, the conduction resistance could become dominant and fin effectiveness decreases by adding more surfaces. Thus, if the gas enters the reactor with high velocity, the fin effectiveness reduces.

Additionally, the quality of the used correlations to estimate the fin effectiveness is considerable but not very significant. However, there is a linear variation between the insulation thickness to insulation thermal conductivity, maximum inside temperature of the reactor, and ambient temperature and insulation thickness is sensitive to these parameters.

CHAPTER 4 Experiments with ACR pilot unit

4.1 Experimental set-up

The ACR pilot unit, occupying an area of 1,5 m×1,5 m, was constructed in the laboratory in spring 2006. As depicted in Figure 0-1 the overall experimental set-up consists of 5 sections. Section (1) is the reactor where the chemical reactions take place. The ACR was wrapped with Kaowool fiber and installed in a metallic box with dimensions 40×40×70 cm. The gas mixture enters first the electrical pre-heater (section (2)) to be heated up to a desired temperature in a typical range of exhaust emissions from NG engines. The pre-heater was also wrapped with Kaowool fiber and placed in a metallic box with dimensions 35×35×40 cm. The feed gas composition simulating the emissions from NG engines was adjusted by mixing in appropriate proportion of compressed air, carbon dioxide, and methane using three mass flow meters (section (3)). Water was added to the gas mixture by water pump (LMI Milton Roy, Model A741) (section (4)). Finally, gas chromatograph (Perkin-Elmer, Sigma 300) (section (5)) was used to monitor methane concentration in the inlet and the outlet gas of the reactor.

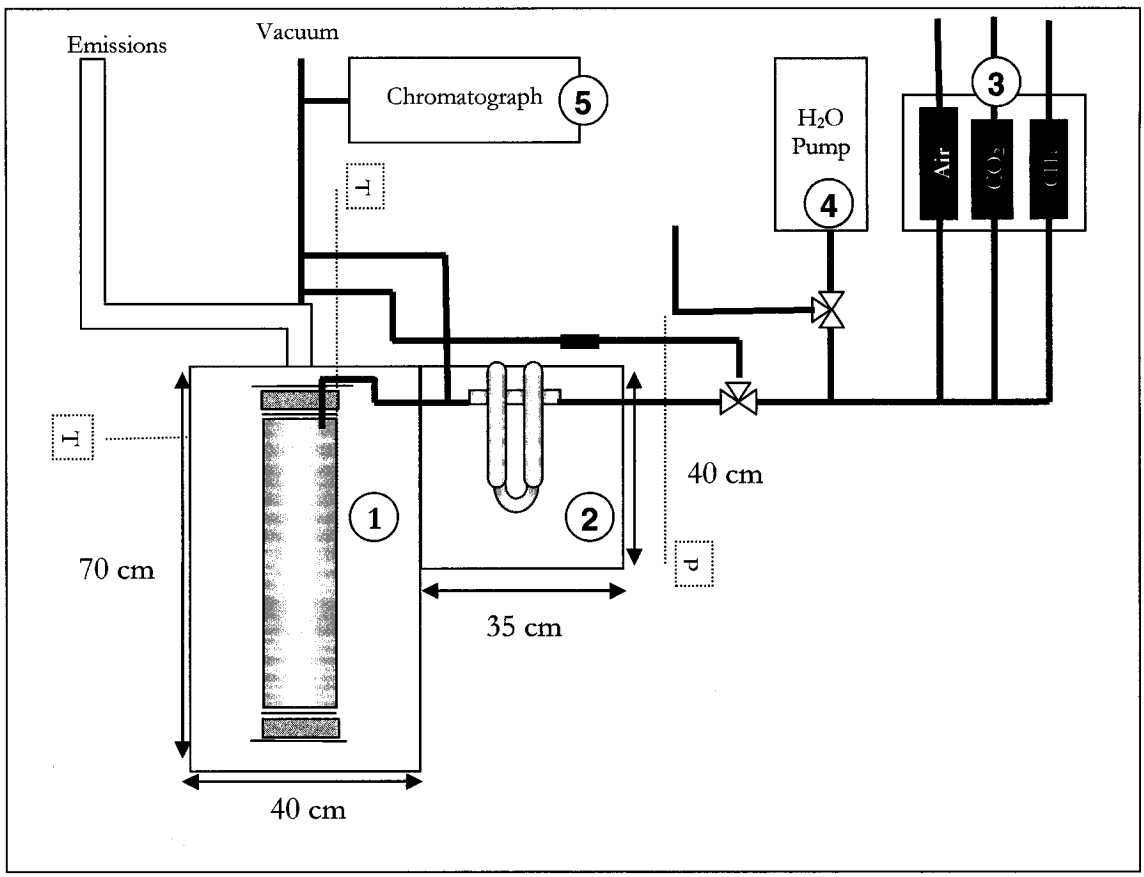

Figure 4-1: Schematic of the ACR experimental set-up 1) ACR, 2) Electrical pre-heater, 3) Gas supply, 4) Water pump, 5)Gas chromatograph

Figure 4-2 shows the reactor, the Kaowool bulk fiber, the metallic box and the fifteen K-type thermocouples. Figure 4-3 presents the dimensions of the reactor made of AISI 304 stainless steel. Figure 4-4 presents the internal tube of the ACR with fourteen fins in order to improve the heat transfer between the outlet of the reactor and entrance.

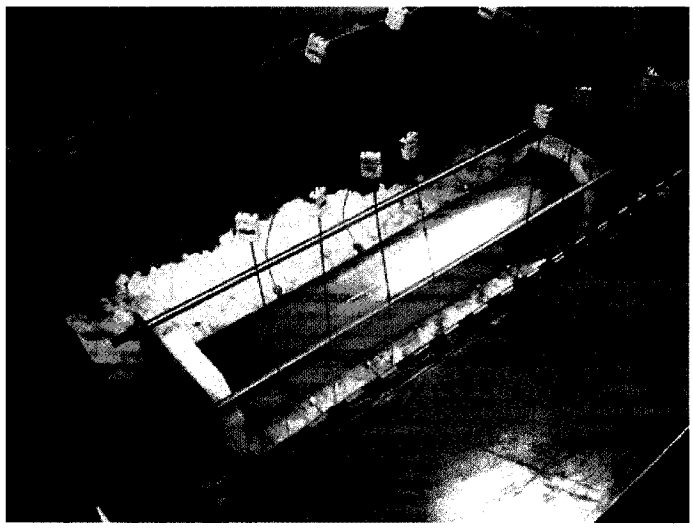

Figure 4-2: ACR with insulation and thermocouples in the metallic box

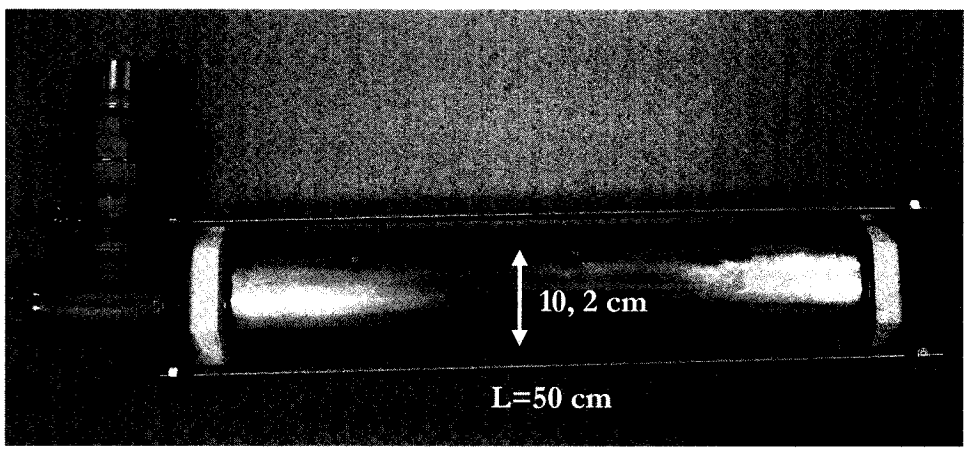

Figure 4-3: Complete ACR

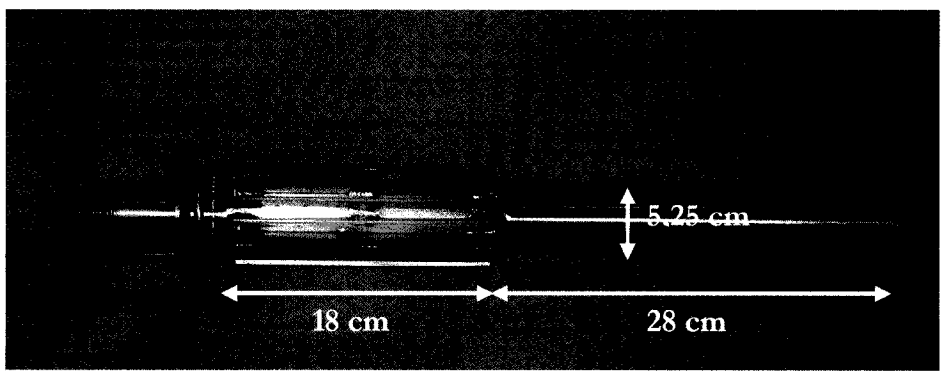

Figure 4-4: Inner tube of the ACR with fins

The space between the fins in the annular tube and cylindrical tube were filled with 3 mm catalyst pellets shown in Figure 4-5. The 0,9% Pd/Al_2O_3 pellets were prepared by enriching the commercial PC263 catalyst with 0,7% Pd as mentioned in section 2.1.1.

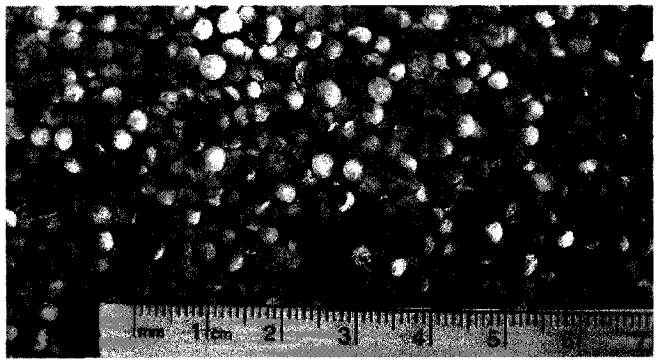

Figure 4-5: Catalyst pellets after impregnation and calcination (0,9% Pd/Al_2O_3)

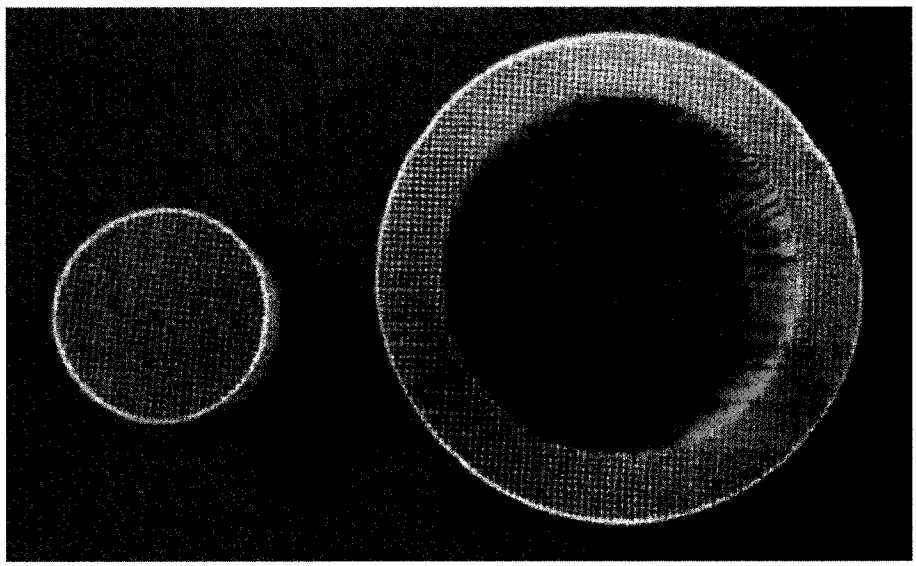

Figure 4-6: Monoliths before impregnation and calcinations (400CPSI)

The other part of the annular and cylindrical tube of the reactor was filled with six pieces of alumina cordierite monolith (400CPSI) (bare shown in Figure 4-6). The monolith pieces

were coated with γ-alumina (9±1%) and impregnated with 1,2±0,05% PdO as explained in section 2.1.1.

It was crucial to assemble the reactor in the way that the gas passes through the pellets and monoliths uniformly. This was simple and direct for the pellet section. However, for the monolith section, because of its fixed structure, it was more complex to make sure that the gas mixture passes exactly through the monoliths and the monoliths are concentric. Thus, to position correctly the monoliths, a space of 4 mm between the monolith and the reactor walls was tightly filled with Kaowool fiber as shown in Figure 4-7. The Kaowool fiber used in this section was impregnated with PdO and calcinated similar to the catalysts to avoid un-reacted gas slippage.

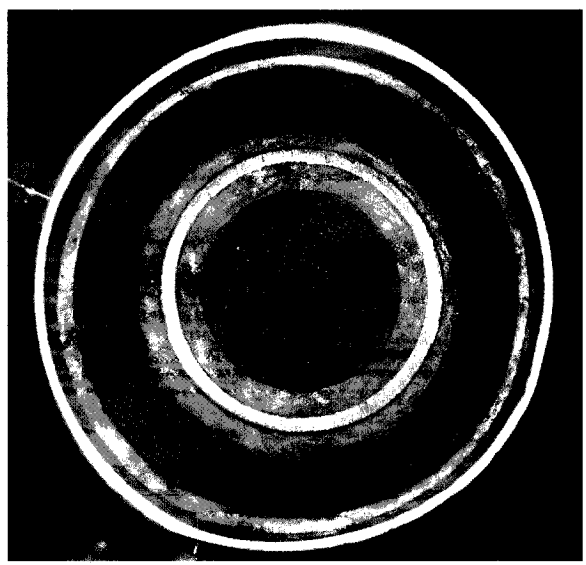

Figure 4-7: Monolith section in ACR

The entrance gas flow rate to the reactor was mostly adjusted to 140 L/min which corresponds to one tenth scale-down of real average flow rate of NG engines of a bus. Desired gas mixture was obtained by selecting appropriate flow rate of individual components (air, CH_4, CO_2). When water was needed, it was injected at the appropriate rate by water pump. Selected experimental gas composition (without methane) is shown in Table 4-1 where it is compared with published exhaust composition. For practical reasons the high O_2 concentration was accepted as a reasonable compromise. In addition, concentration of methane varied between 500 to 3000 ppm.

Table 4-1: The inlet gas composition of the ACR

	Selected laboratory composition	Published Ando *et al.* [26]
CO_2	7,32%	7,32%
H_2O	13,37%	13,37%
N_2	62,66%	73,71%
O_2	16,66%	5,6%

However, initial ACR performance evaluation was carried out with air containing methane (500-3000 ppm).

To monitor the temperatures along the reactor, the ACR was equipped with 15 K-type thermocouples as illustrated in Figure 4-8. There is one thermocouple in the entrance of the reactor (T_{in}), five thermocouples are inserted in the fins section (T_1-T_5), six thermocouples

are situated in the annular part of the monolith section (T_6-T_{11}), two are in the internal pellet section (T_{12}-T_{13}), and one in the outlet of the reactor (T_{out}).

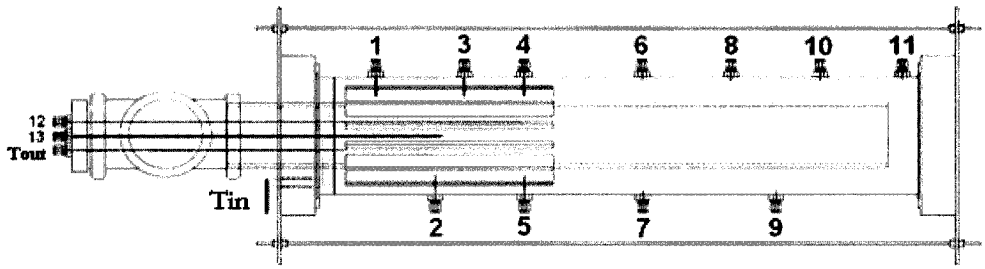

Figure 4-8: Position of 15 thermocouples in the ACR

4.2 Pre-heater operation

As mentioned before, the actual pre-heater consists of four electrical elements 1070 W each, housed individually in a tube where the gas mixture is admitted. To reach the desired temperature of the gas mixture the power of the first and the second element is fixed by Labview application, while the power of the third and the fourth element is regulated using the temperature difference between the required temperature and the measured temperature in the entrance of the reactor. Thus, when the measured temperature is lower than the required temperature, the power of the third and the fourth elements increases in order to reach the required entrance temperature and vice versa. It takes a relatively long time before the required temperature is attained. Example of the pre-heater operation strategy is given in Table 4-2.

Table 4-2: Pre-heater operation (strategy)

ACR entrance required temperature	*Flow [L/min]*	*Total power [%]*	*Time[1] [min]*
350 °C	100	20	40
	120	25	45
	140	30	45
400 °C	100	25	45
	120	30	50
	140	35	50
450 °C	100	30	45
	120	35	50
	140	40	55
500 °C	100	35	50
	120	40	55
	140	45	55
550 °C	100	40	50
	120	45	55
	140	50	55

4.3 Adiabatic temperature rise

The adiabatic temperature is the maximum temperature rise in the reactor for different concentration of fuel when the conversion is complete and there is no heat loss with the exterior of the system. In order to determine the temperature region for the reactor operation, it is useful to make a plot of adiabatic temperature rise as a function of fuel content. The adiabatic temperature is given by

$$\Delta T_{adiabatic} = \frac{-\Delta H_R Y_{CH4}}{Cp}. \tag{4.1}$$

For methane combustion ΔH_R and Cp are considered -802.7 kJ/mol and 32 J/mol.K respectively. Figure 4-9 shows the adiabatic temperature rise for methane combustion with

[1] Time to reach the required temperature

different methane concentrations. For instance, when the concentration of methane is 2000 ppm, the maximum temperature rise in the reactor could be 52°C.

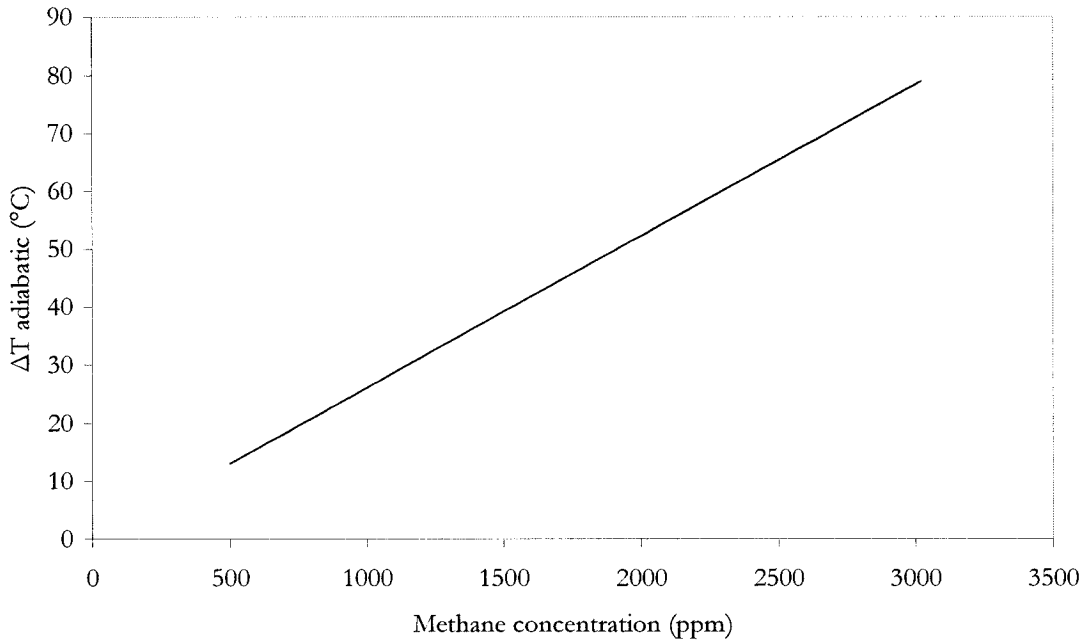

Figure 4-9: Adiabatic temperature rise of methane combustion

4.4 Initial ACR performance evaluation

Several sets of experiments were executed in the laboratory to study the performance of the ACR. For technical reasons the initial ACR performance evaluation was restricted to combustion of methane in air, but under a wide range of inlet temperatures (300 to 450°C) and methane concentration (0,05 to 0,3%), mostly at 140 L/min. Complete evaluation under conditions closely simulating the exhaust gases from the NG engines, conducted by M. Zanoletti, was outside the scope of this thesis.

4.4.1 Time to heat the ACR and light off

As a first step, it was of interest to determine the time it takes to heat the reactor under a selected inlet temperature to a steady state both under air (i.e. without combustion) and in the presence of methane. Two sets of experiments involving monitoring the temperature from the onset of heating until an apparent steady state at a selected inlet temperature was attained. One set covered T_{inlet} = 350°C, the other T_{inlet} = 400°C. In each set the temperature profiles for heating only with flowing air are compared with those obtained when heating under a flow of 0,2% methane in air. By comparing the profiles for heating by hot air with those for heating in the presence of methane, the temperature of light-off and the time it took to be reached were determined for the case of each temperature.

Figure 4-10 and Figure 4-11 show the temperature profiles for these two experiments for the four first thermocouples. The temperatures of 15 thermocouples in transient are presented in Appendix C. When heating the reactor from 25°C to 350°C or 400°C by feeding the 2000 ppm methane in air, the reaction does not initiate immediately because of the low temperature. The reaction starts (lights off) only when a sufficiently high temperature is attained. In these experiments the time needed to attain the reaction was measured. From Figure 4-10 and Figure 4-11 after about 30 minutes, the graph of methane leaves the graph of air, which corresponds to the beginning of the reaction in the reactor.

Furthermore, the reaction in the reactor appears by an increase in temperature. From the graph in Appendix C it was observed that the highest temperature in the reactor, i.e 380°C

when T_{inlet} = 350°C and 430°C when T_{inlet}=400°C, was located at the thermocouple T_2. This indicates that the reaction zone is located in the pellets section between the fins in annular part. Moreover, it can be observed from Figure 4-10 that the temperature of T_2 increases from 332°C (with air) to 380°C (with methane) and in Figure 4-11 T_2 raises from 383 (with air) to 430 (with methane) which indicates the maximum temperature rise of around 50°C. Moreover, no methane was detected in the outlet, indicating a complete conversion. As it was shown in Figure 4-9, $\Delta T_{adiabatic}$ is 52°C for 2000 ppm of methane.

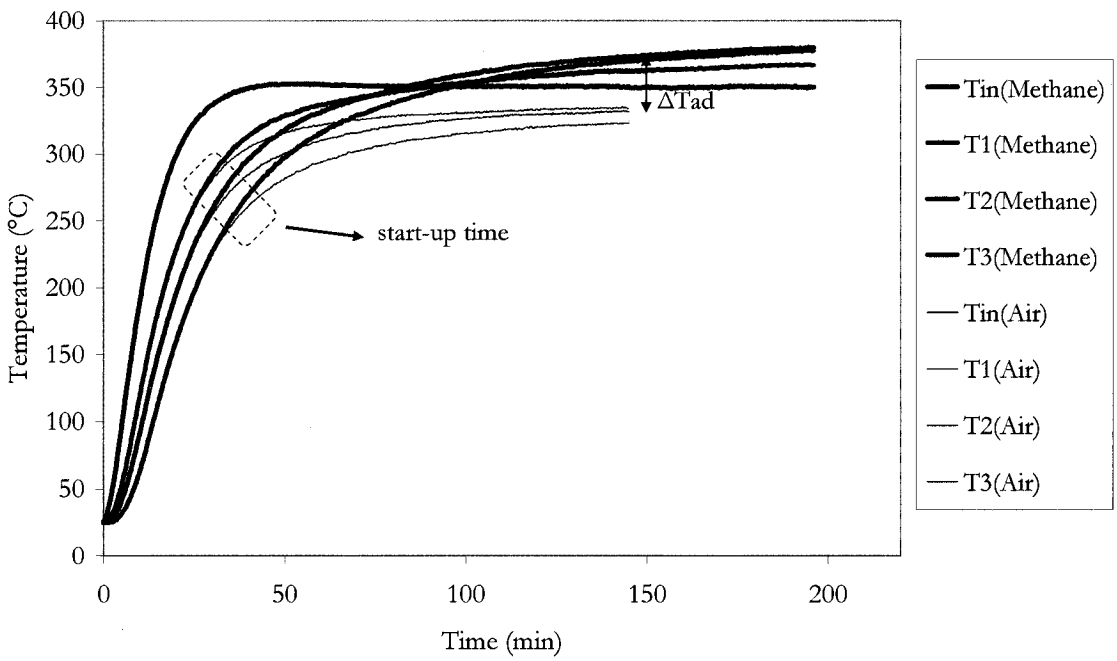

Figure 4-10: Temperature profiles in the ACR as a function of time; T_{inlet} =350°C, 0.2% methane/air

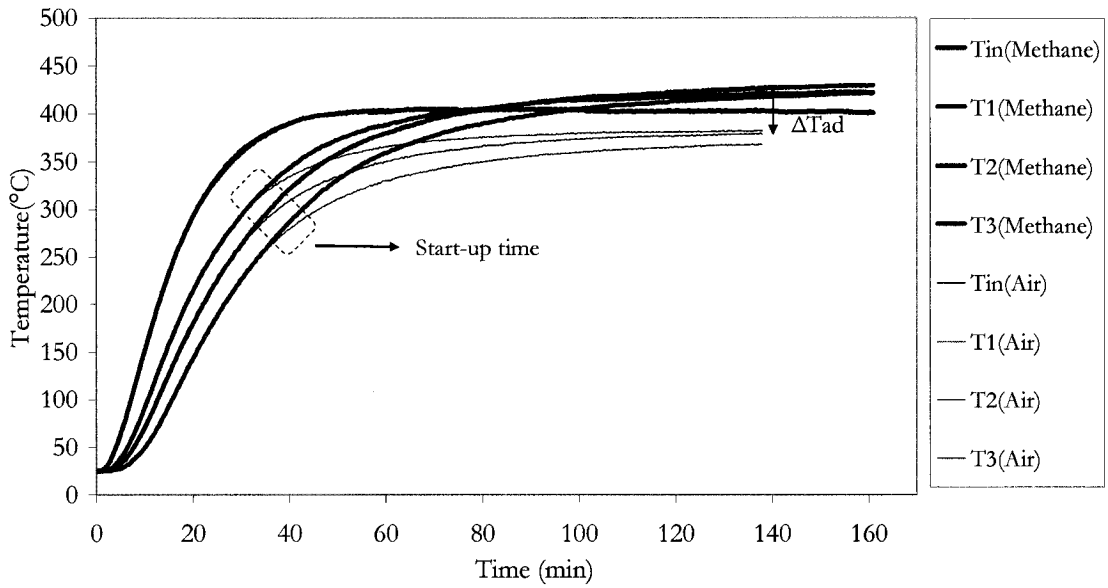

Figure 4-11: Temperature profiles in the ACR as a function of time; T_{inlet}=400°C, 0.2% methane/air

4.4.2 Steady-state temperature profile

The steady state temperature profile in the reactor is illustrated in Figure 4-12 for T_{inlet}=400°C with 2000 ppm (0,2%) of methane in air. There is a rise of temperature on T_2 (between fins-pellets section) which indicates the zone of reaction, then the temperature declines but increases again on T_{13} (internal tube-pellets section). Notice that the position of the maximum temperature in the internal tube (T_{13}) corresponds to the position where there is the maximum temperature in the annular tube (T_2).

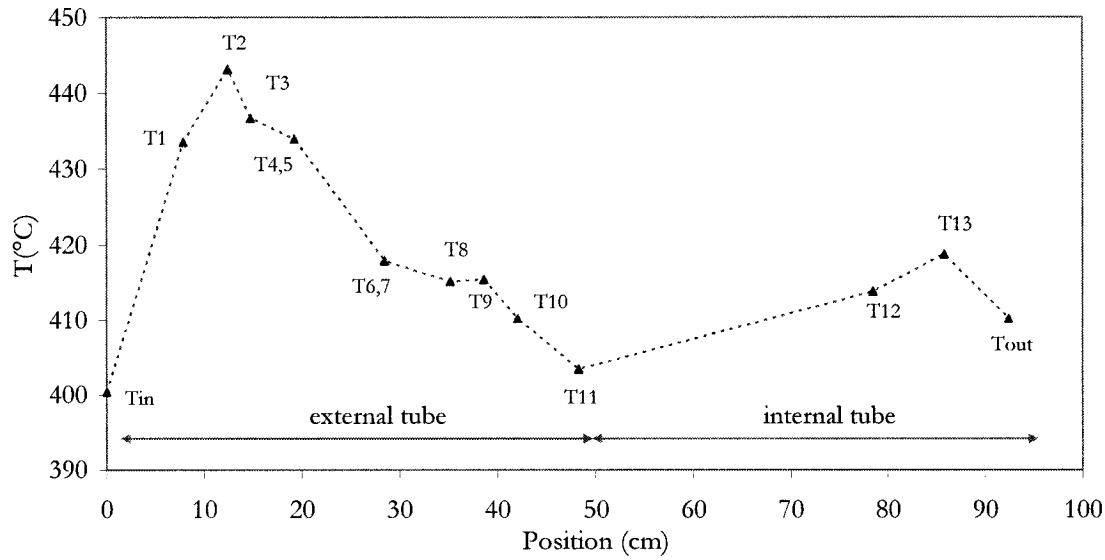

Figure 4-12: Steady-state temperature profiles in the ACR measured after 4-5 hours for 0.2% methane/air flowing at 140 L/min, T_{inlet}=400°C

4.4.3 Response to inlet temperature change

Another experiment was performed to study the response of the reactor to the decrease of inlet gas temperature from 350°C to 300°C with concentration of 2000 ppm of methane and flow rate of 140 L/min. The reactor responded fast to the decrease in temperature, although it took more than two hours to reach a new steady-state (Figure 4-13). Furthermore, as depicted in Figure 4-14 the position of the front (the hottest point) moves along the ACR axis from T_2 to T_4 and T_5.

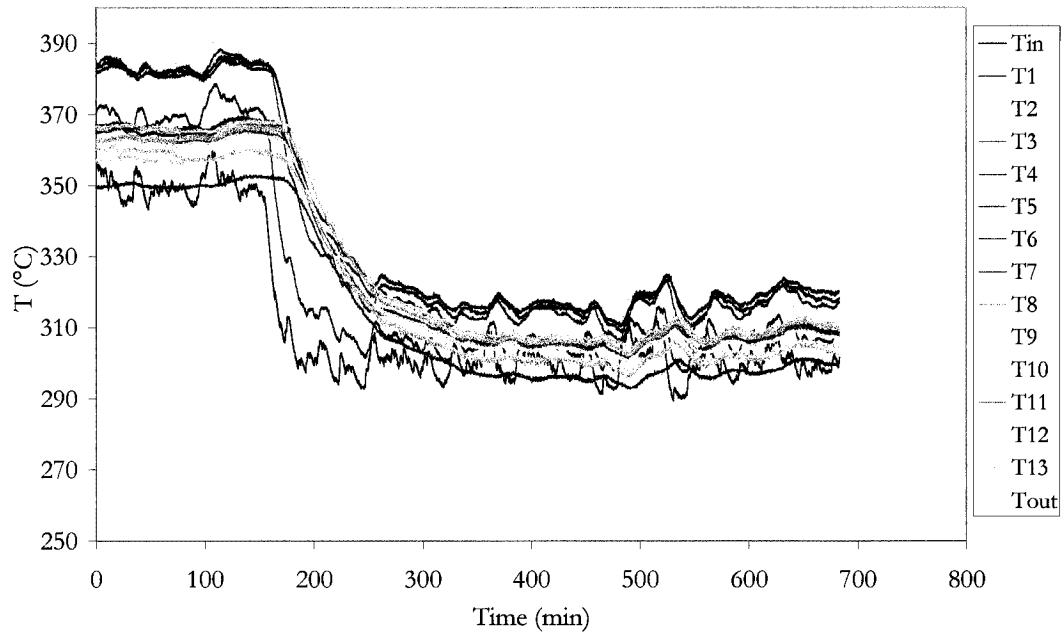

Figure 4-13: The response of the ACR to the decrease in the feed temperature of 0.2% methane/air, flowing at 140 L/min

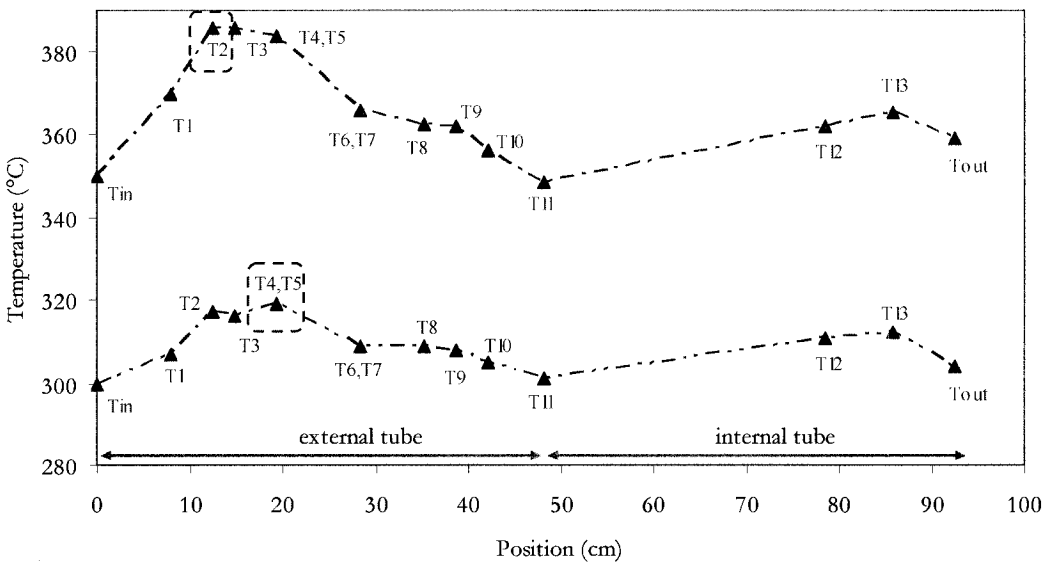

Figure 4-14: Steady-state temperature profile versus position for the entrance temperature change, 0.2% methane/air, flowing at 140 L/min

4.4.4 Conversion as a function of inlet conditions

Maximum methane removal, i.e. high methane conversion is the main requirement for the efficient ACR operation. To delimit the conditions under which acceptable conversion is achieved, a series of experiments was carried out in which the inlet conditions were varied and the response of the ACR was monitored. In addition to the temperature profiles, the conversion of inlet methane concentration was determined when an apparent steady-state was reached, typically after 4-5 h. The inlet temperature was varied from 250 to 500°C for four different methane inlet concentrations: 500, 1000, 2000, and 3000 ppm.

Conversion is a measurement of the amount of reactants that participated in the reaction. The definition of the conversion is

$$X = \frac{C_{CH4\_in} - C_{CH4\_out}}{C_{CH4\_in}}, \tag{4.2}$$

where C_{CH4_in} and C_{CH4_out} are the concentration of methane in inlet and outlet flow of the reactor respectively. To obtain the conversion of the reaction, the concentration of methane in inlet and outlet flow of the ACR is required.

Figure 4-15 presents the experimental results obtained for the methane conversion in the ACR as a function of inlet methane concentration and inlet gas temperature. Results indicate that above an inlet temperature of 350°C the reaction is almost complete for all methane concentrations. Just below this temperature, the conversion is still relatively high, but the reaction will be extinguished more rapidly.

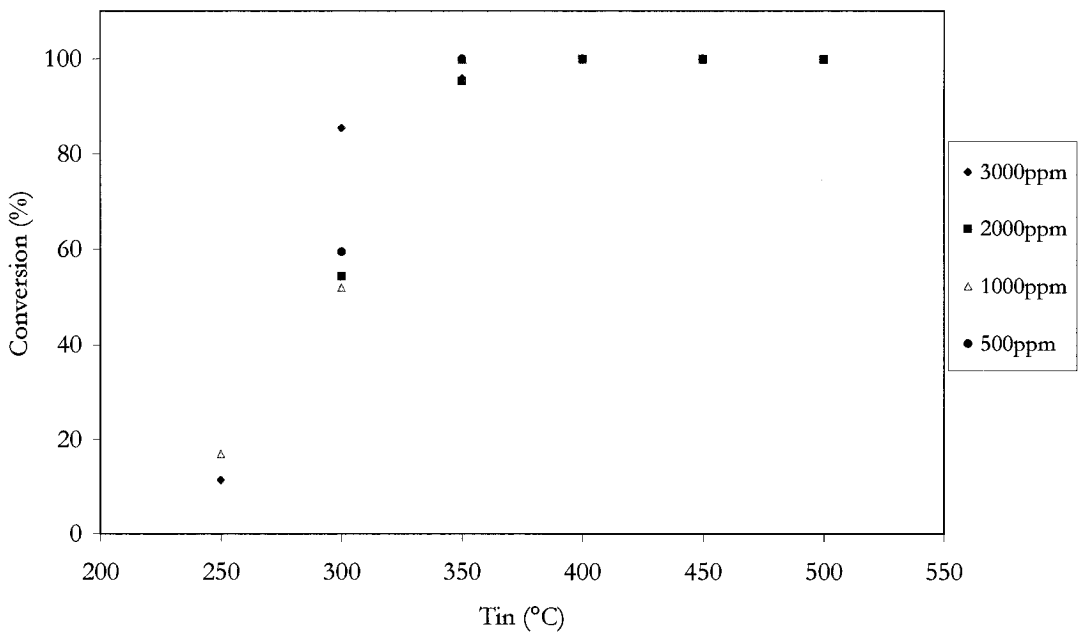

Figure 4-15: Conversion of methane in the ACR as a function of inlet temperature for different inlet methane in air concentrations; 140 L/min

It is also interesting to compare the outlet temperature as a function of the inlet temperature and methane concentration. As seen in Figure 4-16 the higher the concentration of methane, the higher is the outlet temperature of the reactor. Moreover, when the inlet concentration of methane is high, there is more heat of reaction which increases the conversion and leads to higher temperature in the outlet of the ACR. Figure 4-17 presents the maximum temperature inside the reactor as a function of inlet temperature and methane concentration as well. The maximum temperature is mostly located in pellets section between the fins in annular tube.

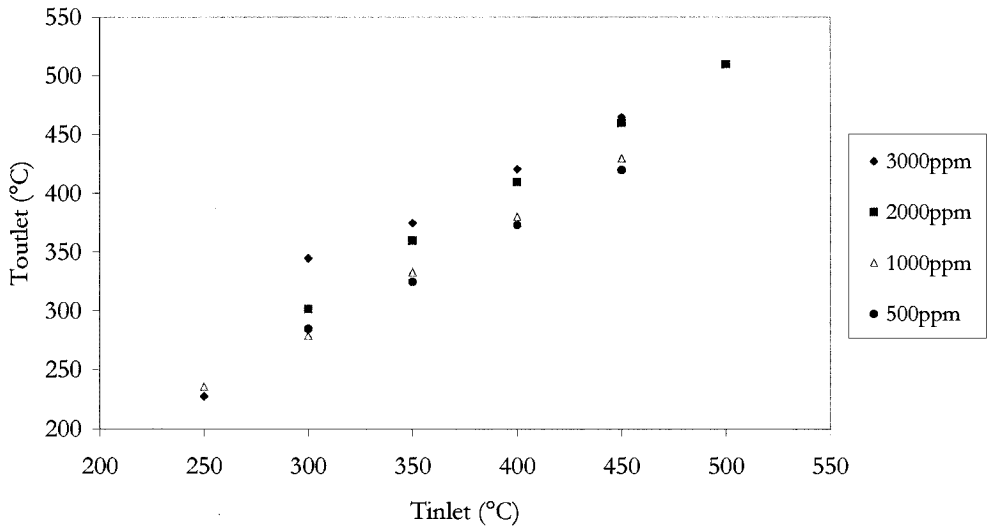

Figure 4-16: Outlet temperature from the ACR versus inlet temperature for different methane concentration

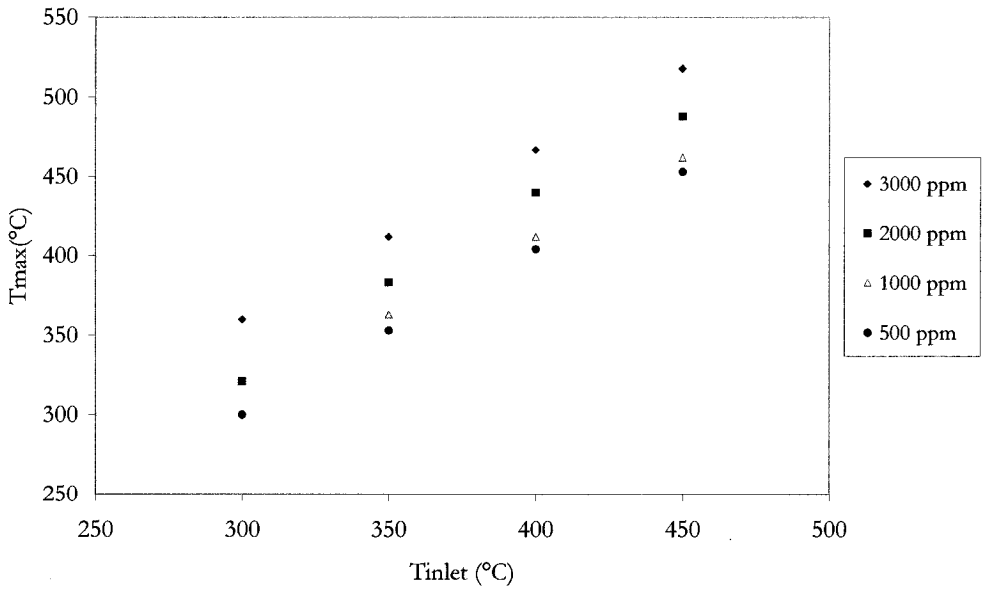

Figure 4-17: Maximum temperature inside the ACR versus inlet temperature for different methane concentration

In Figure 4-15 and Figure 4-16, it is interesting to notice that for T_{inlet}=300°C the conversion and the outlet temperature vary significantly according to concentration. First, it can be observed that higher conversion is obtained for 3000 ppm, because there is more heat generated by the reaction, which promotes reaction and leads to an increase of the conversion and the outlet temperature. Thus, higher concentration of methane results in higher outlet temperature and tends to increase conversion.

However, the conversion at 500 ppm of methane is higher than the conversion of 1000 ppm or 2000 ppm of methane. At low concentration of methane, there is, in proportion, more catalyst surface available for the reaction and that results to a higher conversion at 500 ppm. In other words, for a given quantity of catalyst there is a maximum of methane that can react and that can correspond to a higher conversion at low concentration. Moreover, methane combustion produces CO_2 and H_2O, which are considered as inhibitors to the reaction. So at high concentration, production of these inhibitors can also contribute to limit the conversion.

4.4.5 Heat loss estimation

In order to estimate the heat loss from the reactor at a flow rate Q =140 L/min, two sets of experiments were performed; one was without methane, and the others were with different concentrations of methane. Heat loss was estimated by applying energy balance and using

the measurements of temperature of gas flowing into the reactor given by the thermocouples as well as methane concentration determined by GC analysis. These temperatures corresponded to apparent steady state, i.e. when no measurable temperature variation was observed for about 30 min.

4.4.5.1 Heat loss without methane combustion

To estimate the heat loss from the reactor with air flow, energy balance equation for the case of air flowing at constant mass flow is given by

$$\mathcal{Q}_{loss} = \mathcal{Q}_{inlet} - \mathcal{Q}_{outlet}, \tag{4.3}$$

with

$$\mathcal{Q}_{inlet} = \dot{m} Cp_{inlet} T_{inlet}, \tag{4.4}$$

$$\mathcal{Q}_{outlet} = \dot{m} Cp_{outlet} T_{outlet}, \tag{4.5}$$

where Cp_{inlet} and Cp_{outlet} are the heat capacities of flowing gas at inlet and outlet temperature computed using correlations for air, given in Appendix A. The mass flow rate of air, denoted by $\dot{m}$, is obtained by

$$\dot{m} = \rho \, \mathrm{Q}, \tag{4.6}$$

where Q is the volumetric flow rate of the gas (140 L/min) and ρ is the gas density at atmospheric pressure and ambient temperature obtained from the ideal gas law

$$\rho = \frac{PM}{R_g T}, \tag{4.7}$$

with M as molecular mass of air (28,09 g/mol) and R_g as universal gas constant (R_g=8,314 J/mol.K). At atmospheric pressure and ambient temperature (25°C), density of air (ρ) computed by equation (4.7) is 1,15 kg/m^3, giving a mass flow rate ($\dot{m}$) of 0,00277 kg/s. Thus, for a given inlet temperature (T_{inlet}) of gas (air) entering the reactor the heat loss (Q_{loss}) was estimated by measuring the corresponding outlet gas temperature and solving equations (4.3) to (4.5).

Table 4-3 presents the results of heat loss calculated for these experimentally determined inlet and corresponding outlet temperatures.

Table 4-3: Heat loss from the reactor without methane, Q=140 L/min

T_{inlet}(°C)	T_{outlet}(°C)	Heat loss (W)
350	308	128
400	348	163
450	390	192

As expected, outlet temperature and the corresponding heat loss are almost proportional to the inlet temperature. So, when inlet temperature of air increases, then outlet temperature and total heat loss are higher.

4.4.5.2 Heat loss with methane combustion

When methane is present, heat generated by its combustion, Q_{gen}, has to be added to the energy balance equation, thus

$$Q_{loss} = Q_{inlet} - Q_{outlet} + Q_{gen} \tag{4.8}$$

where Q_{inlet} and Q_{outlet} are the same as equations (4.4) and (4.5) respectively. The heat generation Q_{gen} is given by

$$Q_{gen} = X \Delta H_R \dot{F}_{CH_4}, \tag{4.9}$$

where ΔH_R is heat of reaction (ΔH_R =802,7 KJ/mol), X is conversion measured experimentally from the results of GC analysis as presented in section 4.4.4. The molar flow rate of methane $\dot{F}_{CH_4}$ (mol/s) is computed using the ideal gas law at atmospheric pressure and ambient temperature of 25°C,

$$\dot{F}_{CH_4} = \frac{P\dot{V}_{CH_4}}{R_g T}, \tag{4.10}$$

where $\dot{V}_{CH_4}$ is the volume flow rate of methane defined as the product of the methane concentration C_{CH4} (ppm) and the volume flow rate of gas (140 L/min),

$$\dot{V}_{CH_4} = C_{CH_4} Q. \tag{4.11}$$

In the case of methane combustion the estimation of the heat loss necessitates the temperature of inlet and outlet gas, but also the information about the methane concentration of these streams. Hence, the heat loss with methane combustion was estimated experimentally for selected temperatures and compositions of inlet gas, by measuring the temperature and the concentration of (outlet) gas leaving the reactor when an apparently steady state was observed. By using these data, heat loss was obtained by using equation (4.8) to (4.11)

Experimental results of heat loss at various temperatures and various methane concentrations of inlet gas are summarized in Table 4-4.

Table 4-4: Heat loss from the reactor with methane

CH_4 (ppm)	T_{inlet} (°C)	T_{outlet} (°C)	Heat loss (W)
3000	350	375	143
	400	421	163
	450	465	181
2000	350	360	115
	400	410	121
	450	460	121
1000	350	333	129
	400	380	140
	450	430	141
500	350	325	115
	400	373	123
	450	420	135

As expected, the higher the temperature and methane concentration, the higher is the heat loss from the system.

By comparing the heat loss values obtained experimentally (Table 4-3 and Table 4-4) with the heat loss simulated by FEMLAB in chapter 3 which is 114 W, it is observed that the simulated heat loss is lower than the average experimental heat loss (130 W). This difference could be explained by the fact that the experimental temperatures were not completely stabilized. It takes about one day to reach a true steady state, while the experiments for the heat loss were done in 4-5 hours.

4.4.6 Pressure Drop

To measure the pressure drop in the reactor and pre-heater, a manometer was placed before the pre-heater (Figure 4-18). As it is demonstrated in Table 4-5, the pressure drop in the system is reasonable. Moreover, the pre-heater causes larger pressure drop than the ACR because of the pipe connections.

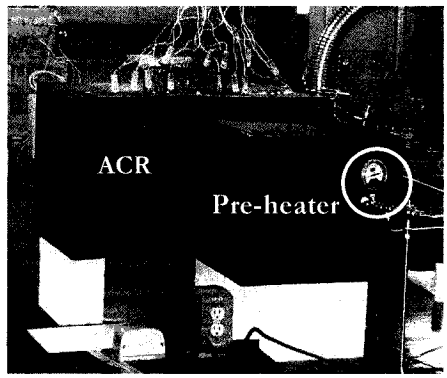

Figure 4-18: Placement of the manometer before pre-heater

Table 4-5: Pressure drop in pre-heater and ACR

	T=25°C			*T=450°C*		
Flow rate	TOTAL	Pre-heater	ACR	TOTAL	Pre-heater	ACR
L/min	PSI	PSI	PSI	PSI	PSI	PSI
100	5.5	3.2	2.3	11	6	5
120	7	4	3	15	8	7
140	9.5	5.9	3.6	19	12	7
160	11	7	4	22	14	8

As it is observed from Table 4-5, the higher the temperature, the higher is the pressure drop. When the temperature increases, the volume of gas raises as well; thus the velocity

increases since the cross sectional area and mass flow are constant which leads to a higher pressure drop.

CHAPTER 5 1D heterogeneous transient model

5.1 Introduction

In this chapter a 1D heterogeneous transient model (HT 1D-t) for the ACR, is presented. This model aims to predict the concentration and temperature of gas flowing in axial direction of the ACR. To develop this model, the conservation equations introduced in chapter 2, were adapted for a 1D problem and transient terms were included. In this simplified model, only the energy and mole balances were considered while the momentum balance equations were neglected because of the small pressure drop. Also, thermal radiation and homogenous reactions were neglected as well.

For simplicity, it was presumed that the reactor is filled only with monoliths with physical dimensions given in Table 2-1. Notice that only one channel of monolith is considered since the concentration and temperature vary only in axial direction. Moreover, the continuity was assumed between the outlet of the annular section and the entrance of the internal tube for temperature and concentration. Also, the heat exchange between the two compartments was not considered in the 1D HT-t model.

5.2 Problem formulation

Table 0-1 resumes the energy and mole balance equations for HT 1D-t model and the boundary conditions for the gas and the solid phase. These equations and boundary

conditions form a system of 4 partial differential equations, with temperature and concentration as unknown variables.

Table 5-1: Energy and mole balance equations in HT 1D-t

Energy balance equations		
Gas phase	$\frac{4}{D_H} h_m (T_s - T_g) - \rho_g Cp_g v_s \frac{\partial T_g}{\partial z} = \rho_g Cp_g \frac{\partial T_g}{\partial t}$	$T_g\big\|_{z=0} = T_{g0}$ $\left.\frac{\partial T_g}{\partial z}\right\|_{z=L} = 0$
Solid phase	$\frac{\partial}{\partial z}(k_w \delta_w \frac{\partial T_s}{\partial z}) - h_m (T_s - T_g) - \eta(1-\varepsilon_m)\Delta H_R k_n C_g Y_{CH_4,s} = \rho_w Cp_w \delta_w \frac{\partial T_s}{\partial t}$	$T_s\big\|_{z=0} = T_g\big\|_{z=0}$ $\left.\frac{\partial T_s}{\partial z}\right\|_{z=L} = 0$
Mole balance equations		
Gas phase	$-\frac{\partial Y_{CH_4}}{\partial z} v_s - \frac{4}{D_H} k_{m,CH_4} (Y_{CH_4,g} - Y_{CH_4,s}) = \frac{\partial Y_{CH_4,g}}{\partial t}$	$Y_{CH_4,g}\big\|_{z=0} = Y_{CH_4,g0}$ $\left.\frac{\partial Y_{CH_4,g}}{\partial z}\right\|_{z=L} = 0$
Solid phase	$k_{m,CH_4} (Y_{CH_4,g} - Y_{CH_4,s}) - \eta k_n Y_{CH_4,s} = 0$	$Y_{CH_4,s}\big\|_{z=0} = Y_{CH_4,g0}$ $\left.\frac{\partial Y_{CH_4,s}}{\partial z}\right\|_{z=L} = 0$

The heat transfer coefficients and physical properties of the gas (air) were presented in chapter 2. The thermal conductivity (k_w) and heat capacity (Cp_w) of the cordierite (monolith wall) were presented in Appendix A. The monolith reactor wall thickness (δ_w), the density of the washcoat (ρ_w), and the monolith porosity was calculated as $1{,}3882\times10^{-4}$ (m), $1{,}5179\times10^{3}$ (kg/m^3), and 0,66 respectively. The related correlations to calculate the effectiveness factor (η), reaction rate constant (k_n), and mass transfer coefficient of methane ($k_{m,CH4}$) are presented in Appendix D [16] .

5.3 Mathematical resolution

Efficient mathematical strategy must be used to solve the 4 differential equations of Table 5-1, which are in fact coupled. In this work, this strategy includes the finite difference method to solve each differential equation in the ACR and iterative procedure to couple these equations together.

5.3.1 Finite difference method

The finite difference method was used to solve each differential equation given in Table 5-1. Using finite difference method, the ACR geometry is described by mesh grid with a set of nodes where the unknown temperature and concentration are solved. Thus, the domain is subdivided into a set of nodes equally distant as shown in Figure 5-1. Also, in the grid the internal tube is placed directly after the annular tube.

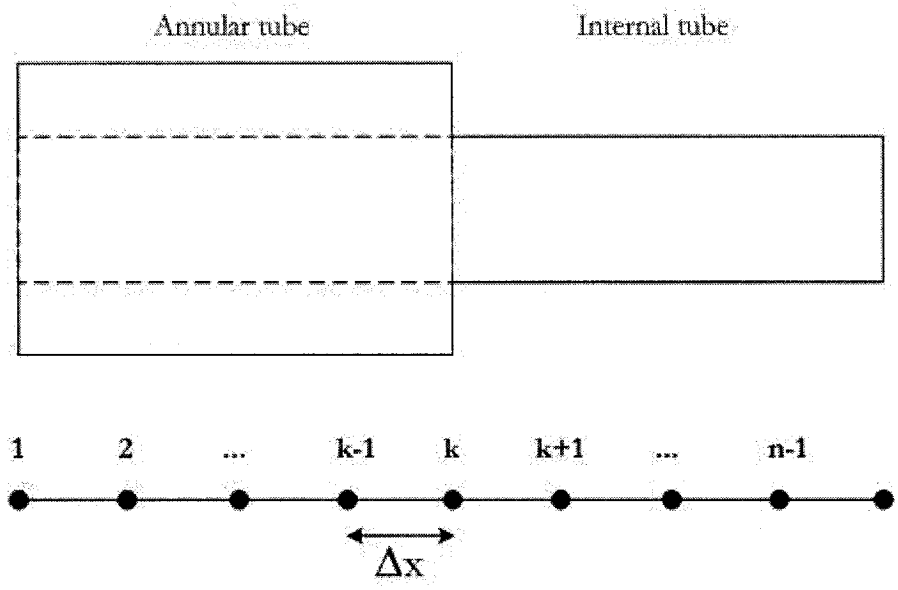

Figure 5-1: Schematic of the grids

In the finite difference method, the first and the second derivatives are approximated using finite difference formula derived from Taylor development. For instance, centered finite difference formula for the first and second derivative are given by

$$\frac{\partial T}{\partial x} = \frac{T_{k+1} - T_{k-1}}{2\Delta x}, \tag{5.1}$$

$$\frac{\partial^2 T}{\partial x^2} = \frac{T_{K+1} - 2T_k + T_{k-1}}{(\Delta x)^2}. \tag{5.2}$$

Using these approximations, an equation can be derived for each node of the grid and be assembled for all the nodes of the grid that leads to a linear system of equations. The resulting system of equations can be solved efficiently by the Jacobi method.

5.3.2 Coupling-scheme algorithm

An algorithm for coupling the 4 differential equations of Table 5-1 was suggested by Hayes and Kolaczkowski [16] (Figure 5-2). This procedure involves using initial estimation of the unknown temperature and concentration and solving each differential equation in turn in order to produce new estimation of the unknown variables. This procedure is repeated iteratively until a final convergence is obtained.

Notice that each of the conservation equations requires various values for physical properties, reaction rates, and mass and heat transfer coefficients. These all depend on the temperature, concentration and velocity in the reactor. The functions of these parameters are stored in a library and called as necessary.

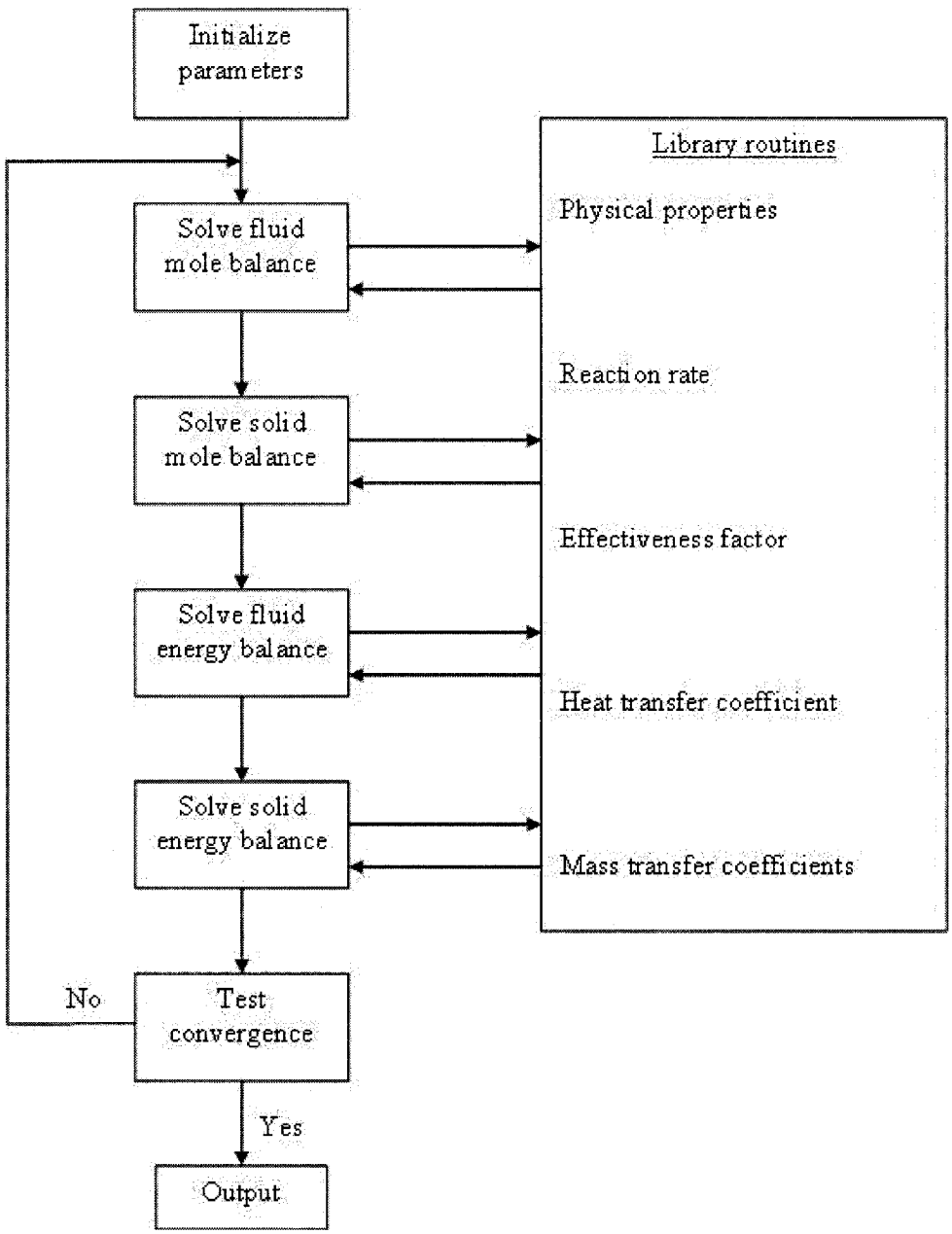

Figure 5-2: Algorithm of the numerical solution according to [16]

5.4 Simulation results

In this section, the simulation results obtained with the HT 1D-t model are presented and compared with available experimental results. The influence of operating conditions of the ACR (inlet temperature, composition, and flow rate) on the temperature and concentration profiles is also investigated.

5.4.1 Comparison with experimental data

First, simulations results of HT 1D-t model were compared with experimental data given for two cases in Table 5-2. The results of these simulations for temperature profile, molar fraction of methane, and conversion are presented in Figure 5-3 to Figure 5-5.

Table 5-2: Available experimental results

	T_{inlet}	C_{CH4_in}	Q
Case 1	400°C	3000 ppm	140 L/min
Case 2	350°C	1000 ppm	140 L/min

Figure 5-3 shows the temperature profile in axial direction in the ACR numerically and experimentally for Case 1 and Case 2. The comparison indicates that the HT 1D-t results exhibit similar trends to experimental data, with values which are mostly in agreement with experimental data. Also, the position of the maximum temperature of numerical prediction corresponds to the experimental data.

Figure 5-4 and Figure 5-5 present the molar fraction and conversion of methane along the reactor. As shown the molar fraction of methane tends to be zero in the outlet of the reactor and the conversion would be close to 100%. In Case 1, the molar fraction of methane reaches the value of zero (position x=0,2 m) more rapidly than in Case 2 (position x=>0,6 m). This can be explained by the fact that the inlet temperature in Case 1 is higher than in Case 2. Furthermore, in Case 1, more heat is released because of higher methane concentration.

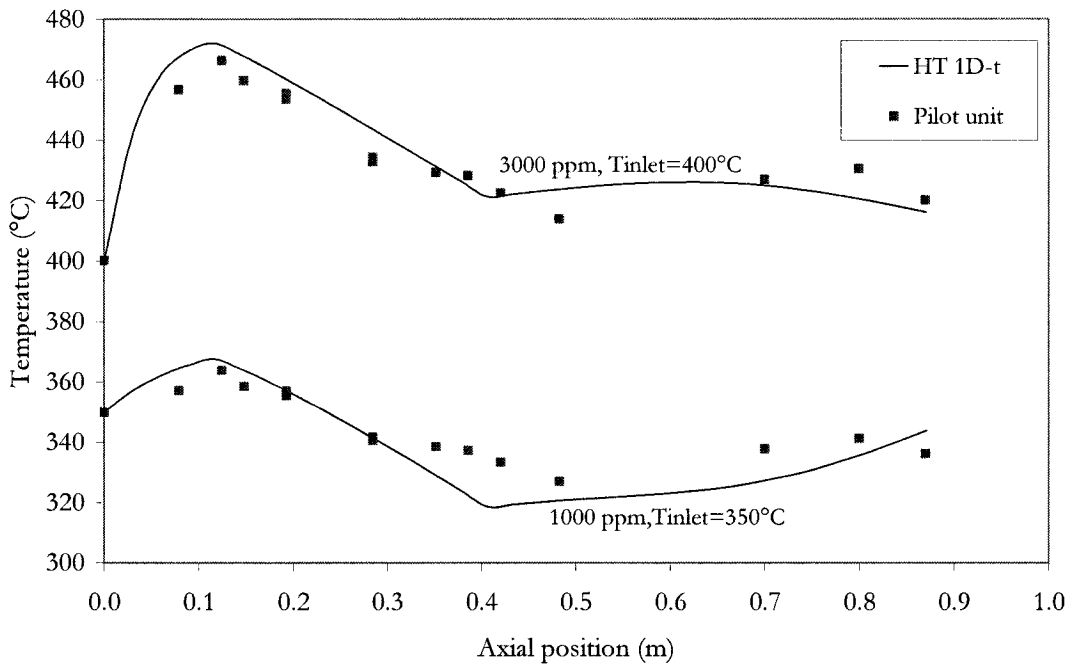

Figure 5-3: Comparison of the simulated temperature profile (lines) with the experimental data (points); 140 L/min

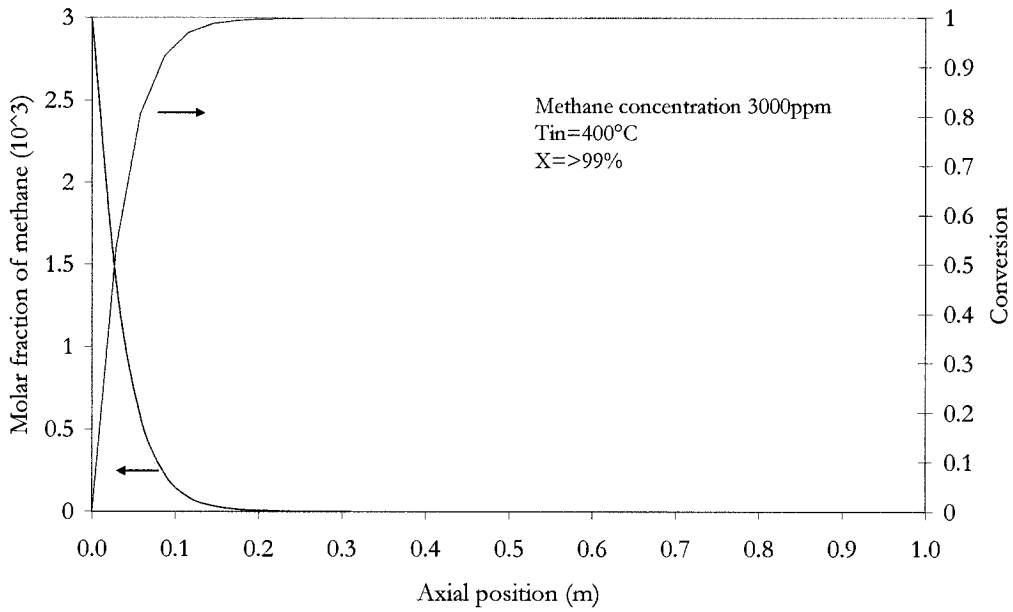

Figure 5-4: Molar fraction and conversion of methane with 0,3% methane/air; T_{inlet}=400°C

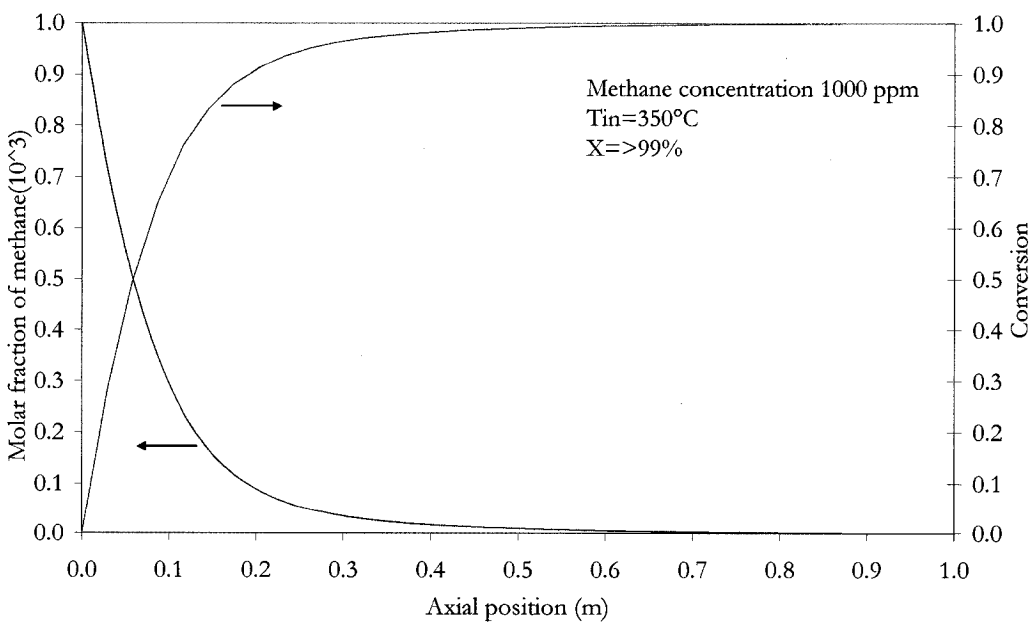

Figure 5-5: Molar fraction and conversion of methane with 0,1% methane/air; T_{inlet}=350°C

5.4.2 Influence of operating conditions

Figure 5-6 shows the influence of different inlet temperatures on axial temperature profile in the reactor for a constant methane concentration of 2000 ppm. It is clear that when the inlet temperature of the reactor is higher, the axial temperature profile will be higher as well. Furthermore, the change in gas temperature from inlet condition is almost the same for all these simulations.

Figure 5-7 shows the influence of flow rate on the temperature profile in the ACR with constant concentration of methane (2000 ppm) and inlet temperature (T_{in}=450°C). It is observed that the higher the volume flow rate, the higher is the temperature profile in the ACR.

As shown in Figure 5-8 when the inlet concentration of methane increases, the axial temperature profile tends to increase in the ACR due to the more generation of heat by the reaction.

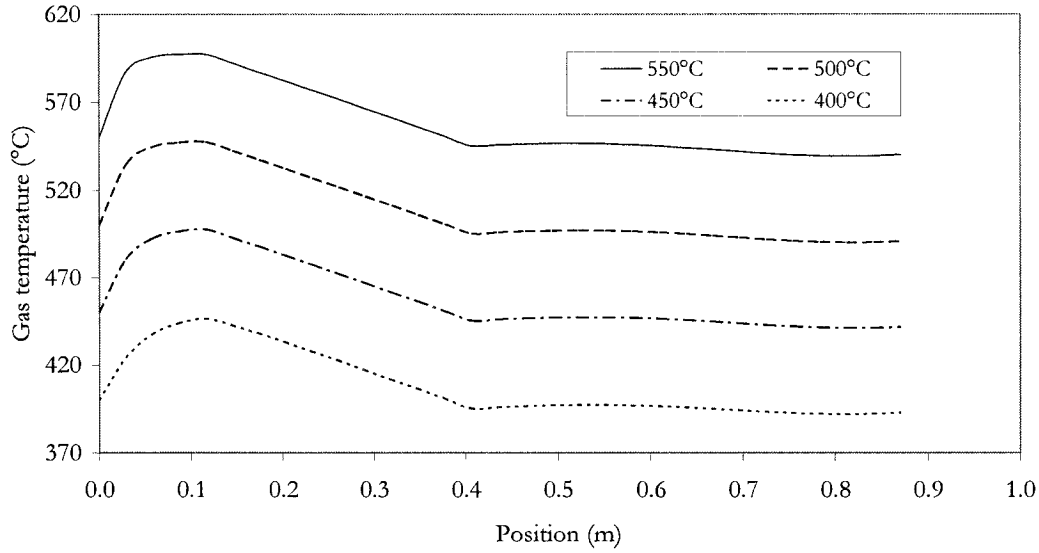

Figure 5-6: Influence of inlet temperature of the ACR on the simulated temperature profile, 0,2% methane/air; 140 L/min

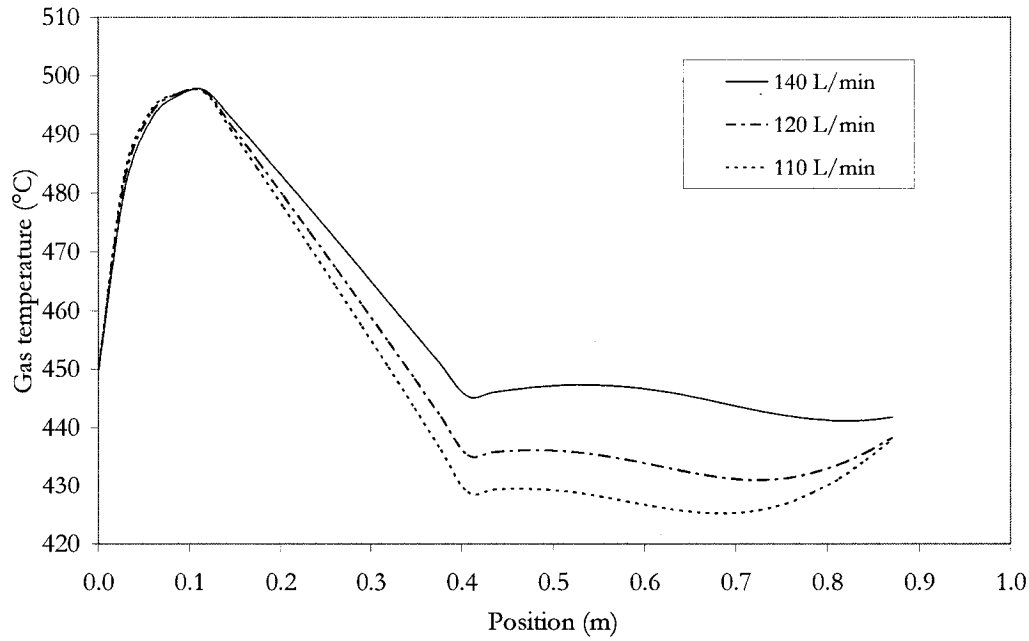

Figure 5-7: Influence of flow rate of the ACR on temperature profile for 0,2% methane/air; T_{inlet}=450°C

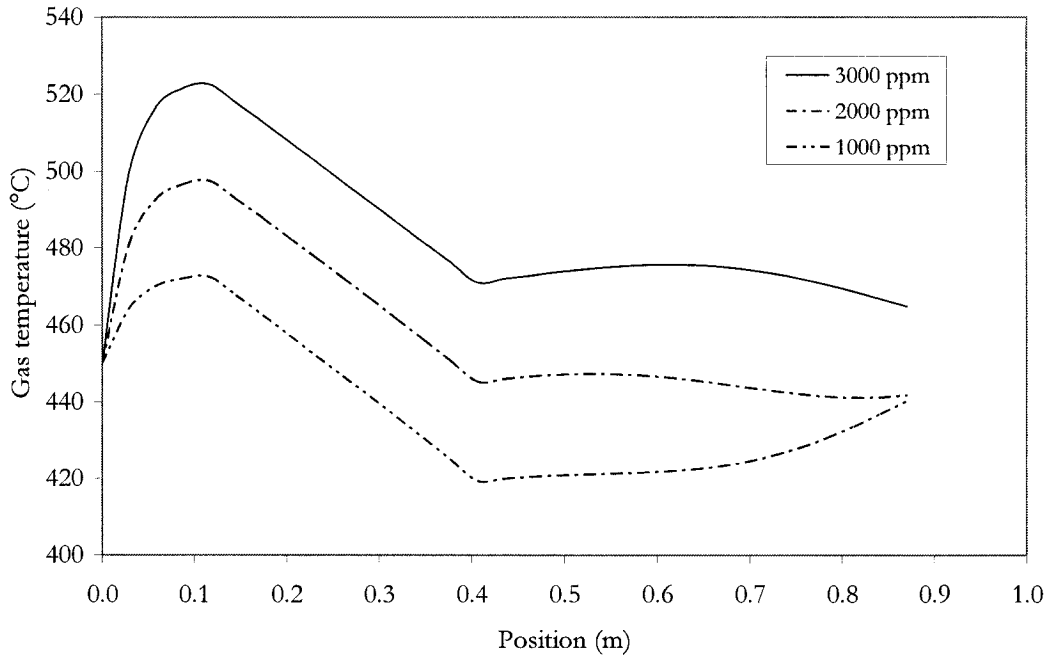

Figure 5-8: Influence of the inlet methane concentration in air on temperature profile in the ACR; 140 L/min and T_{inlet}=450°C

As a conclusion, HT 1D-t model can be used to estimate the temperature and concentration profile in the ACR corresponding to operating conditions defined by inlet temperature, concentration, and flow rate. The comparison between experimental results and simulated values shows that HT 1D-t model produces an appropriate concentration and temperature profile in the ACR.

One dimension was not sufficient to include the heat exchange between two compartments, especially in the fins section in the HT 1D-t. Thus the 3D model should be developed to simulate effectively the transfer phenomena in the ACR.

CHAPTER 6 Conclusions and Recommendations

This Master's Degree work is a part of a research project aiming to eliminate the unburned methane in exhaust emissions from natural gas fueled engines by using an auto-cyclic reactor (ACR). The ACR designed at the Department of Chemical Engineering of Ecole Polytechnique, is a catalytic bed consisting of two concentric tubes: an annular and an internal tube. This configuration takes the advantage of the heat released by reaction to warm up the feed and thus improve the autothermicity of the reactor.

The objective of this (Master Degree) project was to improve understanding of the heat transfer involved in the ACR. The main task was to model the temperature profile in the ACR using numerical methods in order to design the insulation part and to determine the performance of the internal fins. Participation in construction of the experimental ACR and experimental studies of the pilot unit conducted to study the influence of heat transfer on the reactor performance were also an important part of the project. Finally, experimental data were compared with predictions by a simple HT 1D-t numerical model.

The fin performance and the insulation part of the ACR were modeled by numerical simulation of heat transfer in two-dimensions. This 2D model used the commercial software FEMLAB, based on the finite element method, to solve the thermal balance equation with temperature dependent correlations for the physical parameters and the heat transfer coefficients.

Results of 2D model indicate that fin performance is limited by both the conduction and convection resistance of heat transfer. The use of 14 straight fins of stainless steel appears to be a good compromise, which improves the heat transfer in the ACR. However, the conduction resistance of stainless steel is significant and could limit the fin performance when convection resistance is small. From thermal transfer point of view only, the use of material more conductive than stainless steel, for example iron or even copper, would decrease the influence of conduction resistance and increase performance of internal fins. However, for practical reasons, like corrosion, stainless steel is the most reasonable material.

The performance of seven different non-combustible insulation materials was estimated with the 2D model by comparing the temperatures of the reactor side walls for different insulation thickness. As expected, the material having the lowest thermal conductivity needs the smallest insulation thickness to reach the same target for the side wall temperature of the reactor. According to this study, Kaowool bulk fiber was chosen as the insulation material of the laboratory ACR pilot unit. The cross sectional box dimension was estimated as 40×40 cm for reasonable side wall temperatures of 60-65°C.

The HT 1D-t model for the catalytic combustion was elaborated in collaboration with the Ph.D. student M. Zanoletti. The HT 1D-t model was implemented in order to predict the temperature and concentration profiles of gas flowing in axial direction of the ACR. The related balance equations for catalytic combustion were solved by the finite difference method in one dimension. In spite of its simplicity, the HT 1D-t model predicted

reasonably well both the temperature and concentration profiles in the ACR. Thus, this simplified model represents a useful tool for preliminary simulations.

From the experimental monitoring the gas temperature profile and the methane concentration in the inlet and outlet gas, the catalytic combustion of methane in the ACR can be understood. It was found that the combustion reaction is almost complete for all inlet methane concentration if inlet temperature is above 350°C.

It is important to point out that HT 1D-t and 2D models are simplifications of a complex 3D multi-physics problem. To simulate more closely the transfer phenomena in the ACR, in particular the heat exchange between two compartments and in the fins section, a complete 3D model should be developed. However, full 3D multi-physics simulation is a difficult challenge and needs significant computational capacity and time. Nevertheless, the coupling strategy of multi-physics equations used in this project for the HT 1D-t model provides good results and should be adapted for the 3D case.

Also, all the experiments and simulations considered in this study were executed in absence of combustion inhibitors (CO_2, H_2O) in the inlet feed gas of the reactor. Hence, performance of the ACR in real operating conditions should be included in future experimental programs and in the HT 3D-t model.

In resume, this work concerned the modeling of heat transfer in the ACR by using numerical and experimental approach. Simplified 1D and 2D models and also experimental

results on pilot unit were used to improve understanding of thermal transfer in ACR and improve design and operation. In concrete, 2D model allows to design the isolation part of the pilot unit in order to decrease the heat loss from the exterior tube of the reactor and also to study the performance of internal fins to increase the heat transfer between two compartments. Moreover, the HT 1D-t model and the experimental measurements on pilot unit permit to study the performance of the ACR, in term of methane conversion and temperature profile, for different operating conditions of reactor.

In conclusion, this Master's Degree project was contributed to the development of a technology for the treatment of methane emissions from natural gas engines. Models and strategies used in this work permit to understand better the transfer phenomenon in the ACR and improve its design and operation. It is also interesting to highlight that experimental studies almost reached a complete combustion of methane if the inlet temperature of gas is sufficiently high. In this context, the ACR technology seems to be feasible and promising solution to eliminate the unburned methane in emissions from natural gas engines and thus reduce the green-house effect from emissions of buses transportation.

References

[1] Natural Resources Canada, "Canada's 2004 Greenhouse gas inventory; A Summary of Trends," Natural Resources Canada, 2004.

[2] T. E. Lipman and M. A. Delucchi, "Emissions of nitrous oxide and methane from conventional and alternative fuel motor vehicles," *Climatic Change*, vol. 53, pp. 477-516, 2002.

[3] Natural Resources Canada, "Canada's energy market, Natural gas," 2000.

[4] P. Gélin and M. Primet, "Complete oxidation of methane at low temperature over noble metal based catalysts: A review," *Applied Catalysis B: Environmental*, vol. 39, pp. 1-37, 2002.

[5] J. H. Lee and D. L. Trimm, "Catalytic combustion of methane," *Fuel Processing Technology*, vol. 42, pp. 339-359, 1995.

[6] D. Vortmeier and W. Jahnel, "Moving Reaction Zones in Fixed Bed Reactors Under the Influence of Various Parameters," *Chemical Engineering Science*, vol. 27, pp. 1485-1496, 1972.

[7] Y. S. Matros, "Catalytic Processes Under Unsteady Conditions," *Studies in Surface Science and Catalysis*, vol. 43, 1989.

[8] C. Sapundzhiev, J. Chaouki, C. Guy, and D. Klvana, "Catalytic combustion of natural gas in a fixed bed reactor with flow reversal," *Chemical Engineering Communications*, vol. 125, pp. 171-186, 1993.

[9] G. Kolios, J. Frauhammer, and G. Eigenberger, "Autothermal fixed-bed reactor concepts," *Chemical Engineering Science*, vol. 55, pp. 5945-5967, 2000.

[10] Y. S. Matros, G. A. Bunimovich, V. O. Strots, and E. A. Mirosh, "Reversed flow converter for emission control after automotive engines," *Chememical Engineering Science*, vol. 54, pp. 2889-2898, 1999.

[11] B. Liu, R. E. Hayes, M. D. Checkel, M. Zheng, and E. Mirosh, "Reversing flow catalytic converter for a natural gas diesel dual fuel engine," *Chemical Engineering Science*, vol. 56, pp. 2641-2658, 2001.

[12] D. Klvana, J. Kirchnerova, J. Chaouki, and C. Guy, "Apparatus and process for Catalytic Gas Involving Reactions Which are Exothermic," *US Patent Application*, vol. No. 2 273761, 1999.

[13] D. Klvana, J. Chaouki, C. Guy, J. Kirchnerova, and M. Zanoletti, "Performance of auto-cyclic reactor in catalytic combustion of lean fuel mixtures," *Industrial and Engineering Chemistry Research*, vol. 44, pp. 9676-9682, 2005.

[14] M. Sheintuch and O. Nekhamkina, "Comparison of flow-reversal, internal-recirculation and loop reactors," *Chemical Engineering Science*, vol. 59, pp. 4065-4072, 2004.

[15] W. C. Turner and j. F. Malloy, *Thermal Insulation Handbook*. New York: McGraw-Hill, 1981.

[16] R. E. Hayes and S. T. Kolaczkowski, *Introduction to Catalytic Combustion*. Amsterdam: Gordon and Breach Science Publishers, 1997.

[17] R. B. Bird, W. E. Stewart, and E. N. Lightfoot, *Transport Phenomena*, Second ed. New York: John Wiley & Sons, 2002.

[18] S. Yagi and N. Wakao, "Heat and Mass Transfer from Wall to Fluid in Packed Beds," *AIChE Journal*, vol. 5, pp. 79, 1959.

[19] H. J. Lane and P. J. Heggs, "Extended surface heat transfer-the dovetail fin," *Applied Thermal Engineering*, vol. 25, pp. 2555-65, 2005.

[20] P. Razelos and R. N. Krikkis, "On the optimum thermal design of individual longitudinal fins with rectangular profile," *International Communications in Heat and Mass Transfer*, vol. 30, pp. 349-358, 2003.

[21] E. N. Sieder and G. E. Tate, "Heat transfer and pressure drop of liquids in tubes," *Industrial and Engineering Chemistry*, vol. 28, pp. 1429-1435, 1936.

[22] A. G. Dixon and D. L. Cresswell, "Theoretical prediction of effective heat transfer parameters in packed beds," *AIChE Journal*, vol. 25, pp. 663-76, 1979.

[23] T. P. Tiemersma, C. S. Patil, M. V. Sint Annaland, and J. A. M. Kuipers, "Modelling of packed bed membrane reactors for autothermal production of ultrapure hydrogen," *Chemical Engineering Science*, vol. 61, pp. 1602-1616, 2006.

[24] J. P. Holman, *Heat Transfer*, ninth ed. New York: McGraw-Hill, 2002.

[25] F. P. Incropera and D. P. DeWitt, *Fundamentals of Heat and Mass Transfer*, Fifth ed. New york: John Wiley & Sons, 2002.

[26] Thermal Ceramics Company, "Kaowool bulk fiber, Product information." Montreal, 2006.

[27] Y. S. Touloukian, R. W. Powell, C. Y. Ho, and P. G. Clemens, *Thermophysical Properties of Solids*, vol. 2, . New York: Plenum Press, 1970.

[28] T. Ando, Y. Isobe, D. Sunohara, Y. Daisho, and J. Kusaka, "Homogeneous charge compression ignition and combustion characteristics of natural gas mixtures: The visualization and analysis of combustion," *JSAE Review*, vol. 24, pp. 33-40, 2003.

Appendix A: Physical properties of materials

Air [24]

Thermal conductivity

$$k = 1.679\times10^{-2} + 5.073\times10^{-5}\,T \quad \frac{W}{m.K}$$

Heat capacity

$$Cp = -4\times10^{-7}\,T^3 + 0.0009T^2 - 0.3945T + 1053.8 \quad \frac{J}{kg.K}$$

Viscosity

$$\mu = (0.2198T^2 + 609.26T + 17607)\times10^{-5} \quad Pa\cdot s$$

Prandlt number

$$Pr = (-4\times10^{-10}\,T^4 + 5\times10^{-7}\,T^3 + 0.0002T^2 - 0.4398T + 813.09)\times10^{-3}$$

Density

$$\rho = 364.8T^{-1.0053} \quad \frac{kg}{m^3}$$

The values of k, Cp, μ, and Pr are not a strong function of pressure and may be used in the range of 1 to 20 bar. All the temperatures are in Kelvin.

CO_2 [24]

Thermal conductivity

$$k = (0.0411T^2 + 51.452T - 2541.5)\times10^{-6} \quad \frac{W}{m.K}$$

Heat capacity

$$Cp = (0.0006T^2 + 1.2813T + 530.52)\times 10^{-3} \quad \frac{J}{kg.K}$$

Viscosity

$$\mu = (-2\times 10^{-5}T^2 + 0.0587T + 0.7673)\times 10^{-6} \quad Pa\cdot s$$

Prandlt number

$$Pr = (0.0002T^2 - 0.557T + 922.76)\times 10^{-3}$$

Density

$$\rho = 584.69T^{-1.0139} \quad \frac{kg}{m^3}$$

H2O (water vapour) [24]

Thermal conductivity

$$k = (0.0138T^2 + 66.35T - 2673.6)\times 10^{-6} \quad \frac{W}{m.K}$$

Heat capacity

$$Cp = (-0.0006T^3 + 1.3241T^2 - 846.33T + 369709)\times 10^{-5} \quad \frac{J}{kg.K}$$

Viscosity

$$\mu = (0.0001T^2 + 360.64T - 9892.2)\times 10^{-10} \quad Pa\cdot s$$

Prandlt number

$$Pr = (7\times 10^{-7}T^4 - 0.0019T^3 + 2.0904T^2 - 998.41T + 275304)\times 10^{-5}$$

Density

$$\rho = (0.0118T^2 - 21.205T + 12123)\times 10^{-4} \quad \frac{kg}{m^3}$$

O2 [24]

Thermal conductivity

$$k = (0.0333T^2 + 101.88T - 828.92)\times 10^{-6} \quad \frac{W}{m.K}$$

Heat capacity

$$Cp = (0.0001T^3 + 0.1697T^2 - 57.843T + 96993)\times 10^{-5} \quad \frac{J}{kg.K}$$

Viscosity

$$\mu = (-0.3594T^2 + 757.58T + 10624)\times 10^{-10} \quad Pa \cdot s$$

Prandlt number

$$Pr = (-0.0001T^3 + 0.201T^2 - 115.77T + 90491)\times 10^{-5}$$

Density

$$\rho = (-0.0004T^3 + 0.602T^2 - 289T + 57240)\times 10^{-4} \quad \frac{kg}{m^3}$$

N2 [24]

Thermal conductivity

$$k = (-0.0246T^2 + 87.507T + 2048)\times 10^{-6} \quad \frac{W}{m.K}$$

Heat capacity

$$Cp = (-3\times10^{-5}T^{3} + 0.0703T^{2} - 33.348T + 108426)\times10^{-5} \quad \frac{J}{kg.K}$$

Viscosity

$$\mu = (-0.1347T^{2} + 496.62T + 39835)\times10^{-10} \quad Pa\cdot s$$

Prandlt number

$$Pr = (-0.0024T^{4} - 9.8155T^{3} + 15356T^{2} - 9\times10^{6}T + 9\times10^{9})\times10^{-10}$$

Density

$$\rho = 3\times10^{6}T^{-1.0003} \quad \frac{kg}{m^{3}}$$

Stainless steel AISI 304 [25]

Thermal conductivity

$$k = (-0.0044T^{2} + 22.323T + 7789.4)10^{-3} \quad \frac{W}{m.K}$$

Heat capacity

$$Cp = 143.68Ln(T) - 370.51 \quad \frac{J}{kg.K}$$

All the temperatures are in Kelvin.

Cordierite [16]

Thermal conductivity of the monolith wall

$$k_{W} = 0.9558 - 2.09\times10^{-4}T \quad \frac{W}{m.K}$$

Heat capacity

$$Cp_w = 948 + 0.2268T \quad \frac{J}{kg.K}$$

All the temperatures are in Kelvin.

Insulation materials [15]

- Kaolin (Density=48 to 64 $\frac{kg}{m^3}$)

$$k = (0.0024T^2 + 0.3498T - 34.926)10^{-4} \quad \frac{W}{m.K}$$

- Kaolin (Density=96 to 128 $\frac{kg}{m^3}$)

$$k = (0.0028T^2 - 1.0314T + 364.54)10^{-4} \quad \frac{W}{m.K}$$

- Mineral wool (Density=160 to 224 $\frac{kg}{m^3}$)

$$k = (0.0024T^2 - 0.2866T + 281.53)10^{-4} \quad \frac{W}{m.K}$$

- Alumina silica fiber (Density=400 $\frac{kg}{m^3}$)

$$k = (0.0038T^2 - 1.2243T + 301.66)10^{-4} \quad \frac{W}{m.K}$$

- Silica fiber (Density=96 to 152 $\frac{kg}{m^3}$)

$$k = (0.0045T^2 - 3.8757T + 1439.1)10^{-4} \quad \frac{W}{m.K}$$

- Silica fiber (Density=144 $\frac{kg}{m^3}$)

$$k = (0.0019T^2 - 0.3782T + 227.05)10^{-4} \quad \frac{W}{m.K}$$

- Kaowool (Density=128 $\frac{kg}{m^3}$) [26]

$$k = (0.0001T^2 + 0.0321T + 21.526)10^{-3} \quad \frac{W}{m.K}$$

- Kaowool (Density=256 $\frac{kg}{m^3}$) [26]

$$k = (0.0006T^2 + 0.7809T + 50.14)10^{-4} \quad \frac{W}{m.K}$$

T is in Kelvin.

Alumina (Pellets) [27]

Thermal conductivity

$$k = (0.0591T^2 - 74.318T + 32568)10^{-3} \quad \frac{W}{m.^\circ C}$$

T is in Celsius.

Appendix B: Analytical solution of the tube without fins

Here is the energy balance equation

$$\frac{d(rq)}{dr} = 0,$$

$$q = \frac{C_1}{r}.$$

The convection boundary conditions are

$$r = r_1 \rightarrow q_{r_1} = h_1(T_{\infty_1} - T_{w_1}) \rightarrow T_{w_1} = \frac{-C_1}{r_1 h_1} + T_{\infty_1},$$

$$r = r_2 \rightarrow q_{r_2} = h_2(T_{w_2} - T_{\infty_2}) \rightarrow T_{w_2} = \frac{C_1}{r_2 h_2} + T_{\infty_2}.$$

By applying Fourier's law

$$q = \frac{C_1}{r} \rightarrow \frac{\partial T}{\partial r} = \frac{-C_1}{rk},$$

$$T = \frac{-C_1}{k} lnr + C_2,$$

with following boundary conditions

$$r = r_1 \rightarrow T = T_{w1},$$

$$r = r_2 \rightarrow T = T_{w2}.$$

After rearrangement C_1 and C_2 can be computed as

$$C_1 = \frac{T_{\infty 2} - T_{\infty 1}}{a_1 + a_2} \text{ and } C_2 = T_{\infty 1} + C_1 a_1,$$

where

$$a_1 = \frac{1}{r_1 h_1} - \frac{lnr_1}{k} \text{ and } a_2 = \frac{1}{r_2 h_2} + \frac{lnr_2}{k}.$$

Appendix C: Time to heat the ACR and light off

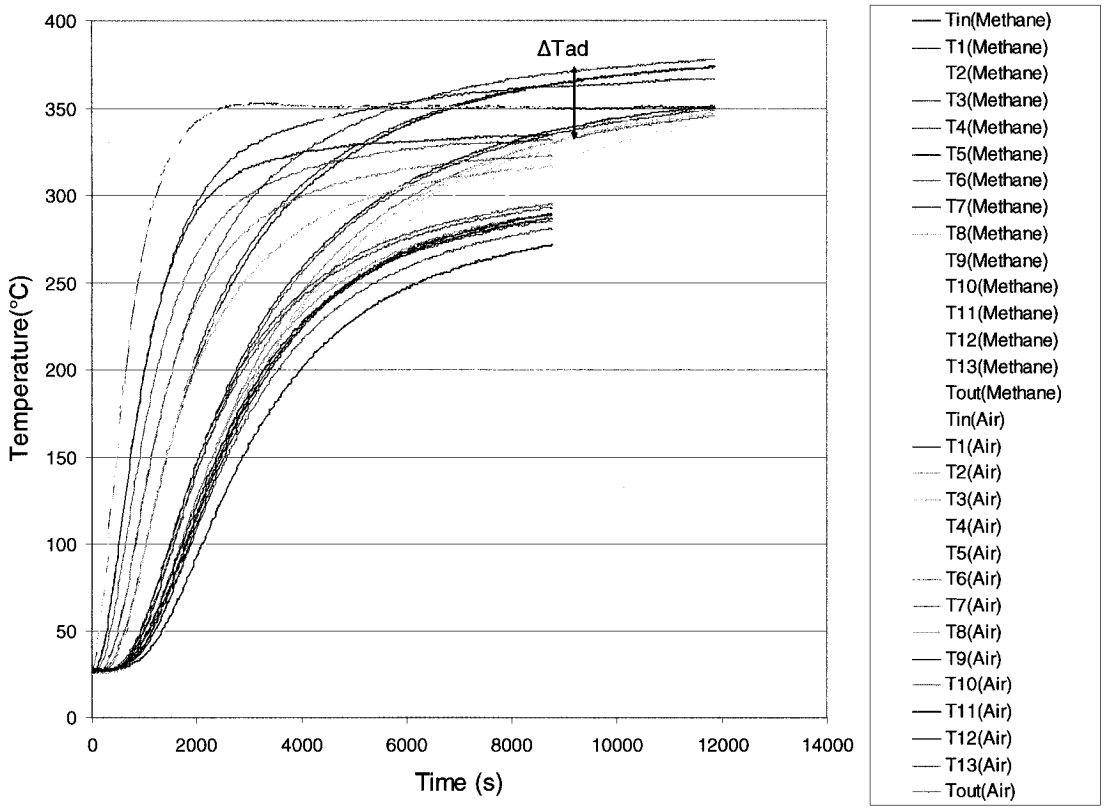

Transient temperature profile in ACR, Tin=350°C, Methane=2000ppm,

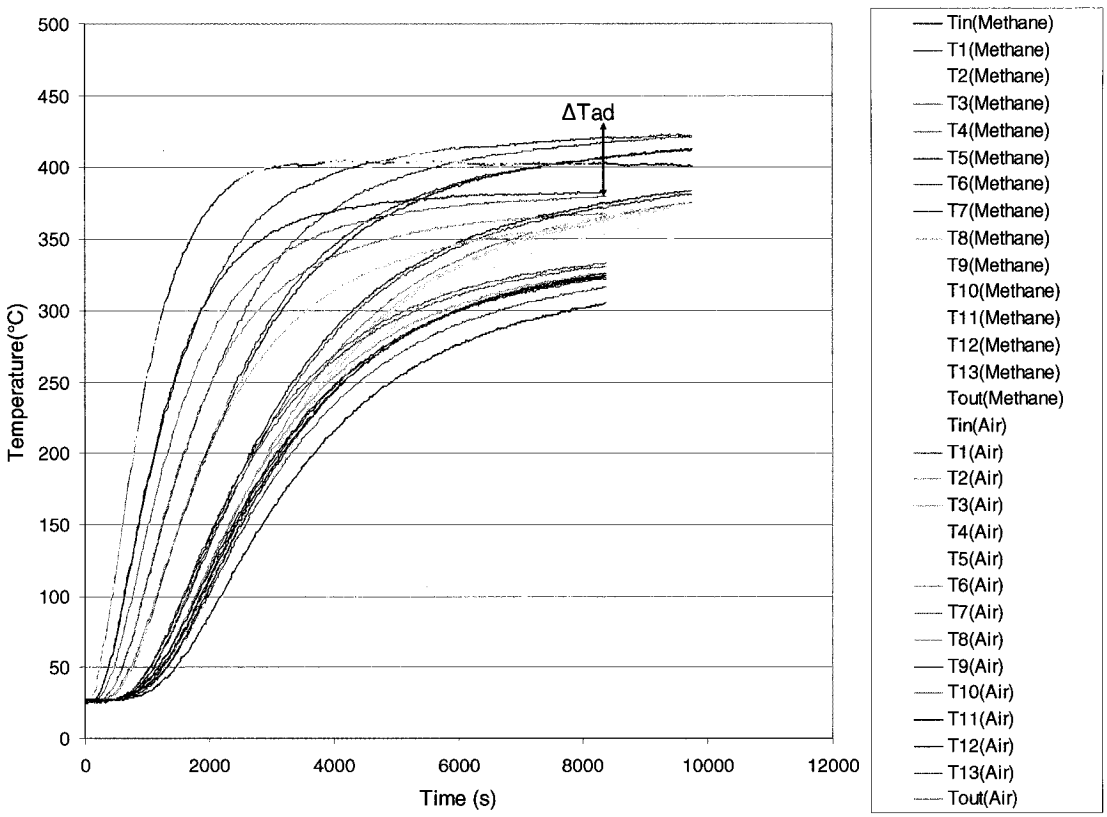

Transient temperature profile in ACR, Tin=400°C, Methane=2000ppm

Appendix D: Mass transfer correlations in HT 1D-t

Mass transfer correlation used for simulations in HT 1D-t presented in chapter 5[4]

Symbol	Description	Formula
η	Effectiveness factor	$\eta = \left[1+\left(\frac{1,002}{\Phi^{0,9794}}\right)^{-1,307}\right]^{\frac{-1}{1,307}}$
Φ	Thiele modulus	$\Phi = \sqrt{\frac{L_C k_s}{D_{eff}}}$
L_C	Effective length (thickness) of washcoat	$L_C = \frac{A_C}{W_P} = 4,6053e\text{-}5$
k_s	Reaction rate constant	$k_s = \exp(12,77)\exp(\frac{-57300}{RT})\frac{RT}{101325}\rho_w(1-\varepsilon_m)L_C$
$Deff$	Effective diffusivity	$D_{eff} = 1,165 D_V$
D_V	Diffusion coefficient inside a pore	$\frac{1}{D_V} = \frac{1}{D_{CH_4,air}} + \frac{1}{D_K}$
$D_{CH_4,air}$	Bulk diffusion coefficient for methane in air	$D_{CH_4,air} = 5,538\times10^{-9}\frac{T_s^{1,75}}{P}$
D_K	Knudsen diffusivity	$D_K = 5,362\times10^{-7}T_s^{0,5}$
k_n	Reaction rate constant	$k_n = \exp(12,77)\exp(\frac{-57300}{RT})\frac{RT}{101325}\rho_w(1-\varepsilon_m)L_C$

[4] Determined by M. Zanoletti

Symbol	Description	Formula
$k_{m,CH4}$	Mass transfer coefficient	$k_{m,CH_4} = \frac{Sh \times D_{CH_4,air}}{D_H}$
Sh	Sherwood number	$Sh = 0,5\,(Sh\_H - D_a \frac{Sh\_H}{Sh\_T} + ((Sh\_H - D_a \frac{Sh\_H}{Sh\_T})^2 + 4 D_a Sh\_H)^{0.5}$
D_a	Damkohler number	$D_a = \frac{\eta k_s D_H}{4 D_{CH_4,air}}$
Sh_T Sh_H	Sherwood	$Sh\_T = 2.977 + 6.854 \times ((1000 / Gz)^{(-0.5174)}) \times \exp(-42.49 / Gz)$ $Sh\_H = 3.095 + 8.933 \times ((1000 / Gz)^{(-0.5386)}) \times \exp(-6.7275 / Gz)$
Gz	Graetz number	$Gz = \frac{D_H \times Pe\_m}{z}$
Pe	Peclet number	$Pe = \mathrm{Re} \times Sc$
Re	Reynolds number	$\mathrm{Re} = \rho_{air} U D_H / \mu_{air}$
U	Velocity	$U = v_s \frac{T}{T_{inlet}}$